ABSTRACT

Title of dissertation: APPLYING MATHEMATICAL MODELS TO STUDY THE ROLE OF THE IMMUNE SYSTEM IN CHRONIC MYELOGENOUS LEUKEMIA

Geoffrey Douglas Clapp
Doctor of Philosophy, 2016

Dissertation directed by: Professor Doron Levy
Department of Mathematics

Although tyrosine kinase inhibitors (TKIs) such as imatinib have transformed chronic myelogenous leukemia (CML) into a chronic condition, these therapies are not curative in the majority of cases. Most patients must continue TKI therapy indefinitely, a requirement that is both expensive and that compromises a patient's quality of life. While TKIs are known to reduce leukemic cells' proliferative capacity and to induce apoptosis, their effects on leukemic stem cells, the immune system, and the microenvironment are not fully understood. A more complete understanding of their global therapeutic effects would help us to identify any limitations of TKI monotherapy and to address these issues through novel combination therapies.

Mathematical models are a complementary tool to experimental and clinical data that can provide valuable insights into the underlying mechanisms of TKI therapy. Previous modeling efforts have focused on CML patients who show biphasic and triphasic exponential declines in BCR-ABL ratio during therapy. However, our patient data indicates that many

patients treated with TKIs show fluctuations in BCR-ABL ratio yet are able to achieve durable remissions. To investigate these fluctuations, we construct a mathematical model that integrates CML with a patient's autologous immune response to the disease. In our model, we define an immune window, which is an intermediate range of leukemic concentrations that lead to an effective immune response against CML. While small leukemic concentrations provide insufficient stimulus, large leukemic concentrations actively suppress a patient's immune system, thus limiting it's ability to respond. Our patient data and modeling results suggest that at diagnosis, a patient's high leukemic concentration is able to suppress their immune system. TKI therapy drives the leukemic population into the immune window, allowing the patient's immune cells to expand and eventually mount an efficient response against the residual CML. This response drives the leukemic population below the immune window, causing the immune population to contract and allowing the leukemia to partially recover. The leukemia eventually reenters the immune window, thus stimulating a sequence of weaker immune responses as the two populations approach equilibrium.

We hypothesize that a patient's autologous immune response to CML may explain the fluctuations in BCR-ABL ratio that are regularly seen during TKI therapy. These fluctuations may serve as a signature of a patient's individual immune response to CML. By applying our modeling framework to patient data, we are able to construct an immune profile that can then be used to propose patient-specific combination therapies aimed at further reducing a patient's leukemic burden. Our characterization of a patient's anti-leukemia immune response may be especially valuable in the study of drug resistance, treatment cessation, and combination therapy.

APPLYING MATHEMATICAL MODELS TO STUDY THE ROLE OF THE IMMUNE SYSTEM IN CHRONIC MYELOGENOUS LEUKEMIA

by

Geoffrey Douglas Clapp

Dissertation submitted to the Faculty of the Graduate School of the
University of Maryland, College Park in partial fulfillment
of the requirements for the degree of
Doctor of Philosophy
2016

Advisory Committee:
Professor Doron Levy, Chair/Advisor
Professor Jacob Bedrossian
Professor Kasso Okoudjou
Professor Sergei Sukharev
Professor Konstantina Trivisa

Acknowledgments

I am extremely grateful to all the people who have made this thesis possible and who have supported me throughout my graduate experience.

First, I'd like to thank my advisor, Professor Levy, for the opportunity to work on such an exciting and challenging project. Applying my mathematical training to problems in medicine has been a truly amazing experience and has kept me motivated throughout my studies. Dr. Levy has been extremely supportive and willing to discuss not only my research project but also my career plans. It has been a great pleasure to learn from such a talented and successful mathematician and researcher.

I would also like to thank Dr. Franck Nicolini, Dr. Thomas Lepoutre, Apollos Besse, and Raouf El Cheikh who have provided valuable clinical and mathematical expertise. Our in-person and Skype meetings have been very informative and have helped to motivate many of the ideas and results presented in this thesis. I would also like to acknowledge Dana Botesteanu and Matt Becker, with whom I have had many thought-provoking discussions, and whose friendship I am extremely grateful to have gained.

I would like to thank my family, who have supported me throughout my life, in all of my personal and professional endeavors. My parents have been amazing role models, who have instilled in me a passion for learning and a dedication to my studies. My parents, my wife Margaret, and my parents-in-law have provided me with all of the love and support I could possibly need. They have always been willing to listen and to reassure me whenever I doubted myself or was feeling overwhelmed, and I feel extremely lucky to have such a great support network.

Lastly, I would like to thank the National Science Foundation for supporting my research through the Graduate Research Fellowship under Grant No. DGE1322106.

Table of Contents

List of Figures

List of Abbreviations

ABM	agent-based model
ALL	acute lymphoblastic leukemia
ATP	adenosine triphosphate
BCR-ABL	the oncogene that causes CML
CML	chronic myelogenous leukemia
CP	chronic phase
DDE	delay differential equation
G-CSF	granulocyte colony-stimulating factor
HSC	hematopoietic stem cell
IFNα	interferon-alpha
IM	imatinib
IS	international standard
M	mature cells (Roeder model)
MMR	major molecular response, a 3-log decrease in BCR-ABL ratio
MMR^4	a 4-log decrease in BCR-ABL ratio
$MMR^{4.5}$	a 4.5-log decrease in BCR-ABL ratio
MP	mercaptopurine
MTX	methotrexate
NK	natural killer
ODE	ordinary differential equation
P	precursor cells (Roeder model)
PDE	partial differential equation
RT-PCR	reverse transcription polymerase chain reaction
TFR	treatment free remission
TGN	thioguanine nucleotide
TKI	tyrosine kinase inhibitor
UMRD	undetectable minimal residual disease, which generally corresponds to a 5-log decrease in BCR-ABL ratio

Chapter 1: Introduction

The goal of this dissertation is to develop and apply mathematical models to study chronic myelogenous leukemia (CML). We take an interdisciplinary approach that combines modeling with patient data, to study various aspects of the dynamics of CML and its treatment. The biological background presented in Chapter 1 provides the foundation of these models.

1.1 Introduction to CML

Hematopoiesis is a complex and tightly regulated process that maintains our body's blood supply, producing between 10^{11} and 10^{12} new blood cells per day. All of these cells are derived from a single type of cell, the hematopoietic stem cells (HSCs). Each day, a small subset of these cells differentiates and expands down the blood cell hierarchy in order to produce the various types of mature blood cells. This process is heavily regulated in order to ensure an appropriate balance of red blood cells, white blood cells, and platelets.

Leukemia is a type of cancer that occurs when a few mutated blood cells escape the normal regulations of hematopoiesis. This type of cancer generally originates in the bone marrow and eventually results in significantly elevated white blood cell counts. Leukemia can be further classified as *acute* or *chronic* and as *myeloid* or *lymphocytic* based on the maturity

and type of the leukemic cells. In this dissertation, we focus on chronic myeloid leukemia (CML), a myeloproliferative disorder that accounts for about 20% of leukemias in adults. CML occurs primarily in adults, with a median age of diagnosis of 65 years. A majority of cases of CML is initiated by the formation of the *BCR-ABL* fusion oncogene, which encodes for a constitutively active tyrosine kinase, that allows these cells to proliferate more rapidly than their healthy counterparts and independently of external regulations. Without treatment, CML patients typically progress from the chronic phase to the accelerated phase, and finally to blast crisis, which is similar to acute leukemia and leads to metastasis, organ failure, and death.

Introduced in the late 1990s, tyrosine kinase inhibitors (TKIs), such as imatinib (IM), dasatinib, and nilotinib, have revolutionized the treatment of CML. These targeted therapies work via competitive inhibition, by binding to the adenosine triphosphate (ATP)-binding site of *ABL* tyrosine kinases, thus preventing these proteins from switching into their active form. Because of their specificity, TKIs are able to target leukemic cells, while healthy cells are left mostly intact. TKI therapy produces hematological and cytogenetic remissions in most patients [34, 73]. Beyond these levels of remission, a patient's response is determined on a molecular level based on their BCR-ABL ratio, a blood measurement that represents the ratio of *BCR-ABL* transcript to a control transcript, either *BCR*, *ABL*, or *GUS*. Many patients achieve a major molecular response (MMR), or a 3-log decrease in BCR-ABL ratio, with some even reaching MMR^4 (4-log decrease), $MMR^{4.5}$ (a 4.5-log decrease), or undetectable minimal residual disease (UMRD) (undetectable by RQ-PCR, or a measured ratio of zero, which generally corresponds to at least a 5-log decrease) [38]. Reaching UMRD may indicate leukemia elimination in some cases, but often small concentrations of leukemic cells can be

detected using more sensitive tests [86]. Still, TKIs have transformed CML into a chronic condition, with patients' life expectancies comparable to those of their healthy counterparts.

Despite their success, it is unclear whether TKIs alone can be curative, and as a result patients typically continue TKI therapy indefinitely, a requirement that is both expensive and compromises their quality of life. A more complete understanding of their global therapeutic effect may lead to improved therapy schedules that would further reduce or eliminate any residual leukemia. While TKIs are known to decrease leukemic cell proliferation [4, 41] and increase apoptosis [24], other effects, such as their impact on the immune cell population or on the microenvironment, may also play a significant role. Gallipoli *et al.* [29] and Rea *et al.* [80] found that quiescent leukemic stem cells (LSCs) are insensitive to TKIs, which suggests that 'cure' in the sense of elimination of the leukemic burden may not be possible with TKIs alone. This finding is further supported by the fact that many patients in long-term remission continue to harbor small residual leukemic loads even after many years of therapy [86]. However, leukemia eradication may not be necessary to achieve an 'operational cure' [31], in which a patient can stop therapy without relapsing, as evidenced in the various treatment cessation trials, which will be discussed in Section 1.2. A better understanding of TKIs would allow us to improve the way that these drugs are administered and also to identify their limitations. If TKIs are incapable of curing most patients, then understanding their mechanisms of action may inform our use of combination therapies.

1.2 Treatment Cessation

Because of the success of TKI therapy for CML, many clinicians have shifted their efforts toward the goal of achieving treatment-free remission (TFR). Currently, CML patients continue TKI therapy indefinitely, regardless of whether they achieve long-term deep remissions. However, treatment cessation is desirable for several reasons. First, although TKIs are generally well-tolerated, these therapies, particularly second-generation TKIs, may have significant side effects that can compromise a patient's quality of life. Second, TKI therapy is expensive, especially over many years. CML patients' life expectancies are comparable to their healthy counterparts', and several decades of treatment can cost hundreds of thousands of dollars per patient [87]. Given these quality of life and financial concerns, reducing the necessary duration of therapy from a patient's lifetime down to 5-10 years would be a significant accomplishment.

Several clinical trials involving over 900 total patients [58] have been conducted in order to evaluate the safety and efficacy of treatment cessation in patients who have responded well to TKI therapy (that is, patients who have at least achieved a durable MMR[4]). Stop Imatinib (STIM) [60] studied treatment cessation in 100 patients who had remained in UMRD for at least two years. After stopping IM, patients' BCR-ABL ratios were measured once per month during the first year, every two months during the second year, and every three months thereafter. Relapse was defined as two consecutive positive measurements (loss of UMRD), where the second measurement represented a 1-log increase in BCR-ABL ratio compared to the first measurement. In TWISTER [86], similar inclusion criteria were used, and patients were monitored every month for the first year and every three months

thereafter. In contrast to STIM, relapse was defined more strictly, as any two consecutive positive measurements. Both trials found that about 60% of patients relapsed, mostly in the first six months of treatment cessation. These patients then resumed IM therapy and were generally able to re-achieve deep remissions. The remaining 40% achieved durable TFRs that lasted for several years.

It is important to note, however, that the inclusion and relapse criteria may be unnecessarily strict, thus excluding patients who would otherwise achieve TFR. ASTIM [88], EUROSKI [92], and STIM2 [59] have explored alternative inclusion and relapse criteria. Specifically, in ASTIM, patients were allowed to show occasional low-levels of *BCR-ABL* expression in the two years prior to treatment cessation. Relapse was defined as loss of MMR (a ratio greater than 0.1%), a much weaker condition than loss of UMRD. Using the original STIM relapse definition, 46% of patients were in TFR at two years, but with their new definition, 64% remained in TFR. In the ongoing EUROSKI trial, patients were required to have remained in MMR^4 for the previous year. Preliminary results include a 6-month TFR rate of 61.5%, which suggests that MMR^4 may be sufficient. In a STIM2 interim report [59], the authors observed a TFR rate of 61%, with median follow-up of 12 months. Interestingly, one-third of TFR patients showed low-level fluctuations in BCR-ABL ratio but maintained their MMR status. These trials suggest that with relaxed inclusion and relapse criteria, more CML patients may be able to achieve TFR. The precise optimal set of requirements remains to be determined.

Based on STIM and TWISTER, approximately 40% of CML patients treated with IM will become eligible for treatment cessation, and about 10-15% will achieve long-term TFR. If the definition of relapse is relaxed to loss of MMR, then this rate may increase to 20-25%

of all CML patients. It remains to be determined why some patients relapse within the first six months of treatment cessation, while others achieve long-term TFR. Factors currently being investigated include Sokal score, duration of IM therapy, the kinetics of response to therapy, time to various levels of remission, duration of remission prior to cessation, prior interferon-alpha (IFNα) therapy, and various immune cell markers. A summary of these factors and remaining questions related to treatment cessation can be found in [58] and [87]. This analysis must also be extended to include patients treated with second-generation TKIs nilotinib and dasatinib. A more complete understanding of the dynamics of TKI therapy and treatment cessation would allow clinicians to identify the patients most likely to achieve TFR.

1.3 The Immune System in CML

As previously mentioned, approximately 10-15% of patients treated with IM are expected to be able to achieve TFR. For the remaining patients, we would like to identify novel strategies aimed at producing deeper remissions and improving their chances of successful treatment cessation. One promising approach is to combine TKIs with an agent that affects a patient's autologous immune system.

There is compelling evidence that a patient's immune response plays a significant role in the dynamics of CML. In general, it is known that immune cells are capable of detecting and eliminating cancer cells [71]. The cancer immune surveillance theory states that our immune systems are continuously recognizing and eliminating newly transformed cells, to prevent them from developing into malignant cancers. Initially, the immune system destroys

these cells until they are eliminated or an equilibrium is reached. In the latter case, a subset of these genetically unstable cells may escape immune surveillance to produce a tumor. Immunotherapy is a major goal of both immunology and cancer research because of the ability of the immune system to target and eliminate abnormal cells while leaving healthy cells intact.

Prior to TKIs, many CML patients were treated with either allogeneic bone marrow transplants [46] or IFNα [96], both of whose success seem to partially depend on inducing an immune response. Following an allogeneic transplant, donor lymphocytes mount a response that reduces and may even eliminate the CML clone. Allogeneic bone marrow transplants may be the only curative therapy for CML but is rarely used because of its toxicity [46].

IFNα works through a variety of mechanisms, including induction of apoptosis, inhibition of growth, suppression of angiogenesis, and activation of immune cells [96]. A patient's immune system may play an especially important role in this therapy. IFNα improves the detection of leukemic cells by increasing expression of tumor-associated antigens and MHC class I molecules [7]. Additionally, CD8+ T cells [33,69,101], natural killer (NK) cells [54,95], and dendritic cells [25,82] are activated by IFNα. T cells specific for an antigen called PR1 are specifically associated with successful IFNα therapy [12,68,69] and are able to identify and eliminate CML progenitor cells [67]. IFNα is able to induce cytogenetic remission in some patients. A few of these patients have even achieved TFR [57,96], despite the persistence of detectable levels of CML [15,35]. Interestingly, PR1-specific T cells are associated with continued remission following IFNα cessation [40], which suggests that a patient's immune system may help to control the residual CML in the absence of therapy.

Several combination therapies involving TKIs and IFNα are currently being investi-

gated [32,72,78], in part, because of their complementary mechanisms of action. While TKIs do not affect quiescent leukemic stem cells [29,80], IFNα has both direct and indirect effects on the immature leukemic population. IFNα may drive quiescent leukemic stem cells into the cell cycle [28,91], where they become exposed to the effects of TKIs. The immunostimulatory effects of IFNα may also help in the elimination of CML cells not directly affected by TKIs. Thus, while TKIs remain the primary first-line therapy for CML and are responsible for eliminating the majority of the CML burden, IFNα may assist in controlling residual CML cells.

Initial results suggest that TKIs combined with IFNα produce improved rates of molecular response during the first few years of treatment [72, 78]. However, in many cases, the toxicity of IFNα limits its effectiveness, and long-term benefits remain to be evaluated. The addition of IFNα may improve a patient's chances of achieving TFR [60], although the observed advantage is not statistically significant, possibly due to small sample size. A 12-patient study found that while the two IM-only patients relapsed after stopping treatment, six out of ten patients who had received a combination of IM and IFNα remained in remission [89]. Despite these promising results, the toxicity of IFNα remains a significant barrier, and further research is required to determine an optimal schedule for combining these potentially complementary therapies.

The role of the immune system in the dynamics of CML is further supported by the results of the IM cessation trials. Similar to the results of IFNα cessation studies, many patients who achieve TFR continue to express *BCR-ABL* DNA and mRNA [59,86]. Moreover, in [14], patients still harbored *BCR-ABL*+ leukemic stem cells, despite having remained in TFR for up to eight years. In these cases, since treatment did not completely eradicate the

disease, some other mechanisms, such as the autologous immune system, must be preventing this residual cancer population from expanding. The hypothesis that the immune system controls the residual leukemic burden during TFR is further supported by the association of TFR with prior IFNα therapy and the activity and presence of various immune populations. Specifically, several independent groups [39, 66, 74, 81] have observed that higher NK cell count and functionality are associated with TFR. Additionally, Usuki *et al.* [102] found higher memory CD8+ T cell concentrations and lower naïve CD8+ T cell concentrations in patients who remained in TFR. A recent and promising 2015 study [11] shows that higher concentrations of CD86+ dendritic cells are associated with relapse. Moreover, the authors proposed a specific mechanism driving this phenomenon, namely, that CD86+ dendritic cells interact with the CTLA-4 inhibitory receptor of T cells, which impedes T cells that would otherwise participate in the body's anti-leukemia immune response. Together, these findings suggest that a patient's autologous immune system may play a critical role in the future of CML treatment, by providing biomarkers that guide clinical decisions, and by serving as an additional therapeutic option to complement TKIs.

1.4 Outline of Thesis

The remainder of this dissertation is organized as follows. In Chapter 2, we present an overview of the recent contributions of mathematical modeling groups to the study of leukemia and lymphoma. Although our list is not exhaustive, it does provide a representation of the types of contributions mathematicians can make to understanding these diseases. At the end of the chapter, we focus on the models of Michor *et al.* [65], Kim *et al.* [43], and

Roeder *et al.* [85] and their applications to CML. These three models serve as a starting point for our own mathematical modeling efforts.

In Chapter 3, we revisit the model of Roeder *et al.* [85], which we modify in order to produce a model that more accurately reflects the biology of CML. We incorporate asymmetric division, a variable lifetime for precursor cells, and feedback from mature cells into the model. We present an implementation of this model as a system of difference equations, followed by numerical simulations and a discussion of our results.

We present our own mathematical model of CML and the autologous immune system in Chapter 4. We use this model to study the role of the immune system during IM therapy, by applying it to patient data. A detailed analysis of this model is presented in Chapter 5, followed by additional applications and extensions in Chapter 6. Finally, we conclude with discussion of our work and future directions in Chapter 7.

Chapter 2: Mathematical Models of Leukemia and Lymphoma

2.1 Motivation

Recently, there has been significant effort in the mathematical community aimed at developing quantitative tools for studying leukemia and lymphoma. Mathematical models complement clinical and experimental data and can be used to identify underlying mechanisms driving an observed phenomenon, or to determine a quantity that is not experimentally accessible. In a clinical setting, mathematical modeling can be applied to evaluate and improve the scheduling of an existing therapy or to propose novel drug combinations.

Mathematicians, clinicians, and experimentalists have complementary skill sets and perspectives that, when combined, can lead to significant improvements in patient care and wellbeing. Leukemia and lymphoma research can benefit greatly from a collaborative and interdisciplinary approach that allows each group to utilize the others' expertise. Mathematicians depend on clinicians' and experimentalists' understanding of a disease's biology in order to produce a realistic mathematical representation, and on their data in order to validate their resulting models. Likewise, mathematical modeling provides an inexpensive and efficient setting for preliminary testing of hypotheses before they reach the clinical and experimental phase. Additionally, these models can guide experimental design and identify critical parameters that should be measured. Ultimately, a research environment in which

ideas and data are shared across disciplines will lead to more rapid discoveries that will improve our ability to treat leukemia and lymphoma.

2.2 Summary of Mathematical Models

We begin with an overview of the recent contributions of mathematicians to the study of leukemia and lymphoma. While the focus of this dissertation is CML specifically, these works as a whole provide valuable insight into the clinical questions that mathematicians can help to answer and some of the tools available to study these diseases. Although this summary is not exhaustive, it does describe the contributions of many modeling groups to the study of hematopoiesis, cancer genesis, therapy, and drug resistance. The rest of Section 2.2 was published in [20].

2.2.1 Hematopoiesis

Hematopoiesis is the process by which our body creates new blood cells. Mathematical models of hematopoiesis provide a framework for mathematicians to study cancer genesis and treatment strategies. Hematopoiesis can be modeled as a system of discrete maturity stages starting with hematopoietic stem cells (HSCs) and ending with mature blood cells. Within each stage, a balance between self-renewal and differentiation must be achieved. When a cell divides, each daughter cell remains in its current compartment with a certain probability, referred to as the renewal fraction, or differentiates and enters the next stage. This complex and well-regulated process produces more than 10^{11} cells per day in order to maintain the equilibrium levels of cells in the erythroid, lymphocyte, and myelocyte lines.

Despite the complexity of hematopoiesis, several simple ordinary differential equation (ODE) models have provided insight into the process. Michor *et al.* [65] divide blood cells into four categories based on maturity - stem, progenitor, differentiated, and terminally differentiated - and represent each by a single ODE. Healthy cells and cancer cells are assumed to both progress through these differentiation stages, differing only in their rates of differentiation and their ability to compete for resources.

Marciniak-Czochra *et al.* [61] also model hematopoiesis with a system of ODEs but incorporate feedback inhibition via cytokines. It is known that environmental signals, such as granulocyte colony-stimulating factor (G-CSF) [79] and erythropoietin [93], play a significant role in regulating hematopoiesis [83]. In order to explore these regulatory mechanisms and, specifically, their role in the rapid recovery of the mature blood cell population following chemotherapy [45], the authors in [61] implement feedback inhibition from mature cells that affects proliferation rates and/or renewal fractions of the less mature compartments. This feedback is assumed to take the form of a single cytokine, such as G-CSF. When the population of mature blood cells is large, the cytokine is consumed by these cells. When the population of mature blood cells declines, the cytokine becomes more abundant, and its presence triggers an increase in proliferation, an increase in renewal fraction, or both. Numerical simulations suggest that regulation of renewal fractions alone leads to a more rapid regeneration of the mature blood cells than does regulation of proliferation rates alone, although combining the two leads to slightly faster recovery [61]. This model has also been applied to studying the dynamics of leukemogenesis [94].

By incorporating time delays or accounting for spatial or age heterogeneity, more complex models have been constructed in order to better capture the biology of the system. Time

delays have been added to account for events such as cell divisions (for instance [1], [2]) and the interactions between cancer and immune cells (for instance [43]). In [2], Adimy and Crauste present three delay differential equation (DDE) models of cycling and quiescent HSCs, with constant, distributed, and state-dependent delays. These delays represent the time to complete one cell division. The system with distributed delays is derived from an age-structured partial differential equation (PDE) in [1]. All three models have been applied to studying periodic hematological diseases, which are characterized by oscillations in various blood cell populations. It is concluded that although all three models produce periodic solutions, the nature of the oscillations depends on the type of delay [2].

To explore oscillations that occur in multiple cell lines simultaneously, Colijn and Mackey [21] combine constant DDEs representing HSCs, leukocytes, erythrocytes, and platelets. This model includes more biological detail than those mentioned earlier, in that it replaces the generic mature cell compartment with three different cell lines. The model is later applied to cyclical neutropenia and G-CSF therapy [55].

In general, deterministic ODE and DDE models, like the ones presented so far, can serve as good approximations of the average behavior of a system when the populations are large. However, when considering small cell populations, stochasticity plays a key role in the emerging dynamics. In [52], larger populations of mature cells are represented by ODEs, while a stochastic model is used for the smaller populations of less mature cells. Using a bivariate Markov process and its deterministic approximation, Chrobak *et al.* [16] model the competition between healthy and precursor T-cell lymphoma cells, for a survival stimulus. Cancer T cells are assumed to be more competitive and able to accept a wider variety of stimuli. Simulations show that healthy T cells with more specific receptors survive

longer than healthy T cells with less specific receptors, while cancer T cells, despite their lack of specificity, are able to out-compete normal cells. To study drug resistance, branching processes [53, 100] and birth-death processes [47, 49] with mutations have been applied to calculate mutation probabilities and sizes of mutant clones at the time of cancer diagnosis. Stochastic models are especially useful when considering cancer genesis and resistance mutations, as both processes start from a single cell.

In contrast to the previous population-based models, the agent-based model (ABM) of Roeder *et al.* [85] treats each individual cell as an autonomous agent. The model considers quiescent and cycling stem cells, progenitors, and mature cells. Each stem cell is characterized by an affinity variable, which represents its tendency to either cycle or remain quiescent. Though ABMs retain valuable information about individual cells and their interactions, they are very computationally demanding, and simulations involving a realistic number of cells may not be feasible. To address this limitation, Kim *et al.* [44] reduce the Roeder model [85] to systems of difference equations, while Kim *et al.* [42] and Roeder *et al.* [84] reduce the model to a system of PDEs . Although some detail is lost in these reductions, both systems can be used to quickly capture quantities of interest, such as the steady state distribution of stem cells, with a realistic number of cells, as computation time does not depend on the total number of cells.

Once these models have been parameterized and validated using experimental and clinical data, they serve as useful tools for studying cancer treatment and drug resistance. The models mentioned above have been applied to several diseases within the leukemia and lymphoma families, including chronic myeloid leukemia (CML) [26, 30, 36, 43, 52, 65, 85, 97], acute myeloid leukemia (AML) [1], T-cell lymphoma [16], and periodic hematological diseases

[2, 21, 55].

2.2.2 The Dynamics of Treatment

One of the main goals of mathematical modeling of cancer is to improve treatment, either by optimizing the way existing therapies are being administered, or by motivating novel therapies. The optimal timing and dosage schedule remains an open question for many drugs used to treat leukemia and lymphoma. Mathematical models have been utilized to investigate treatment strategies, by considering, for instance, impulse versus continuous doses [30] as well as the number of drugs to be used and their order [49, 53, 85]. Using sensitivity analysis and numerical simulation, the dependence of a treatment outcome on specific model parameters can be determined. Mathematical models can be applied to interpret experimental or clinical data, or to evaluate a treatment strategy before it is tested in an experimental or clinical setting.

Models of a single cell are useful for studying intracellular drug accumulation and concentrations of substances involved in cell fate decisions. In [77], intracellular and extracellular concentrations of methotrexate (MTX), a treatment for acute lymphoblastic leukemia (ALL), are modeled. In vivo measurements indicate that levels of intracellular MTX are greater in leukemia B cells than in T cells. Simulations show that increasing the dose can only partially compensate for the lower levels of intracellular MTX in T cells. It is hypothesized that extending the infusion time would lead to greater MTX accumulations in leukemia T cells and may enhance the effectiveness of the therapy [77]. A follow-up study [76] that compares infusion times of four and twenty-four hours, in a clinical trial and with an extended MTX

model that includes the drug's effects on the folate pathway, supports this hypothesis.

Alarcon *et al.* [3] take a similar modeling approach to attempt to understand the factors that determine the fate of lymphoma B cells during antibody treatment. Treatment of lymphoma B cells with a specific antibody causes either apoptosis or quiescence. In order to determine how to induce apoptosis in these B cells, an ODE model of intracellular substances involved in cell fate decisions is developed. The modeling results suggest that Myc plays a crucial role in cell fate decision of lymphoma B cells during antibody therapy.

A significant amount of attention has been given to modeling the treatment of CML. Although we briefly cover some of these studies here, a more detailed description of these models and their applications can be found in Section 2.3. These models have been applied to investigate the underlying mechanisms of action of TKIs, which can then be used to identify any limitations of these drugs. Several groups [52, 85, 99] have argued that IM affects all leukemic cells and therefore may be able to cure patients after many years of treatment. Others [26, 65] claim that certain subsets of leukemic cells are protected from the effects of IM, and therefore a residual population of leukemia will remain indefinitely. These models have also been applied to treatment cessation [36, 97] and combination therapy [30, 43].

2.2.3 Drug Resistance

Drug resistance remains a major challenge in leukemia and lymphoma therapy. Mathematical models can be used to assess a patient's risk of relapse upon diagnosis and to identify strategies that minimize the probability of treatment failure.

Panetta *et al.* [75] conduct an experiment in which ALL T cells, of varying drug re-

sistance, are treated with mercaptopurine (MP), and cell cycle distributions and apoptosis rates are measured. Using this data, they construct a mathematical model of the cell cycle and apoptosis during MP treatment. The model divides cells into normally cycling cells; cells that are cycling with thioguanine nucleotides (TGNs), a byproduct of MP, incorporated in their DNA and RNA; apoptotic cells; and necrotic cells. Interestingly, the model parameterizations suggests that the rate of TGN incorporation is greater in resistant cells than in sensitive cells. However, this difference is overcome by the higher rates of entry into apoptosis found for the sensitive cell line compared to the resistant lines. This result suggests that although the drug is able to incorporate itself into the cancer cells' DNA, resistance is explained by an inability of resistant cells to detect damaged TGN-incorporated DNA [75].

Using branching processes [53, 100] and birth-death processes with mutations [47, 49], several groups have sought to quantify the probability of resistance and the size and diversity of resistant clones, at the time of diagnosis. In both types of models, cancer initiates from a single cell, with a birth rate, death rate, and a small probability of mutation per division. Mutations can lead to several different resistance clones, each with its own growth kinetics. The time of diagnosis is estimated by the time at which the cancer population reaches a certain size. Using both simulation and analysis techniques, the aforementioned quantities can be determined.

Tomasetti and Levy [100] construct a model of cancer stem cells in which the cells may divide in one of three ways. A stem cell may divide into two stem cells (symmetric renewal), differentiate into two progenitor cells (symmetric differentiation), or divide asymmetrically into one stem cell and one progenitor cell. By incorporating data on the relapse rate of patients that are treated with IM [34], it is concluded that cancer stem cells tend

to symmetrically renew, as opposed to their healthy counterparts that predominantly divide asymmetrically [100]. In a later paper [99], Tomasetti argues that, based on modeling results [100] and clinical data [60], IM affects leukemic stem cells the same way it affects all leukemic cells, by decreasing their proliferation rates.

Leder *et al.* [53] and Komarova *et al.* [47, 49] use their models to determine when combination therapy can be administered to minimize the chance of resistance mutations. In [53], the authors calculate that if a patient is diagnosed at an early stage of cancer, then there is only a 12% chance of having a resistance mutation. However, when diagnosed at a late stage, the risk increases, and multiple mutations become possible [53]. Their modeling results demonstrate the importance of early detection and also suggest that combination therapy is advantageous when the cancer is detected at a late stage. Komarova and Wodarz [47] create a mathematical framework to study resistance to targeted therapies. It is found that the combination of three drugs should prevent resistance in the treatment of CML. Komarova *et al.* [49] later consider specific resistance mutations to TKI treatment of CML. They evaluate the effectiveness of combinations of IM, dasatinib, and nilotinib. Most of the known resistance point mutations confer resistance to only one of the three, but the T315I mutation causes resistance to all three [4]. It is concluded that two-drug combination therapies can increase the probability of treatment success, but adding a third drug does not lead to further improvements [49].

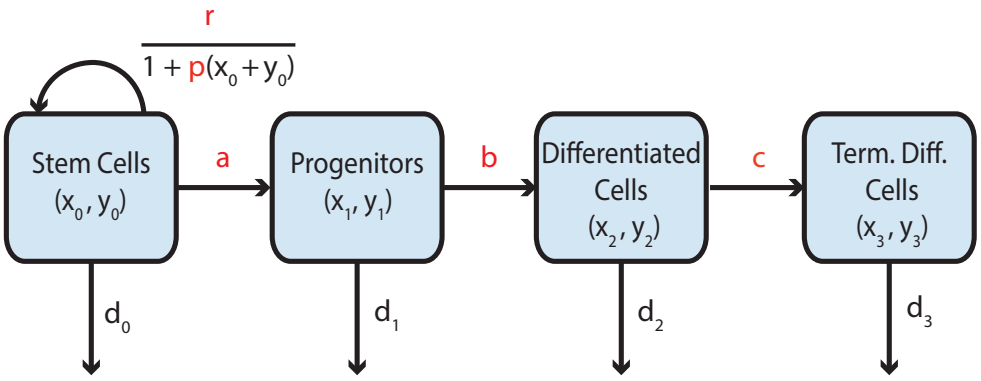

Figure 2.1: The Michor model divides healthy cells (x) and leukemic cells (y) into stem cells (x_0, y_0), progenitors (x_1, y_1), differentiated cells (x_2, y_2), and terminally differentiated cells (x_3, y_3). Healthy cells x_i and leukemic cells y_i are assumed to have the same death rates d_i for each compartment i, but to differ in their stem cell growth rates r and their differentiation rates a, b, and c. The parameters in red (r_y, a_y, and b_y) are those affected by IM therapy.

2.3 Models of CML

We now shift our focus to mathematical models of CML, specifically the Michor model [65], the DDE model of Kim *et al.* [43], and the Roeder model [85]. For each, we will present the details of each model and then discuss their applications. Ultimately, these three models serve as a basis from which we constructed our own CML model (see Chapter 4).

2.3.1 The Michor Model

The Michor model [65] is an ODE model that divides both healthy cells (x) and leukemic cells (y) into stem cells (x_0, y_0), progenitors (x_1, y_1), differentiated cells (x_2, y_2), and terminally differentiated cells (x_3, y_3). These populations are described by the following

system of equations.

$$\dot{x}_0 = (r_x\phi - d_0)x_0, \tag{2.1a}$$

$$\dot{x}_1 = a_x x_0 - d_1 x_1, \tag{2.1b}$$

$$\dot{x}_2 = b_x x_1 - d_2 x_2, \tag{2.1c}$$

$$\dot{x}_3 = c_x x_2 - d_3 x_3, \tag{2.1d}$$

$$\dot{y}_0 = (r_y\psi - d_0)y_0, \tag{2.2a}$$

$$\dot{y}_1 = a_y y_0 - d_1 y_1, \tag{2.2b}$$

$$\dot{y}_2 = b_y y_1 - d_2 y_2, \tag{2.2c}$$

$$\dot{y}_3 = c_y y_2 - d_3 y_3. \tag{2.2d}$$

In the equations above, r is the maximum division rate of stem cells, and p is the sensitivity of each population to crowding. The parameters a, b, and c are differentiation and expansion rates of the stem cells, precursors, and differentiated cells. Lastly the $\{d_i\}$ are the death rates of each compartment. The terms $\phi = 1/(1 + p_x(x_0 + y_0)$, and $\psi = 1/(1 + p_y(x_0 + y_0))$ incorporate competition between healthy and leukemic stem cells. The parameters p_x and p_y represent each population's sensitivity to crowding. Although these terms are not in the original model [65], they are introduced in [26] and are included in future works [97, 98]. A diagram representing this model can be found in Figure 2.1

Leukemic cells are assumed to have a greater stem cell proliferation rate ($r_y > r_x$), a greater stem cell differentiation rate ($a_y > a_x$), and to be less sensitive to crowding ($p_y < p_x$) than healthy cells. Healthy and leukemic cells are assigned the same death rates. IM therapy

decreases the proliferative capacity of leukemic cells, by decreasing the parameters r_y, a_y, and b_y to values r'_y, a'_y, and b'_y.

By analyzing patients' initial response to IM therapy, Michor *et al.* [65] find that many patients show a biphasic exponential decline in BCR-ABL ratio. In their model, the first, sharper decline is explained by the decreased proliferative capacity of differentiated cells ($a'_y < a_y$), which causes both the differentiated and terminally differentiated populations to shrink. After 3-6 months, these populations reach an equilibrium relative to the progenitor compartment. During months 6-12, there is a second, slower exponential decline that is explained by a similar effect on progenitors ($b'_y < b_y$), until they reach an equilibrium with the stem cell population. The parameters a'_y and b'_y are calculate based averages of their patient data, and are assumed to be the same for all patients. The slopes of these two declines are interpreted as the death rates of the progenitors (d_1) and differentiated cells (d_2), which are allowed to vary between patients.

In their initial fits, the authors assume that IM has no effect on leukemic stem cells (that is, $r'_y = r_y$). The leukemic stem cell population continues to grow during therapy. Eventually, all simulated patients relapse, a result that does not accurately represent the long-term effects of IM seen in most patients. However, their initial data only includes the first year of IM therapy, so their fits are largely unaffected by this assumption. In a later analysis of patients' long-term responses over many years of IM therapy [98], these assumptions are adjusted to allow IM therapy to also affects leukemic stem cells, by decreasing their growth rate ($r_y < r'_y$). Some patients show a triphasic exponential decline in leukemic load. The authors hypothesize that the third decline may represent an effect on a less mature leukemic population, such as the leukemic stem cells. In [26], it is suggested that a successful therapy

must target leukemic stem cells in order to eliminate the leukemic clone, a result which motivates the question of whether IM alone may be curative.

In [97], Tang *et al.* attempt to understand the contrasting results of the STIM trials [60]. They first sought to determine whether TFR indicates cure in some patients, or whether these patients continue to harbor small residual leukemic clones. However, both cure and non-cure statistical models were in agreement with the STIM data, suggesting that a longer follow-up time was necessary to make any conclusions. By parameterizing the Michor model based on STIM survival curves, it is found that the leukemic population has significantly slower growth kinetics after treatment than before treatment. This result suggests that selection pressures during IM therapy lead to different subsets of the heterogeneous leukemic population surviving, which in part explains the disparate outcomes of the trial. The author notes that this selection effect may act in combination with suppression of the leukemia by the immune system, crowding, or the microenvironment.

2.3.2 DDE Model of CML and the Immune System

In [43], Kim *et al.* present the following DDE model of CML and the immune system in order to study the anti-leukemia immune response during IM therapy.

$$\dot{y}_0 = (r_y - d_0)y_0 - q_C p(C,T)y_0, \tag{2.3a}$$

$$\dot{y}_1 = a_y y_0 - d_1 y_1 - q_C p(C,T)y_1, \tag{2.3b}$$

$$\dot{y}_2 = b_y y_1 - d_2 y_2 - q_C p(C,T)y_2, \tag{2.3c}$$

$$\dot{y}_3 = c_y y_2 - d_3 y_3 - q_C p(C,T)y_3, \tag{2.3d}$$

$$\dot{T} = s_T - d_T T - p(C,T)C + q_T 2^n p(C_{n\tau}, T_{n\tau})C_{n\tau}, \tag{2.3e}$$

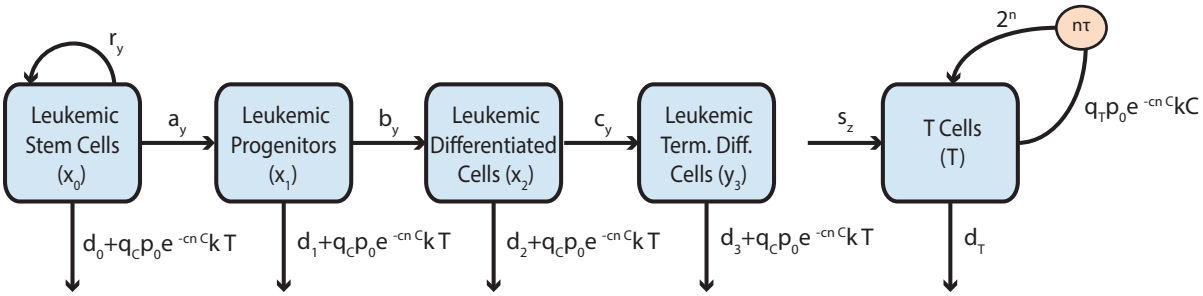

Figure 2.2: The DDE model of Kim et al. [43] considers leukemic stem cells y_0, progenitors y_1, differentiated cells y_2, and terminally differentiated cells y_3, which are all modeled as in the original ODE model of Michor *et al.* [65] An additional T cell compartment T is described by a DDE, where the delay $n\tau$ accounts for the time to complete n cell divisions, each of which requires time τ, following stimulation by a leukemic cell.

where

$$\begin{aligned} C_{n\tau} &= C(t - n\tau), \\ T_{n\tau} &= T(t - n\tau), \\ p(C, T) &= p_0 e^{-c_n C} kT, \\ C &= \textstyle\sum_{i=0}^{3} y_i. \end{aligned}$$

In this model, which is depicted in Figure 2.2, the variables $\{y_i\}$ represent leukemic stem cells, progenitors, differentiated cells, and terminally differentiated cells, and an additional variable T is introduced that represents anti-leukemia T cells. As in the Michor model (see Equations (2.1a)-(2.2d)), r_y is the growth rate of leukemic stem cells, which are assumed to grow exponentially in the absence of an immune response. The parameters a_y, b_y, and c_y are differentiation rates, while $\{d_i\}$ are natural death rates. The last terms $p_0 q_C e^{-c_n C} kT y_i$ in the leukemic cell equations represent an anti-leukemia immune response. The rate of interaction between T cells T and each leukemic subpopulation y_i is described by a mass-action term kTy_i with coefficient k. The constant p_0 is the probability that a T cell engages, while q_C is the probability that the leukemic cell dies because of that engagement. This probability $p_0 q_C$ is decreased by a factor $e^{-c_n C}$ in order to incorporate immune suppression by the total leukemic population $C = \sum_{i=0}^{3} y_i$.

Lastly, T cells are assumed to have a constant source term s_T and a constant death rate d_T. The third term on the right side represents T cells that engage leukemic cells and commit to n rounds of cell division. The last term represents the population increase due to immune cells that committed to division at a time $n\tau$ in the past, where τ is the time to complete one cell division. The variables $C_{n\tau}$ and $T_{n\tau}$ are the leukemic and T cell concentrations at time

$t - n\tau$. A T cell survives the encounter with the leukemic cell with probability q_T, and if it survives, it produces 2^n new T cells. We note that the precise interactions between leukemic and immune cells are not known, and so there are several alternate ways of representing these interactions, as shown in [50] and [70].

Without an immune response, and assuming no effect of IM on leukemic stem cells, the leukemic stem cells continue to grow exponentially. The model therefore predicts that all patients will relapse after about 3 years of therapy. On the other hand, simulations of this model with an immune response produce long-term remissions that are in agreement with patient data. These contrasting outcomes suggest that a patient's immune system may play a critical role during IM therapy.

The authors therefore sought to characterize patients' individual immune responses to CML. They fit their model to individual patient data by choosing patient-specific values of s_T, d_T, c_n, n, and $y_0(0)$. They define an optimal load zone for leukemic cells that maximizes the anti-leukemia immune response. This zone coincides with the range of leukemic loads C where the rate of immunostimulation $p_0 k e^{-c_n C}$ exceeds the T cell death rate d_T and is therefore patient-specific, as it depends on the parameters c_n and d_T. Based on their modeling results and data measuring patients' immune responses during IM therapy, they hypothesize that IM may drive the leukemia below the optimal load zone. As a result, after an initially strong immune response, the T cells contract, allowing the leukemic population to survive and partially recover. This result suggest that carefully-timed patient-specific vaccines may help to maintain a patient's strong immune response in order to further reduce or even eradicate the leukemic population.

2.3.3 The Roeder Model

In this section, which is taken from our publication [19], we provide a brief overview of the Roeder model [85]. The Roeder model is an ABM that considers hematopoietic cells in three compartments: stem cells (STC), proliferating precursor cells (P), and mature cells (M). Stem cells are either quiescent, denoted by A, or cycling, denoted by Ω. Let $A(t)$ and $\Omega(t)$ represent the total number of quiescent and cycling stem cells at time t. Each individual stem cell is characterized by an affinity variable $a(t) \in [a_{min}, a_{max}]$ which determines the probability that the cell will be quiescent or cycling. At each time step, which represents one hour, a quiescent stem cell will enter the cell cycle with probability ω, and a cycling stem cell will become quiescent with probability α, where

$$\omega(\Omega(t), a(t)) = \frac{a_{min}}{a(t)} f_\omega(\Omega(t)), \tag{2.4}$$

$$\alpha(A(t), a(t)) = \frac{a(t)}{a_{max}} f_\alpha(A(t)). \tag{2.5}$$

Thus, cells with affinity $a(t)$ close to a_{max} tend to remain or become quiescent, while cells with $a(t)$ close to a_{min} tend to remain or become cycling. The functions f_ω and f_α are defined by

$$f_\omega(\Omega(t)) = \frac{1}{\nu_1 + \nu_2 \exp\left(\nu_3 \frac{\Omega(t)}{N_\omega}\right)} + \nu_4, \tag{2.6}$$

$$f_\alpha(A(t)) = \frac{1}{\mu_1 + \mu_2 \exp\left(\mu_3 \frac{A(t)}{N_\alpha}\right)} + \mu_4. \tag{2.7}$$

Both functions, f_ω and f_α, are decreasing sigmoidal functions whose shapes depend on the parameters ν_i and μ_i. The parameters N_ω and N_α are scaling factors for $\Omega(t)$ and $A(t)$. Given the values of f_ω at $\Omega(t) = 0$, $N_\omega/2$, N_ω, and ∞, we can compute the coefficients ν_i as

follows:

$$\begin{aligned}
\nu_1 &= (h_1 h_3 - h_2^2)/(h_1 + h_3 - 2h_2), \\
\nu_2 &= h_1 - \nu_1, \\
\nu_3 &= \log((h_3 - \nu_1)/\nu_2), \\
\nu_4 &= f_\omega(\infty),
\end{aligned}$$

where

$$\begin{aligned}
h_1 &= 1/(f_\omega(0) - f_\omega(\infty)), \\
h_2 &= 1/(f_\omega(N_\omega/2) - f_\omega(\infty)), \\
h_3 &= 1/(f_\omega(N_\omega) - f_\omega(\infty)).
\end{aligned}$$

A similar set of formulas can be used to determine the parameters μ_i of f_α. These functions are constructed so that cells that are in the less-populated compartment are less likely to move.

Quiescent cells that remain quiescent during a time step increase their affinity by a factor of r, until they reach the maximum affinity a_{max}. Cycling cells that continue to cycle during a time step decrease their affinity by a factor of d, until they reach the minimum affinity a_{min}. In other words, cells that remain in A or Ω become more likely to stay in A or Ω in the future.

Cycling cells are also characterized by a cell cycle counter $c(t)$, which represents their place in the cell cycle. In [85], the cell cycle lasts 49 hours, so $c(t) \in \{0, 1, ..., 48\}$. The first 32 hours represent the G1 phase, where cells grow and can transition to quiescence. Cells that reach $c(t) = 32$ commit to division and must go through the S, G2, and M stages of the

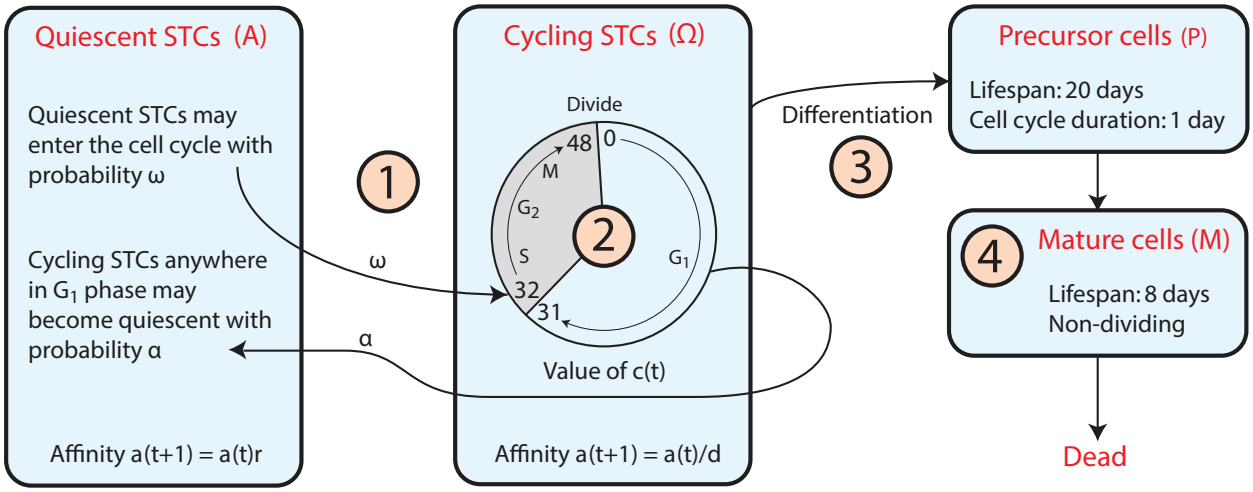

Figure 2.3: A diagram for the Roeder model. (1) At each time step, quiescent stem cells enter the cell cycle with probability ω, while cycling cells in G1 become quiescent with probability α. Quiescent stem cells that remain quiescent during a time step increase their affinity by a factor of r, up to a maximum value of a_{max}. Cycling stem cells that continue to cycle decrease their affinity by a factor of d. (2) Cycling stem cells progress through G_1, S, G_2, and M. The cell cycle counter $c(t) \in \{0, 1, ..., 48\}$ indicates the cell's phase in the cell cycle. Stem cells enter the cell cycle at hour $c(t) = 32$. At hour $c(t) = 48$, the cell divides, and its daughter cells reset their cell cycle counters to $c(t) = 0$. (3) A cycling stem cell whose affinity reaches a_{min} differentiates into a precursor cell, which lives for 20 days and divides once per day. (4) In the last division, precursor cells differentiate into mature cells, which do not divide and die after 8 days.

cell cycle. After the cell divides ($c(t) = 48$), each daughter cell reenters G1 ($c(t) = 0$) and becomes an uncommitted cycling cell that may transition to quiescence. Quiescent cells that enter the cell cycle have their cell cycle counter initialized to $c(t) = 32$, which means that they commit to at least one division. Stem cells that reach affinity $a(t) = a_{min}$ differentiate into precursor cells. Precursors (P) live for a fixed amount of time and undergo a fixed number of divisions. They then differentiate into mature cells (M), which do not divide and die after a fixed amount of time. Figure 2.3 summarizes the Roeder model.

Both healthy (Ph-) and cancer cells (Ph+) cells differentiate through the maturity

stages discussed above. Ph- cells and Ph+ cells compete at the stem cell level through the functions f_ω and f_α, whose inputs are the total number of cycling cells and quiescent cells, respectively. Ph+ cells differ from Ph- cells in their transition functions f_ω and f_α. It is assumed that Ph+ stem cells are more likely to transition between quiescence and cycling and that the probability of a quiescent Ph+ stem cell transitioning to cycling is only slightly affected by the current number of cycling stem cells. Cancer genesis is characterized by a long latency period of 5 to 7 years, in which Ph+ and Ph- populations coexist. Without treatment, Ph+ cells are eventually able to out-compete Ph- cells and take over the system.

Treatment with IM is assumed to have two effects on Ph+ stem cells while not directly affecting Ph- cells. First, all cycling Ph+ stem cells are killed at a rate r_{deg}. In addition, all cycling Ph+ stem cells become IM-affected with probability r_{inh}. Once a Ph+ stem cell becomes IM-affected, its transition function f_ω is decreased significantly, making it much less likely for quiescent Ph+ stem cells to enter the cell cycle. Note that there is no direct action of IM on quiescent Ph+ stem cells.

The effect of the treatment is evaluated by monitoring levels of BCR-ABL fusion transcript in the blood. These levels are reported relative to an endogenous control transcript, BCR or ABL, in order to normalize the BCR-ABL measurements. This relative value, known as the BCR-ABL ratio, is estimated in [85] by

$$\text{BCR-ABL ratio} = \frac{100 \times (\#\text{ of mature Ph+ cells})}{2 \times (\#\text{ of mature Ph- cells}) + (\#\text{ of mature Ph+ cells})}. \tag{2.8}$$

The contributions of stem cells and precursors to this ratio are negligible because these populations are small relative to the mature cells, and the mature cells are the dominant population in the blood. In each healthy Ph- cell, there are two copies of the control gene,

while Ph+ cells are assumed to possess one copy of the BCR-ABL fusion gene and one copy of the control gene. Thus, BCR-ABL transcript levels should be proportional to the number of mature Ph+ cells, while the control transcript levels should be proportional to twice the number of mature Ph- cells plus the number of mature Ph+ cells. This quantity is multiplied by 100 so that it represents a percentage.

In simulations, treatment leads to a biphasic exponential decline in BCR-ABL levels, with a rapid first decline followed by a slower second decline. However, small populations of Ph+ cells persist over many years of treatment, and cessation of treatment generally leads to a rapid relapse.

The Roeder model is later applied to study the combination of TKIs and IFNα [30]. In their modeling framework, IFNα is assumed to stimulate quiescent cancer cells to enter the cell cycle, where they are more likely to be affected by IM. It is shown that pulsed IFNα with continuous IM is nearly as effective as administering both drugs continuously, but with significantly less toxicity. Moreover, since the initial response to IM alone is very strong, the authors suggest that pulsed IFNα should be started after 9-12 months of IM-only therapy. Simulations of this combination therapy suggest that the addition of IFNα may reduce the time to CML eradication from 25 years with IM alone down to as few as three years.

Using patient-specific data, the Roeder model is used in [36] to determine which patients can be safely taken off IM without relapsing. The slopes of each patient's biphasic decline are used to estimate the parameters r_{deg} and f_ω (which is constant for leukemic cells during treatment). Treatment cessation is then simulated in order to determine whether a patient would relapse or remain in remission. Their model predicts that 14% of patients will be cured after 15 years of therapy while an additional 16% will remain in TFR for at

least two years despite harboring residual leukemic populations. The authors provide model-based and model-independent criteria for selecting the best treatment cessation candidates. Together with other clinical markers, their criteria may be used to improve the number of patients who achieve TFR.

Chapter 3: Incorporating Asymmetric Stem Cell Division into the Roeder Model

3.1 Overview

In this chapter, we propose several modifications to the Roeder model [85] (described in Section 2.3.3), in order to construct a model that more closely represents hematopoiesis. Specifically, we incorporate asymmetric division of stem cells and precursors, allow precursors to live a variable amount of time before maturing, and introduce feedback inhibition from mature cells to stem cells and precursors. These modifications result in more accurate simulations of cancer genesis and treatment. We begin by presenting a reduction of the Roeder model to a system of difference equations. Then, we discuss the additional biological details that we incorporate into the model, which we then incorporate into the system of difference equations. Lastly, we present results of numerical simulations and discuss the implications of our findings. The content of the remainder of this chapter was previously published in [19].

3.2 Reducing the Agent-Based Model to a System of Difference Equations

Although the Roeder model has the advantage of being able to capture the dynamics of cell-cell interactions, simulations with a realistic number of agents is computationally very expensive. In the simulations in [85], the number of cells is down-scaled to 1/10 of normal patient values, resulting in approximately 10^5 stem cells. Even with this reduction in the number of agents, a simulation of 20 years requires approximately 175,000 steps for each of the 10^5 agents (Precursors and mature cells can be represented as populations, so the total number of agents is the total number of stem cells.) To address this limitation, the Roeder model is reduced to a system of PDEs in [42] and [84] and a system of difference equations in [44]. In this section we follow [44] and provide a brief summary of the system of difference equations. A modified version of this system is used for the numerical simulations that we present in Section 3.4.

In order to decrease the number of variables, Kim *et al.* [44] discretize the affinity state space. In [85], $d = 1.05$ and $r = 1.1$, so $\log(d) = \rho = 0.0488 \approx \log(r)/2$. By setting $d = e^{\rho}$ and $r = e^{2\rho}$, any cell whose initial affinity is of the form $a(t) = e^{-k\rho}$ for an integer k will continue to have this form. Since $0.002 \leq a(t) \leq 1$, k is restricted to $0 \leq k \leq 127$. Because of the negative in the exponent, the maximum affinity corresponds to the minimum k value, and the minimum affinity corresponds to the maximum k value. More importantly, though, with these new values of r and d, it is no longer necessary to track individual agents. Rather, we can group stem cells into populations whose affinity $a(t) = e^{-k\rho}$, for each of the finitely many k values.

Define $A_k(t)$ and $\Omega_{k,c}(t)$ as follows:

$$A_k(t) = \text{Number of cells in } A \text{ at time } t \text{ with } \log a(t) = -k\rho \tag{3.1}$$

$$G_{k,c}(t) = \text{Number of cells in } \Omega \text{ at time } t \text{ with } \log a(t) = -k\rho \text{ and } c(t) = c \tag{3.2}$$

As mentioned earlier, $k \in \{0, ..., 127\}$, and $c \in \{0, ..., 48\}$. Given this discretization, the Roeder model is represented by the following system of difference equations:

$$A_k(t+1) = \begin{cases} (A_0(t) - B_0(t)) + (A_1(t) - B_1(t)) + (A_2(t) - B_2(t)), & k = 0 \\ (A_{k+2}(t) - B_{k+2}(t)) + \sum_{c=0}^{31} \Psi_{k,c}(t), & k = 1 \dots 125 \\ \sum_{c=0}^{31} \Psi_{k,c}(t), & k = 126, 127 \end{cases} \tag{3.3}$$

$$\Omega_{k,c}(t+1) = \begin{cases} B_0(t), & k = 0,\ c = 32 \\ 2\Omega_{k-1,48}(t), & k > 0,\ c = 0 \\ \Omega_{k-1,c-1}(t) - \Psi_{k-1,c-1}(t), & k > 0,\ c = 1, \dots, 31 \\ (\Omega_{k-1,31}(t) - \Psi_{k-1,31}(t)) + B_k(t), & k > 0,\ c = 32 \\ \Omega_{k-1,c-1}(t), & k > 0,\ c = 33, \dots, 48 \\ 0 & \text{otherwise} \end{cases} \tag{3.4}$$

The terms B_k represents the number of cells that leave A_k and enter the cycling compartment $\Omega_{k,32}$. $\Psi_{k,c}$ is the number of cells that leave $\Omega_{k,c}$ and enter the quiescent compartment A_k. These terms are defined by

$$B_k(t) \sim \text{Bin}\left(A_k(t), \omega(\Omega(t), e^{-k\rho})\right), \tag{3.5}$$

$$\Psi_{k,c}(t) \sim \text{Bin}\left(\Omega_{k,c}(t), \alpha(A(t), e^{-k\rho})\right), \qquad c = 0, ..., 31, \tag{3.6}$$

where, $\Omega(t) = \sum_{k,c} \Omega_{k,c}(t)$ and $A(t) = \sum_k A_k(t)$ are the total number of cycling and quiescent stem cells, and the functions ω and α are defined in Equations (2.4) and (2.5). In

our simulations, we replace these stochastic variables with their expected value and allow populations to be continuous variables.

At each time step, a quiescent cell may remain quiescent or enter the cell cycle. Cells that remain quiescent increase their affinity by a factor of r, which translates to a decrease in k by two. Equation (3.3) describes the number of quiescent cells in each compartment, at time $t+1$. The first line ($k=0$) represents the number of cells entering A_0, namely those cells previously in A_0, A_1, or A_2, that remain quiescent. In the second line ($k=1,...,125$), cells previously in A_{k+2} that remain quiescent enter A_k. The summation term is the number of cycling cells in $\Omega_{k,c}$ that become quiescent. The sum is over $c \in \{0,...,31\}$ because only cells in G1 can become quiescent. Lastly, when $k=126$ or $k=127$, there are no quiescent cells with $k>127$ to feed these compartments. Therefore, the only cells entering these compartment are cycling cells that become quiescent.

On the other hand, cycling cells that continue to cycle decrease their affinity by a factor of d, which translates to an increase in k by one. At each step, the cell cycle counter also increases by one. The cycling cells are described by Equation (3.4). The first line ($k=0, c=32$) represents cells that have maximum affinity who are entering the S phase of the cell cycle. Since there are no cycling cells with greater affinity, the only cells entering this compartment are quiescent cells that have just entered the cell cycle. The second line ($k>0, c=0$) represents cells that have just completed the cell cycle. The constant 2 represents division into two daughter cells, whose cell cycle counters are reset to $c(t)=0$. The third line ($k>0, c=1,...,31$) represents cycling cells in the G1 phase. The right hand side is the number of cycling cells in the $(k-1)^{st}$ compartment that continue to cycle. The beginning of the S phase, marked by $c(t)=32$, is where transitioning quiescent cells enter

the cell cycle. The fourth line ($k > 0, c = 32$) is similar to the third, with an additional term for the quiescent cells that begin cycling. The fifth line ($k > 0, c = 33, ..., 48$) represents cells in S, G2, and M. Because these cells have committed to division, they all progress to the next step in the cell cycle and increase their k value by one, until division. All other cycling cell compartments are zero at all times.

When a cycling cell's affinity reaches its minimum, corresponding to k taking its maximum value of 127, the cell differentiates into a precursor cell. The precursor cell divides once per day for twenty days (480 hours). Upon the last division, both daughter cells differentiate into mature cells, which live for another eight days without dividing, and then die. The equations for these compartments are

$$P_j(t+1) = \begin{cases} \sum_{c=0}^{48} \Omega_{127,c}(t) - \sum_{c=0}^{31} \Psi_{127,c}(t), & j = 0 \\ 2P_{j-1}(t), & j = 24, 48, 72, ..., 456 \\ P_{j-1}(t), & \text{otherwise} \end{cases} \tag{3.7}$$

$$M_j(t+1) = \begin{cases} 2P_{479}(t), & j = 0 \\ M_{j-1}(t), & \text{otherwise} \end{cases} \tag{3.8}$$

Here, $P_j(t)$ is the number of cells that have been precursors for j hours, where $j \in \{0, ..., 479\}$. $M_j(t)$ is the number of cells that have been mature for j hours, where $j \in \{0, ..., 191\}$. In Equation (3.7), the first line on the right hand side represents cycling stem cells that reach minimum affinity ($k = 127$), continue to cycle, and become precursors. The second line accounts for the division of precursor cells, which occurs every 24 hours. For all other values of j, cells increase their age j by one per time step. In Equation (3.8), precursor cells completing their final division become mature, which is the first line. The second line represents the fact that mature cells continue to age without dividing.

As in the Roeder model, cancer genesis is simulated by initializing a single Ph+ stem cell into the Ph- cell steady state. Both populations are described by the system of difference equations (Equations (3.3), (3.4), (3.7), (3.8)). The two populations compete at the stem cell level and differ in their transition functions f_ω and f_α.

In simulating treatment, we divide the Ph+ population into two categories: those that are not affected by IM, which we denote Ph+/R, and those that are, which we denote Ph+/I. These two Ph+ populations differ in their transition function f_ω, with the Ph+/I stem cells being much less likely to transition from quiescence to cycling. At the beginning of treatment, all Ph+ cells are not IM-affected. The effects of treatment are assumed to occur at the beginning of every time step. For each k and c, let $\Omega_{k,c}^{+/R}(t)$ be the number of cycling Ph+/R cells, and let $\Omega_{k,c}^{+/I}(t)$ be the number of Ph+/I cells. Each cell in $\Omega_{k,c}^{+/R}$ will become IM-affected with probability r_{inh}. The number of cells in $\Omega_{k,c}^{+/R}$ that becomes IM-affected at that time step is given by $\Omega_{k,c}^{+/I,new}(t) \sim \text{Bin}(\Omega_{k,c}^{+/R}(t), r_{inh})$. We set

$$\Omega_{k,c}^{+/R}(t) := \Omega_{k,c}^{+/R}(t) - \Omega_{k,c}^{+/I,new}(t), \tag{3.9}$$

$$\Omega_{k,c}^{+/I}(t) := \Omega_{k,c}^{+/I}(t) + \Omega_{k,c}^{+/I,new}(t). \tag{3.10}$$

We additionally assume that all cycling Ph+ cells will apoptose with probability r_{deg}. We therefore remove these cells from the Ph+ populations at the beginning of each time step, by subtracting them from Equations (3.9) and (3.10). In our simulations, we choose to make the effects of IM deterministic by setting the number of cells that become IM-affected and apoptose to the expected values rather than taking them from their binomial distributions. Once the values of $\Omega_{k,c}(t)$ are updated, all three populations (Ph-, Ph+/R, Ph-/I) evolve following Equations (3.3), (3.4), (3.7), and (3.8).

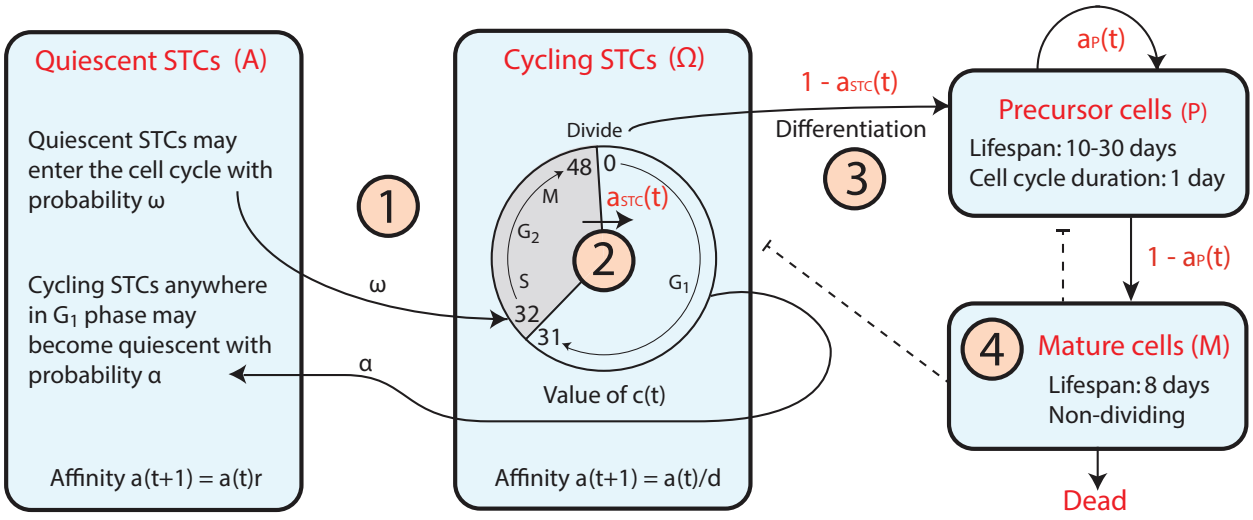

Figure 3.1: A diagram of the modified Roeder model. (1) Stem cell transitions between quiescence and the cell cycle are unchanged. The affinity variable is updated in the same way as in the original model. (2) Cycling stem cells progress through G_1, S, G_2, and M. Stem cells enter the cell cycle at hour $c(t) = 32$. (3) At hour $c(t) = 48$, the cell divides, and each daughter cell will remain a stem cell with probability $a_{STC}(t)$ and will differentiate into a precursor with probability $1 - a_{STC}(t)$. Precursor cells symmetrically renew ten times. For all subsequent divisions, up to a total of thirty divisions, the daughter cells will remain precursors with probability $a_P(t)$ and will differentiate into mature cells with probability $1 - a_P(t)$. (4) On the last division, both precursor cells differentiate into mature cells. Mature cells provide feedback, marked by dashed lines, that affects the renewal fractions $a_{STC}(t)$ and $a_P(t)$ of the stem and precursor cells. After 8 days, mature cells die.

3.3 Modifications to the Roeder Model

In this section we propose several modifications to the Roeder model [85]. Our model is summarized in Figure 3.1. First, we consider three types of stem cell division:

1. Asymmetric division, in which one daughter cell remains a stem cell and the other differentiates into a precursor cell

2. Symmetric differentiation, in which both daughter cells differentiate into precursors

3. Symmetric renewal, in which both daughter cells remain stem cells.

In the Roeder model, all dividing stem cells symmetrically renew. Differentiation into precursor cells is not tied to a division event, and stem cells whose affinity reaches a_{min} instantaneously transform into precursor cells. Thus, the affinity variable controls both cell cycle transitions and differentiation.

By incorporating these three types of cell division, each with probability a', b', and c', where $a'+b'+c' = 1$, we provide a mechanism for differentiation that is independent of affinity, while still allowing a cell's affinity to control transitions between quiescence and cycling. Several other modeling groups have represented differentiation in this way, including [61] and [100]. Moreover, in [100], it is suggested that cancer stem cells tend to symmetrically renew, while healthy stem cells tend to divide asymmetrically. By associating differentiation with a cell division, it becomes possible to implement this hypothesis in the model.

Secondly, we allow precursor cells to divide a variable number of times before they differentiate into mature cells. To implement this, we allow precursors to go through the same three types of divisions as stem cells. Precursors can divide between 10 and 30 times before differentiating into mature cells. This range is centered around 20 divisions, which is assumed for all precursor cells in [85]. The lower bound to the number of divisions enforces a minimum number of divisions before maturation, and the upper bound prevents any precursor cells from living forever.

Lastly, it is known that hematopoiesis is a very closely regulated process that is affected by many different signals and cytokines [64]. For instance, G-CSF is known to play a significant role in granulopoiesis [64,79]. Motivated by [61], we implement feedback inhibition

from mature cells that affects less mature cells (precursors and stem cells). Consider a cytokine $S(t)$ that is produced at a constant rate α, degraded at a constant rate d, and is consumed by mature cells at a rate β. Then

$$\frac{dS}{dt} = \alpha - dS - \beta SM, \tag{3.11}$$

where $M(t)$ is the number of mature cells. Since the cytokine dynamics occur on a faster time scale than cell division, we may assume that the cytokine exists at its quasi-steady state, which when scaled to $s(t) \in [0, 1]$, is

$$s(t) = \frac{1}{1 + kM(t)}, \tag{3.12}$$

where $s = dS/\alpha$ and $k = \beta/d$. We define the renewal fraction a of the stem cell population as

$$a = \frac{a'}{2} + c'. \tag{3.13}$$

This quantity represents the probability that a daughter cell of a stem cell will also be a stem cell. In [61], feedback inhibition affects proliferation rates, renewal fractions, or both, in the less mature compartments. It is found that regulation of self-renewal fractions is essential for the system to be able to recover from events such as chemotherapy that deplete the mature blood cell population. Therefore, we choose to focus on feedback inhibition that affects renewal fractions a_{STC} and a_P of stem cells and precursors by defining

$$a_{STC}(t) = \frac{a_{STC,max}}{1 + kM(t)}, \tag{3.14}$$

$$a_P(t) = \frac{a_{P,max}}{1 + kM(t)}. \tag{3.15}$$

Here, $a_{STC,max}$ and $a_{P,max}$ define the maximum renewal fractions of the stem cell and precursors, respectively. As $M(t)$ becomes smaller, the renewal fractions of both stem cells and precursors increases, in order to expand both pools, which ultimately leads to an increase in mature cells.

We incorporate these changes into the system of difference equations defined by Equations (3.3), (3.4), (3.7), and (3.8). These changes do not change the form of Equation (3.3). Line 2 in Equation (3.4) is replaced by

$$\Omega_{k,c}(t+1) = 2a_{STC}(t)\Omega_{k-1,48}(t), \qquad 0 < k < 127,\ c = 0, \tag{3.16}$$

in order to incorporate asymmetric division of stem cells. Each of the two daughter cells of the dividing stem cell will remain a stem cell with probability $a_{STC}(t)$. Note that instead of choosing the number of daughter stem cells from a binomial distribution, we use the expected value. All other lines in Equation (3.4) are unchanged, for $0 \leq k < 127$. However, when $k = 127$, we must account for the fact that cycling cells with minimum affinity are no longer differentiating into precursors but instead remain stem cells. Thus, when $k = 127$, we replace Equation (3.4) with

$$\Omega_{127,c}(t+1) = \begin{cases} 2a_{STC}(t)(\Omega_{126,48}(t) + \Omega_{127,48}(t)), & c = 0 \\ \sum_{k=126}^{127} \Omega_{k,c-1}(t) - \Psi_{k,c-1}(t), & c = 1 \ldots 31 \\ \sum_{k=126}^{127} (\Omega_{k,31}(t) - \Psi_{k,31}(t)) + B_k(t), & c = 32 \\ \Omega_{126,c-1}(t) + \Omega_{127,c-1}(t), & c = 33, \ldots, 48 \end{cases} \tag{3.17}$$

The precursor cells are described by

$$P_j(t+1) = \begin{cases} 2(1-a_{STC}(t))\sum_k \Omega_{k,48}(t), & j = 0 \\ 2P_{j-1}(t), & j = 24, 48, 72, ..., 240 \\ 2a_P(t)P_{j-1}(t), & j = 264, 288, 312, ..., 696 \\ P_{j-1}(t), & \text{otherwise} \end{cases} \tag{3.18}$$

Since the precursors can now live for up to 30 days, $j = 0, ..., 719$. Line 1 in Equation (3.18) represents new precursor cells. Stem cells differentiate into precursors during cell divisions, each of which produces two daughter cells. Each daughter cell will become a precursor with probability $1 - a_{STC}(t)$. All progenitor cells divide every 24 hours. The first 10 divisions are symmetric renewals, which is represented by line 2 in Equation (3.18). For each subsequent division, up to a total of 30 divisions, daughter cells will remain precursors with probability $a_P(t)$. For all other times, precursor cells age by one hour.

The mature cells are described by

$$M_j(t+1) = \begin{cases} 2P_{719}(t) + 2(1-a_P(t))\sum_{d=11}^{29} P_{24d-1}(t), & j = 0 \\ M_{j-1}(t), & \text{otherwise} \end{cases} \tag{3.19}$$

The only difference from Equation (3.8) is when $j = 0$. This line represents the source of mature cells. The first term of line 1 of Equation (3.19) represents precursors who are completing their 30^{th} division and must undergo symmetric differentiation. The second term represents the contributions of all precursors who are completing their d^{th} division, where $d = 11, ..., 29$. For these divisions, each of the two daughter cells differentiates with probability $1 - a_P(t)$. We use this modified system of difference equations to produce the simulations that are discussed in Section 3.4.

3.4 Numerical Results

For our simulations, we use the system of difference equations in [44], modified to incorporate the changes discussed in Section 3.3. For all parameters that are present in the original Roeder model, we choose the same values given in [85]. In order to allow the stem cell compartment to grow or shrink, we must set $a_{STC,max} > 0.5$. We choose $a_{STC,max} = 0.52$ and $a_{P,max} = 0.51$. In determining the value of k, we observe that at steady state, the total number of stem cells should be constant. In this model, this occurs when the renewal fraction of the stem cells $a_{STC}(t) = 0.5$. Thus, if we want a steady-state solution with $M(t) = M'$, then we should choose

$$k = \frac{2a_{STC,max} - 1}{M'}. \tag{3.20}$$

We set $M' = 6.8246 \cdot 10^{10}$ cells, which is the mature healthy cell steady state value in [44] and apply Equation (3.20) to determine k.

Using these parameters, numerical simulations of healthy cells produce a shift in the stem cell population toward their cycling state, when compared to the simulations in [44] and [85]. This shift had to be addressed since it is known that the stem cells tend to be quiescent [5]. In order to restore the quiescent stem cell population, we reduce the function f_ω by a factor of 10, in comparison to the function used in the original Roeder model. In other words, we reduce the probability that a quiescent stem cell will enter the cell cycle. This modification restores the balance of stem cells, with 91% in quiescence at steady state. The parameters, including this modification of f_ω, are given in Table 3.1.

In implementing carcinogenesis, as in [85], we introduce a single Ph+ stem cell into the healthy cell population at its steady state. As mentioned previously, in [85], Ph- and

Parameter	Description	Ph-	Ph+/R, Ph+/I
a_{min}	Minimum value of affinity a	0.002	0.002
a_{max}	Maximum value of affinity a	1.0	1.0
ρ	Affinity factor	0.0488	0.0488
d	Differentiation coefficient	e^{ρ}	e^{ρ}
r	Regeneration coefficient	$e^{2\rho}$	$e^{2\rho}$
τ_{c}	Cell cycle duration	49 hours	49 hours
τ_{S}	Duration of S phase	8 hours	8 hours
$\tau_{\mathrm{G_2/M}}$	Duration of G_2 and M phases	8 hours	8 hours
λ_{p}	Lifespan of proliferating precursor cells	10-30 days	10-30 days
λ_{m}	Lifespan of mature cells	8 days	8 days
$\tilde{\tau}_c$	Cell cycle of proliferating precursors	24 hours	24 hours
$f_\alpha(0)$	Transition characteristic for f_α	0.5	1.0
$f_\alpha(N_\alpha/2)$	Transition characteristic for f_α	0.45	0.9
$f_\alpha(N_\alpha)$	Transition characteristic for f_α	0.05	0.058
$f_\alpha(\infty)$	Transition characteristic for f_α	0.0	0.0
N_α	Scaling factor	10^5	10^5
$f_\omega(0)$	Transition characteristic for f_ω	0.05	0.1, 0.00500
$f_\omega(N_\omega/2)$	Transition characteristic for f_ω	0.03	0.099, 0.00499
$f_\omega(N_\omega)$	Transition characteristic for f_ω	0.01	0.098, 0.00498
$f_\omega(\infty)$	Transition characteristic for f_ω	0.0	0.096, 0.00496
N_ω	Scaling factor	10^5	10^5
$a_{STC,max}$	The maximum renewal fraction of stem cells	0.52	0.52
$a_{P,max}$	The maximum renewal fraction of precursors	0.51	0.51
M'	The steady state number of mature cells	$6.8246 \cdot 10^{10}$	$1.36492 \cdot 10^{10}$

Table 3.1: Parameters for the simulations in Section 3.4. We replace the constant lifespan $\lambda_p = 20$ days of precursors with a range of 10-30 days. Additionally, all parameters related to f_ω are decreased by a factor of 10 compared with the values in [44], to restore the population of quiescent stem cells. For all other parameters included in the original Roeder model, we choose the same values given in [44]. The last three parameters arise because of our modifications to the model. The parameter M' is used in Equation (3.20) to determine the value of k.

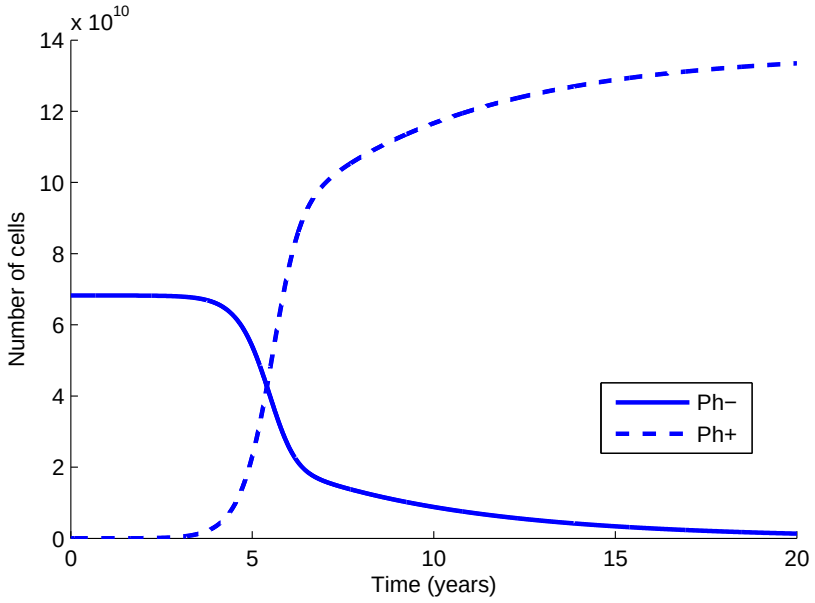

Figure 3.2: A simulation of cancer genesis. The solid line represents mature Ph- cells, and the dashed line represents mature Ph+ cells.

Ph+ cells compete at the stem cell level. They differ in their transition functions f_ω and f_α. We decrease f_ω for both populations by a factor of 10, in order to maintain the same relative difference between these functions for the Ph- and Ph+ cells. We additionally assume that Ph- and Ph+ stem cells compete for cytokine, which is consumed by the mature cells of both populations. We choose a smaller value of k for the Ph+ population, which represents cancer's decreased sensitivity to environmental signals. Specifically, we set $k_{cancer} = k_{healthy}/2$.

Figure 3.2 shows a simulation of cancer genesis for the parameters values described above. The simulation shows a long latency time during which Ph- (solid) and Ph+ (dashed) cells coexist. The Ph+ population becomes greater than the Ph- population between years 5 and 6. These simulations show similar behavior to the simulations of cancer genesis in [44]

and [85].

A simulation of a treatment is shown in Figure 3.3. The initial conditions are taken from the end of the cancer simulation in Figure 3.2. The number of quiescent stem cells, number of mature cells, and BCR-ABL ratio are displayed as functions of time. In comparison with results from [44,85], we observe a much slower decline in the BCR-ABL ratio and the number of cancer cells during treatment. This difference can be understood by considering the Ph+ stem cells. First, recall that quiescent Ph+ stem cells are assumed to be unaffected by IM. These cells are only affected by IM if they enter the cell cycle. Thus, a decrease in the transition rate of stem cells from quiescence to cycling results in quiescent Ph+ stem cells that will remain quiescent for longer periods of time, during which they will remain protected from IM. Figure 3.3(a) illustrates this phenomenon, as the number of quiescent Ph+ stem cells decreases by less than one order and remains above 10^4, after 20 years of treatment. As a result, the number of mature Ph+ cells, shown in Figure 3.3(b), remains above 10^7. The BCR-ABL ratio, shown in Figure 3.3(c), decreases by about 3.5 orders. The simulated patient achieves a MMR, or a 3-log decrease in BCR-ABL ratio, at year 4. However, MMR^4 (a 4-log decrease in BCR-ABL ratio) and MMR^5 (a 5-log decrease) are not achieved.

We consider varying the two treatment parameters, r_{deg} and r_{inh}, in order to simulate patients that achieve MMR^4 and MMR^5. We find that increasing r_{deg}, the rate at which IM kills cycling Ph+ stem cells, results in an increase in the rate at which cancer is cleared, as illustrated in Figure 3.4. By increasing r_{deg}, our simulated patient achieves MMR^4 ($r_{deg} = 0.066$ hour^{-1}) and MMR^5 ($r_{deg} = 0.132$ hour^{-1}).

On the other hand, r_{inh} has a non-monotonic relationship with the rate of cancer clearance. The parameter r_{inh} describes the rate at which cycling Ph+ stem cells become IM-

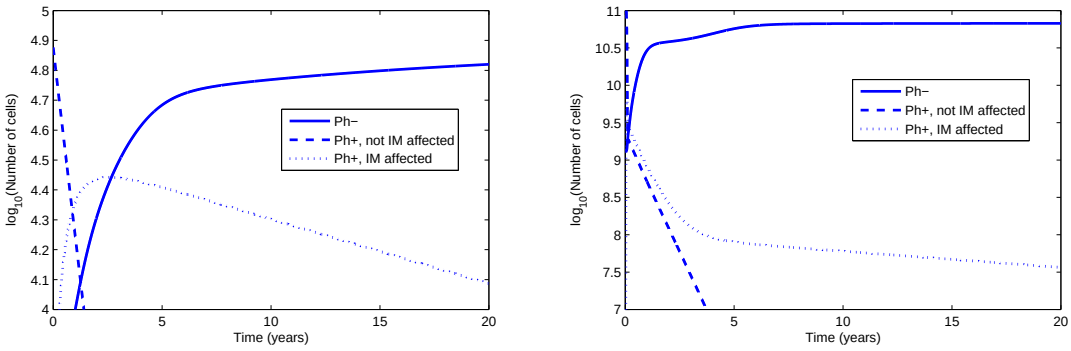

(a)

(b)

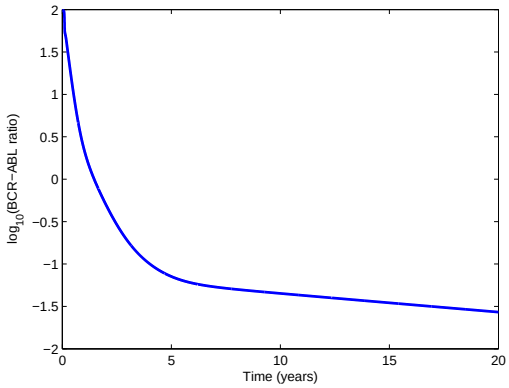

(c)

Figure 3.3: A simulation of treatment. (a) Quiescent stem cells. (b) Mature cells. (c) BCR-ABL ratio. In Figures (a) and (b) Ph- cells are represented by a solid line, Ph+ cells that are not affected by IM are represented by a dashed line, and Ph+ cells that are affected by IM are represented by a dotted line.

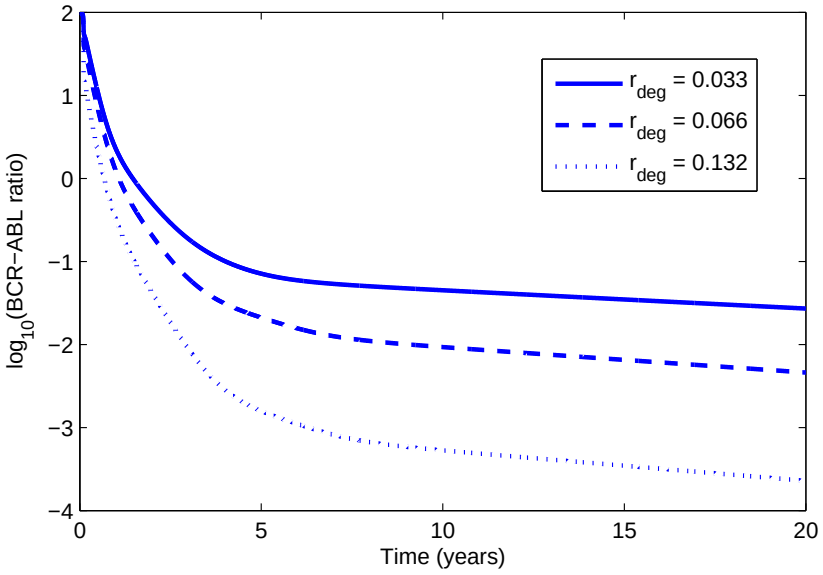

Figure 3.4: BCR-ABL ratio is plotted during treatment, for three different values of r_{deg}: 0.033 hour^{-1} (solid), 0.066 hour^{-1}(dashed), and 0.132 hour^{-1} (dotted). As r_{deg} increases, the BCR-ABL ratio declines more rapidly. For all three simulations, $r_{inh} = 0.05$ hour^{-1}.

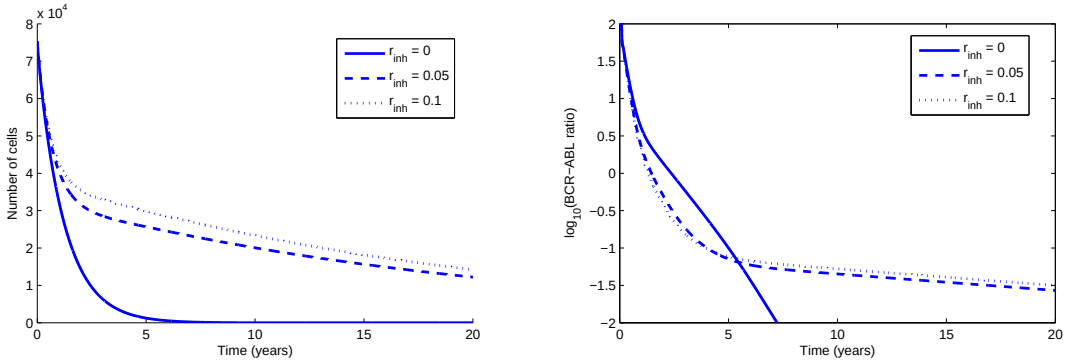

(a) (b)

Figure 3.5: Number of quiescent Ph+ stem cells and BCR-ABL ratio during treatment, for three different values of r_{inh}: 0 hour^{-1} (solid), 0.05 hour^{-1} (dashed), 0.1 hour^{-1} (dotted). (a) Quiescent Ph+ stem cells. (b) BCR-ABL ratio. Initially, a higher value of r_{inh} leads to faster cancer clearance, but later the lower values of r_{inh} become more favorable. For all three simulations, $r_{deg} = 0.033$ hour^{-1}.

affected, meaning they become less likely to enter the cell cycle. Decreasing the transitions of quiescent Ph+ stem cells to cycling has two contrasting effects. On one hand, Ph+ stem cells are prevented from cycling, limiting the number of mature Ph+ cells. On the other hand, these quiescent Ph+ stem cells cannot be eliminated from the stem cell population, as IM does not kill non-cycling Ph+ stem cells.

For large r_{inh}, the Ph+ population rapidly shifts toward these decreased transition rates. As a result, initially the simulations show a sharper decline in mature Ph+ cells, compared to simulations with smaller r_{inh} values. However, Ph+ stem cells with IM-affected transition rates remain quiescent for longer periods of time and are protected from the degradation effect of IM. Eventually, the number of mature Ph+ cells for r_{inh} large becomes greater than the number of mature Ph+ cells for r_{inh} smaller. Figure 3.5(b) shows the effects

of treatment on mature Ph+ cells over time, for different values of r_{inh}.

Figure 3.5(a) shows the number of quiescent Ph+ stem cells over time for different values of r_{inh}. Here, the relationship is more straight-forward. As r_{inh} increases, Ph+ stem cells become IM-affected more rapidly, and as a result, the number of quiescent Ph+ stem cells increases.

3.5 Discussion of Modified Roeder Model Results

In this chapter we modified the Roeder model [85] by adding more biological detail. Specifically, we incorporate asymmetric division of stem cells and precursors, allow precursors to live for a variable amount of time before maturing, and add feedback inhibition from mature cells that affects stem cells and precursors. A more accurate representation of hematopoiesis can lead to more realistic simulations of CML genesis and treatment.

Parametrization of our model suggests that healthy stem cells transition between the quiescent and proliferating compartments at rates that are lower than the rates obtained in the original Roeder model. In the Roeder model, at healthy steady state, approximately 1 quiescent stem cell enters the cell cycle per 1000 quiescent stem cells per time step. Thus, quiescent cells enter the cell cycle, on average, once per 1.4 months. In contrast, in our simulations, 1 quiescent stem cell enters the cell cycle per 10,000 cells, which translates to quiescent cells entering the cell cycle, on average, once every 14 months. This lower rate of entry into the cell cycle by stem cells is supported by [56] and [90].

Lower stem cell transition rates have a significant effect on the results of IM therapy. In our model, we assume that IM only affects cycling Ph+ cells. By decreasing the transition

rates of Ph+ stem cells, quiescent Ph+ stem cells can better evade the effects of IM during treatment. During 20 years of simulated treatment, we see an initial phase of a few months when IM kills most cycling Ph+ stem cells. Once the cycling Ph+ population is depleted, the majority of the remaining Ph+ stem cell population is quiescent and is therefore protected from IM. What follows is a very slow decline in the number of quiescent Ph+ cells over time, since only a few of these cells enter the cell cycle every hour. Our treatment simulations indicate a much larger residual cancer population than those in [85]. These results suggest that IM alone, acting through the implemented mechanisms, can never fully eradicate the cancer population.

The Stop Imatinib trial [60] sought to determine whether patients who responded well to IM therapy could be safely taken off treatment without relapsing. They found that while 61% of patients relapsed, 39% remained in remission for the duration of the two-year study. It is possible that some of the patients in sustained remission had no Ph+ cells remaining when they stopped IM. If this is the case, it may imply that there is an additional action of IM that is not included in the model. Alternatively, patients that remain in sustained remission after stopping IM may still harbor small populations of Ph+ cells. Remaining in remission after stopping IM would then require some other mechanism (e.g. the immune response) to control the Ph+ population and prevent it from expanding.

Still, the fact that many patients do relapse after being taken off IM motivates studying methods by which IM therapy can be improved. Our results suggest that IM therapy may greatly benefit from quiescent Ph+ stem cell activation. IFNα has been shown to activate quiescent stem cells [28] and is therefore a strong candidate for combination therapy. A detailed analysis of immunotherapy in this context is left for a future study.

Chapter 4: The Role of the Autologous Immune System During Imatinib Therapy

The majority of this chapter is taken from [17] and [18].

While TKIs have transformed chronic phase (CP) CML into a long-term survivable and manageable condition, these drugs are not curative in the majority of cases. As a result, patients need to continue therapy indefinitely, a requirement that is both expensive and impairs their quality of life. Further study of the underlying mechanisms of action of TKIs will elucidate whether this limitation is the result of a suboptimal therapy schedule (that is, if changes in the timing and dosage might actually result in a curative therapy), or whether TKIs alone are simply insufficient and combination therapy is necessary. Mathematical modeling is a valuable and complementary tool to clinical data that can be used both to investigate existing therapeutic strategies and to propose novel combinations.

Several mathematical modeling groups have studied various aspects of CML and TKI therapy (see Chapter 2). Both Michor *et al.* [65] and Roeder *et al.* [85] observed that at the beginning of IM therapy, leukemic loads exhibit an initial sharp exponential decline, followed by a second, slower exponential decline. While Michor *et al.* argued that the biphasic exponential decline is the result of decreased proliferative capacities of leukemic progenitors and differentiated cells, Roeder *et al.* hypothesized that IM affects cycling leukemic stem

cells while having no direct effect on quiescent cells.

Although both modeling frameworks capture some characteristic initial responses to therapy, they do not include mechanisms that allow oscillations in the BCR-ABL/ABL ratio to develop. While some patients' leukemic loads continue to monotonically decline, resulting in a triphasic exponential decline [98], our patient data indicates that the leukemic loads of many responding patients exhibit fluctuations. These fluctuations do not necessarily indicate relapse but appear to be an integral part of the response to TKI therapy. The inability of these modeling frameworks to reproduce these fluctuations suggests that an additional mechanism, not included in either model, plays a significant role in the dynamics of TKI therapy. In order to address this limitation, we construct a mathematical model that integrates CML and the autologous immune response.

4.1 Our Model of CML and the Autologous Immune System

We develop an ODE model of CML and the immune system, to study the dynamics of IM therapy. Specifically, we seek to understand patients whose BCR-ABL ratios vary non-monotonically during therapy.

Let y_0, y_1, and y_2, and y_3 represent the concentrations of quiescent leukemic stem cells, cycling leukemic stem cells, progenitor leukemic cells, and mature leukemic cells. Let

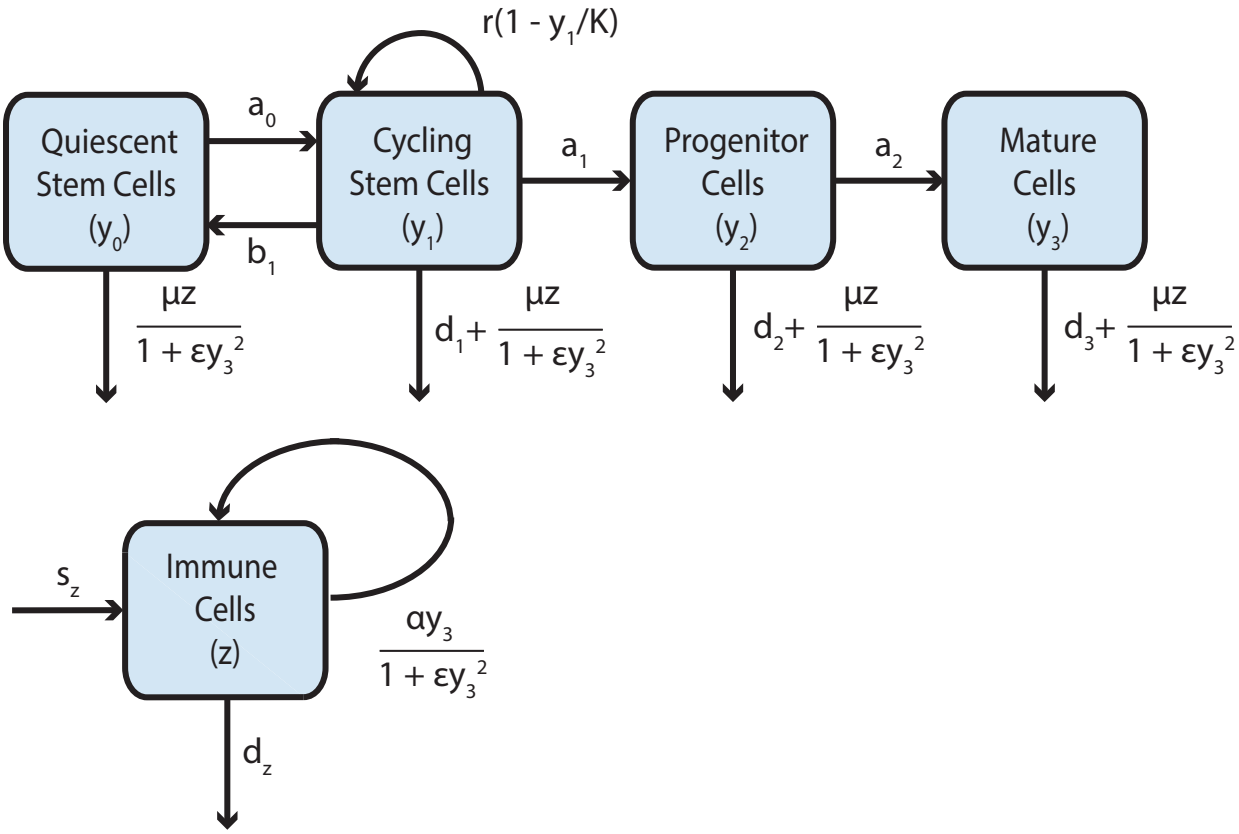

Figure 4.1: Mathematical model including the intervention of the autologous immune system. In our model of CML and the immune response, we divide leukemic cells into quiescent stem cells (y_0), cycling stem cells (y_1), and progenitors (y_2), and mature cells (y_3). Stem cells transition between quiescence and cycling, and some cycling stem cells differentiate into progenitors cells, which can further differentiate into mature cells. Leukemic cells can die naturally at rates d_i or as a result of an interaction with immune cells (z). Immune cells are supposed in this disease to be supplied at a constant rate s_z and to die at a rate d_z. They can also be stimulated by leukemic cells to divide to produce more immune cells. Large leukemic populations are able to suppress the autologous immune system, by limiting immune cell expansion and limiting immune effector cells' ability to kill cancer cells.

z denote the concentration of immune cells. We consider the following system of ODEs.

$$\dot{y}_0 = b_1 y_1 - a_0 y_0 - \frac{\mu y_0 z}{1+\epsilon y_3^2}, \tag{4.1a}$$

$$\dot{y}_1 = a_0 y_0 - b_1 y_1 + r y_1 (1 - \frac{y_1}{K}) - d_1 y_1 - \frac{\mu y_1 z}{1+\epsilon y_3^2}, \tag{4.1b}$$

$$\dot{y}_2 = \frac{a_1}{inh_1} y_1 - d_2 y_2 - \frac{\mu y_2 z}{1+\epsilon y_3^2}, \tag{4.1c}$$

$$\dot{y}_3 = \frac{a_2}{inh_2} y_2 - d_3 y_3 - \frac{\mu y_3 z}{1+\epsilon y_3^2}, \tag{4.1d}$$

$$\dot{z} = s_z - d_z z + \frac{\alpha y_3 z}{1+\epsilon y_3^2}. \tag{4.1e}$$

In Equations (4.1a) and (4.1b), a_0 and b_1 represent the transition rates of leukemic stem cells from quiescence to cycling and cycling to quiescence, respectively. We assume logistic growth of cycling stem cells, with growth rate r and carrying capacity K. Cycling stem cells die naturally at a rate d_1. In Equation (4.1c), the first term represents the differentiation of stem cells into progenitors. The coefficient a_1 is the product of the differentiation rate and the amplification factor upon differentiation due to cell proliferation. Progenitors die naturally at a rate d_2. Equation (4.1d) is similar to Equation (4.1c), with differentiation rate a_2 and death rate d_3. The last terms in Equations (4.1a)-(4.1d) represent the death of leukemic cells caused by an immune response. The mass action term $\mu y_i z$ represents the killing of leukemic cells by the immune system, where μ is the maximal rate (per immune cell) at which an immune cell will engage and kill a leukemic cell. Equation (4.1e) represents the concentration of autologous immune cells. The first term s_z is a constant source term. Immune cells die at a rate d_z. The mass action term $\alpha y_3 z$ represents the expansion (proliferation) of the immune cell pool in response to its leukemia stimulus, which occurs with maximal rate per leukemic cell α. We include only the contributions of the mature leukemic cells y_3 to immune stimulation since they are a much larger population than the immature leukemic

cells ($y_{total} \approx y_3$).

Our model is based on the assumption that immunosuppression acts in two ways. First, mature leukemic cells inhibit the expansion of immune cells. In Equation (4.1e), the immune cell expansion term $\alpha y_3 z$ is divided by $1 + \epsilon y_3^2$, where the constant ϵ determines the strength of the immunosuppression. Second, mature leukemic cells are assumed to decrease the killing capacity μ of activated immune cells, also by a factor of $1 + \epsilon y_3^2$. This effect is represented in the last terms in Equations (4.1a)-(4.1d). This approach is similar to the one used in [43]. By implementing immunosuppression in this way, we encode an autologous immune response that is effective only with intermediate levels of leukemic cells. When the leukemic load is small, only a small number of immune cells is stimulated to respond. On the other hand, although large leukemic loads provide a stronger stimulus, the leukemic cells are able to suppress the efficacy of the immune system. Thus, the immune response will be negligible when the leukemic load is either very small, at levels undetectable by the immune system, or very large, at levels that overwhelm and suppress the immune system. A strong immune response can occur only when the leukemic load y_3 is at an intermediate level, within a range $[y_{min}, y_{max}]$ that we call the immune window. In our model, we define the immune window as the range of y3 for which the rate of immune stimulation $\frac{\alpha y_3}{1+\epsilon y_3^2}$ exceeds the death rate d_z. IM therapy may be used to drive the leukemic load into this immune window, allowing the autologous immune system to assist the drug in the elimination of the leukemic cells. Our model is summarized in Figure 4.1.

IM is known to block the kinase activity of the BCR-ABL protein, which results in a significant decrease in the proliferation rates of the *BCR-ABL+* leukemic cells [4, 41] and apoptotic death [24]. However, we focus here on the effects of IM on proliferation and leave

incorporation of other mechanisms to a future work. We implement IM therapy, starting at time $t = 0$, by decreasing the differentiation/amplification rates a_1 and a_2 to lower values $a_1' = \frac{a_1}{inh_1}$ and $a_2' = \frac{a_2}{inh_2}$. It is unknown how IM affect leukemic stem cells and whether quiescent leukemic stem cells are affected at all, so we assume no direct effect of IM on these populations. However, our model provides a framework for testing various mechanisms of actions of IM, which we leave for a future work.

It is also unclear whether IM is capable of completely eliminating the leukemic cell burden, or whether small residual populations will persist indefinitely. In our model, a leukemic load of zero can only be approached asymptotically, so we define cure as a cancer stem cell concentration less than $1.67 \cdot 10^{-4}$ cells/mL, which corresponds to less than one leukemic stem cell. We stop all simulations of the model whenever this is achieved.

4.2 Materials and Methods

A group of 104 patients with CML was monitored during IM therapy in the Centre Hospitalier Lyon Sud. These patients were all treated with first-line IM 400 mg daily. Patients' BCR-ABL ratios were measured in the same laboratory according to the guidelines of European LeukemiaNet, with the same techniques at diagnosis, months 3, 6, 9, and 12 of therapy, and every 6 months thereafter; in order to limit variability, each measurement was run in duplicate, and the two resulting measurements were averaged. Overall, the patients had an average follow-up time of 62.76 months (range: 2.96 - 148.70), with an average of 12.69 measurements taken (range: 2 - 26). We excluded patients who changed TKIs for safety reasons ($n = 33$) and patients whose disease progressed ($n = 14$), as we focused

exclusively in this study on patients obtaining a residual disease on IM. Thus, a population of 65 patients who responded well to IM remained for analysis.

BCR-ABL ratios were serially measured by quantitative RT-PCR in the peripheral blood of patients in the same laboratory according to the European standards of European Leukemia Net recommendations [6, 22] and expressed as a percentage on the International Scale (IS) [37]. Each sampling was run in duplicate in order to reduce variability and additionally run in parallel to the previous (frozen) sample from each patient in order to exclude technical problems, at each time point (except diagnosis) for all patients. A two-fold variation was considered as significant [8].

Our mathematical model (Equation (4.1)) divides leukemic cells into quiescent stem cells (y_0), cycling stem cells (y_1), progenitors (y_2), and mature cells (y_3). We also represent a single autologous immune cell population (z). For simplicity, we do not distinguish further between immune subpopulations. Leukemia cells stimulate immune cells to proliferate at a maximum rate α, while immune cells kill leukemia cells at a maximum rate μ. We incorporate immunosuppression by inhibiting the proliferation of the immune cells as well as their action on leukemic cells. Our model is summarized in Figure 4.1. A more thorough description of the model is provided in Section 4.1.

As was previously discussed in Sections 1.1 and 2.3.3, the BCR-ABL ratio is a blood measurement that quantifies the amount of *BCR-ABL* transcript relative to a control gene transcript, in our case *ABL*. Each leukemic cell (y_3) possesses the *BCR-ABL* gene and the normal allele of *ABL* gene, while healthy cells (x) possess two alleles of the *ABL* gene. Therefore, *BCR-ABL* transcripts are proportional to y_3 (the immature leukemia cell populations are much smaller than the mature population and can be neglected), while control

transcripts are approximately proportional to $2x + y_3$. For simplicity, the number of healthy cells (x) is assumed to be constant and is estimated based on the patient's initial BCR-ABL ratio at diagnosis. For all later measurements, the BCR-ABL ratio is approximated by

$$\text{ratio} = 100\beta\frac{y_3}{2x + y_3}. \tag{4.2}$$

This equation is similar to Equation (2.8) used in [85], with an additional multiplication factor β that accounts for differences in mRNA expression between *BCR-ABL* and the control gene. We multiply by 100, in order to convert the ratio into a percentage when $\beta = 1$ and a value between 0 and 100β otherwise.

4.3 Results

Many patients who otherwise respond well to therapy exhibit oscillations in their BCR-ABL ratios. Of the 104 patients in our data set, only 15 showed monotonically decreasing BCR-ABL ratios throughout therapy. Each of the remaining 89 patients showed increases in BCR-ABL ratios in, on average, 28.82% of their measurements. Two representative patients are shown in Figure 4.2. These fluctuations occurred in many patients who responded well to IM therapy and did not have any adverse events. This lack of monotonicity in patients who responded well to therapy motivated this study.

We applied our mathematical model, which is summarized in Figure 4.1, to the patient data in order to study these oscillations. As previously mentioned, our model represents leukemic cells of varying maturity and a single immune cell population. We applied Latin hypercube sampling in order to determine the effect of the drug (a_1' and a_2') and the immune parameters (μ, d_z, α, and ϵ). The parameters d_z, α, and ϵ determine the patient's immune

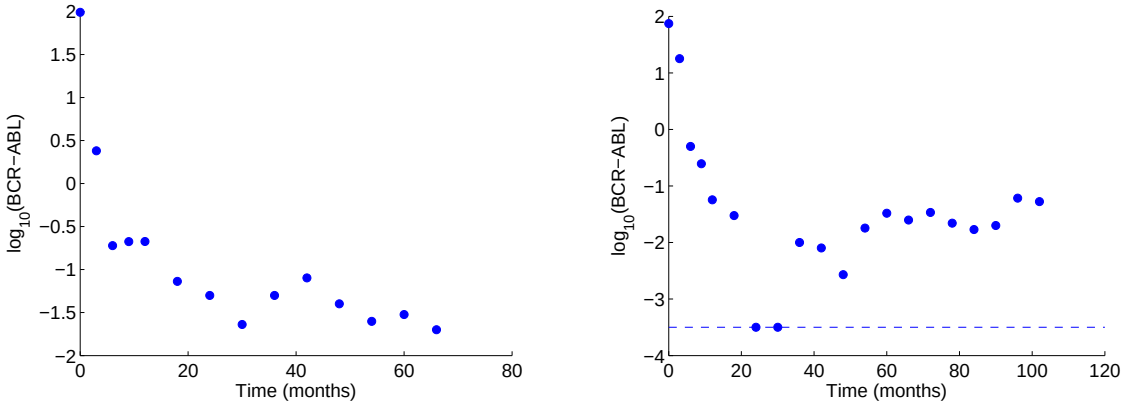

(a) (b)

Figure 4.2: Oscillations of the BCR-ABL ratio in two representative patients. During TKI therapy, a patient's progress is monitored by measuring their BCR-ABL ratio, which is a ratio of *BCR-ABL* mRNA expression to the expression of a control gene, in this case *ABL*. Both patients shown above were treated with standard IM 400 mg daily. During treatment, both patients show multiple increases in BCR-ABL ratio without overt relapse. Here, dots represent clinical data, and the dashed line approximates the detection threshold, or the lowest detectable leukemia level. Dots along this line indicate measurements of zero, meaning the leukemia was undetectable within the limits of the assay. These figures correspond to patients 4 and 12 in Table 4.2.

window $[y_{min}, y_{max}]$, or the range of leukemia loads that will stimulate a strong immune response. We define $[y_{min}, y_{max}]$ by the range of y_3 for which the level of immune stimulation exceeds the death rate. For each patient, we selected the parameter set that minimizes the squared log-distance between the patient data and the results of the model simulation (sampled at the same time as the data). All other parameters were held constant across all patients; their values can be found in Table 4.1. Figures 4.3 and 4.4 show representative fits of our model to patient data. Keeping in mind that these fits are plotted on a logarithmic scale, we see that our model is able to reproduce many patients' dynamics during therapy.

Parameter	Description	Value	Source
$y_0(0)$	Initial leukemic quiescent stem cell concentration	37.5000	Estimated based on [65]
$y_1(0)$	Initial leukemic cycling stem cell concentration	4.1667	Estimated based on [65]
$y_2(0)$	Initial leukemic progenitor concentration	$1.6667 \cdot 10^4$	[65]
$y_3(0)$	Initial leukemic mature cell concentration	$1.5 \cdot 10^8$	[23]
$z(0)$	Initial autologous immune cell concentration	120	Estimated based on [23]
a_0	Stem cell transition rate to cycling	0.0027	Estimated
b_1	Stem cell transition rate to quiescence	0.0247	Estimated
r	Cycling stem cell growth rate	0.08	Estimated based on [43]
K	Cycling stem cell carrying capacity	4.2872	Estimated
a_1	Differentiation rate and expansion factor for progenitors	24.0005	Estimated
a_2	Differentiation rate and expansion factor for mature cells	899.9820	Estimated
d_1	Cycling stem cell death rate	0.00225	[43]
d_2	Progenitor cell death rate	0.006	[43]
d_3	Mature cell death rate	0.0375	[43]

s_z	Source term for autologous immune cells	120 d_z	Estimated
β	Adjustment factor for BCR-ABL ratio	3	Estimated based on patient data

Table 4.1: Universal parameter estimates. This table provides the values of the universal parameters. Cell concentrations are in cells/mL. The initial values $y_0(0) + y_1(0)$ and $y_2(0)$ are chosen based on the initial number of leukemic stem ($2.5 \cdot 10^5$ cells) and precursor cells (10^8 cells) in [65], converted to cells/mL by assuming a blood volume of 6 L. The value $y_3(0)$ is estimated in [23]. The value $z(0)$ is also based on [23], assuming a concentration of $6 \cdot 10^5$ cells/mL, of which about 1/5000 is specific to leukemia. Quiescent stem cells enter the cell cycle infrequently [43], so we set a0 equal to 1/365 day^{-1}. The parameter b_1 is set to $9a_0$ so that most stem cells in our model are quiescent, which is in agreement with [56]. Thus, the two stem cell populations will approximately have a 1:9 ratio, so we set $y_0(0) = 0.9(y_0(0) + y_1(0))$ and $y_1(0) = 0.1(y_0(0) + y_1(0))$. The death rates d_1, d_2, and d_3 are set to those in [43]. The stem cell growth rate is also based on the value in [43]. We increase the original value ($r = 0.008$) by a factor of 10 to account for the fact that only 10% of the stem cells in our model contribute to growth, while all stem cells contribute to growth in [43]. The parameters K, a_1, and a_2 are selected so that the initial conditions represent a steady state when the immune response is removed from the model. (That is, $y_1(0) = K(r - d_1)/r$, $y_0(0) = b_1 y_1(0)/a_0$, $y_2(0) = a_1 y_1(0)/d_2$, and $y3(0) = a_2 y_2(0)/d_3$.) We assume that $z(0) = s_z/d_z$, so the value of d_z determines s_z. Lastly, the adjustment factor β is selected based on the maximum BCR-ABL ratio (269) in our data set.

The patient data and modeling results suggest that patients who respond well to IM therapy go through three to four phases of tumor reduction. During the first few months, there is a rapid exponential decline in BCR-ABL ratio. In our model, this effect is due primarily to the action of the drug on the mature leukemic population. The immune response

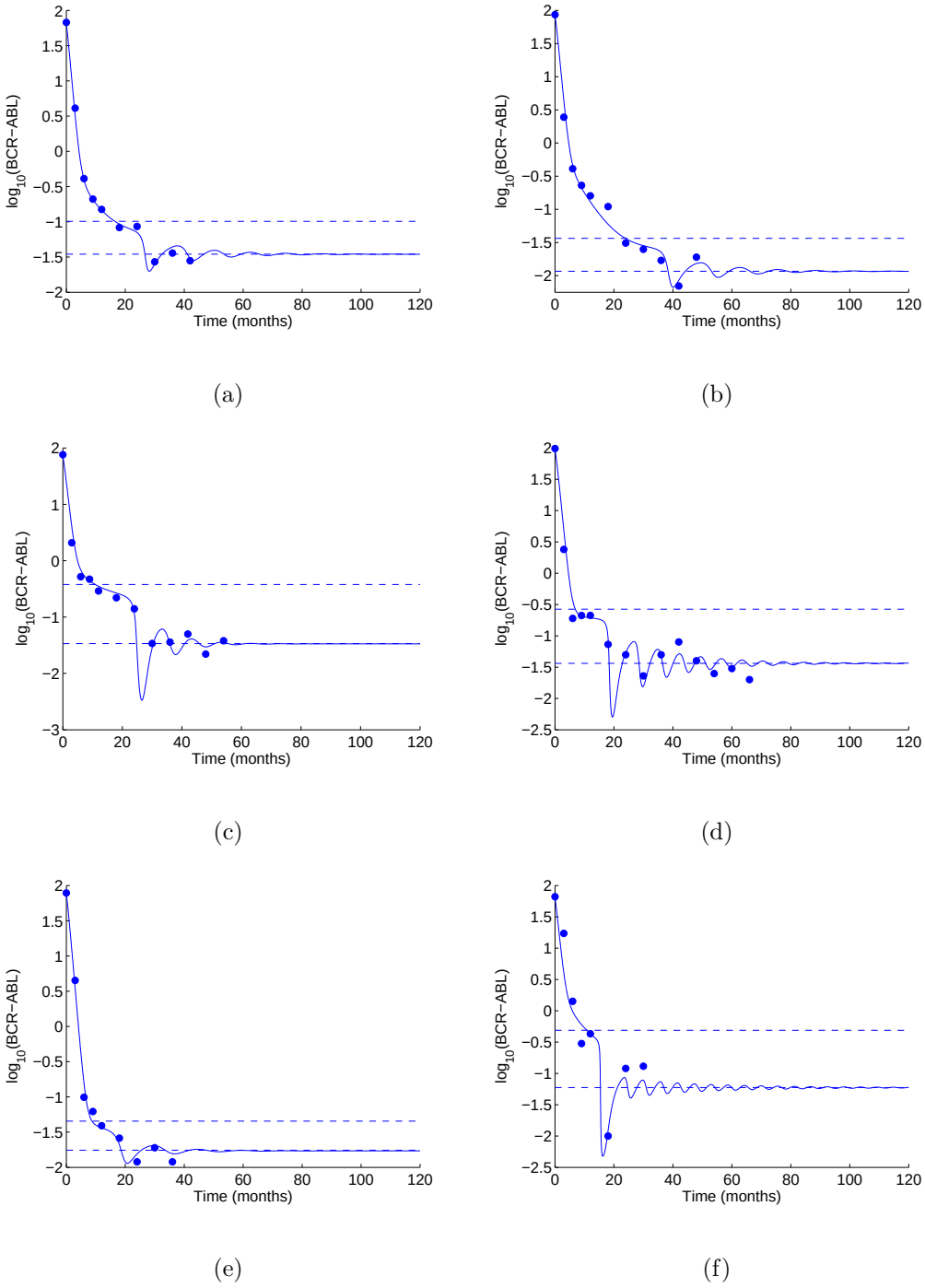

Figure 4.3: Fits of our mathematical model to six representative patients. The base-10 log of the BCR-ABL ratio is plotted against time, in months. The dots represent patient data, and the solid lines represent our simulations. Dashed lines show the BCR-ABL ratios that correspond to the ends of immune window, y_{min} and y_{max}. These figures correspond to patients 1-6 in Table 4.2.

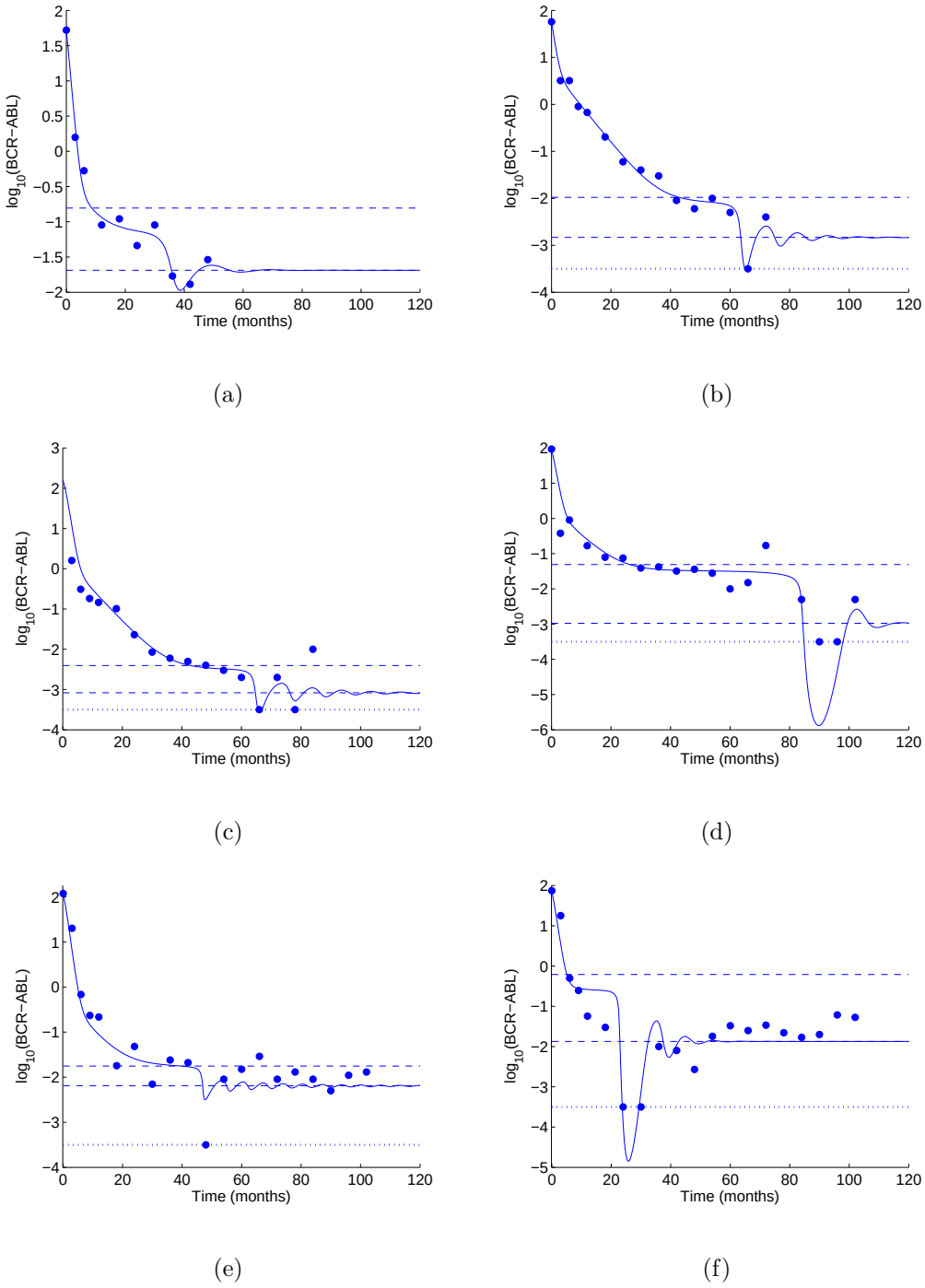

Figure 4.4: Fits of our model to six additional patients. The base-10 log of the BCR-ABL ratio is plotted against time, in months. Dots represent patient data, and the solid lines represent our simulations. Dashed lines show the BCR-ABL ratios that correspond to the ends of immune window, y_{min} and y_{max}. Dotted lines approximate the minimum leukemic level that is detectable by RT-PCR. Dots along this line represent zero measurements, meaning CML cells were not detected. These figures correspond to patients 7-12 in Table 4.2.

is negligible at this stage because the large leukemic load suppresses the immune system. Beginning around month six, there is a second, slower exponential decline in BCR-ABL ratio. In some patients, the second phase is a plateau in BCR-ABL ratio rather than a decline (see Figure 4.3(d)). The location of this plateau is determined primarily by the direct effects of IM on the leukemic cell population (parameters inh_1 and inh_2). This biphasic exponential decline has been previously observed in [65] and [85]. A few patients show a triphasic exponential decline (Figures 4.4(b)-4.4(d)), which was discussed in [98]. The duration of the biphasic or triphasic decline can vary significantly between patients, from the first two years (Figures 4.3(a), 4.3(c), 4.3(d), and 4.4(f)) to several years of therapy (Figures 4.4(b)-4.4(d)).

After this period of monotonic decline, many patients' leukemic loads begin to vary non-monotonically. These fluctuations are often preceded by a sudden sharp decline in the leukemic population, as illustrated in Figures 4.3(f), 4.4(b), and 4.4(d)-4.4(f). If this effect is sufficiently strong, the leukemic stem cell population may be driven to less than one cell, which we interpret as cure in our model. Otherwise, the leukemic population is able to partially recover. Several oscillations in both the leukemic and immune cell populations follow, with their amplitudes decreasing over time as the populations approach an equilibrium, as seen in Figure 4.5.

Patient-specific parameter values are given in Table 4.2 and are summarized in Table 4.3. Of the six parameters varied, the fits seem to be most sensitive to inh_1 and inh_2, followed by y_{min} and y_{max}. The parameters d_z and μ seem to be less important. This is not surprising, as inh_1 and inh_2 determine the effect of the drug, and y_{min} and y_{max} determine at what point the autologous immune response becomes significant. Scatter plots depicting parameter sensitivities for a representative patient are shown in Figure 4.6.

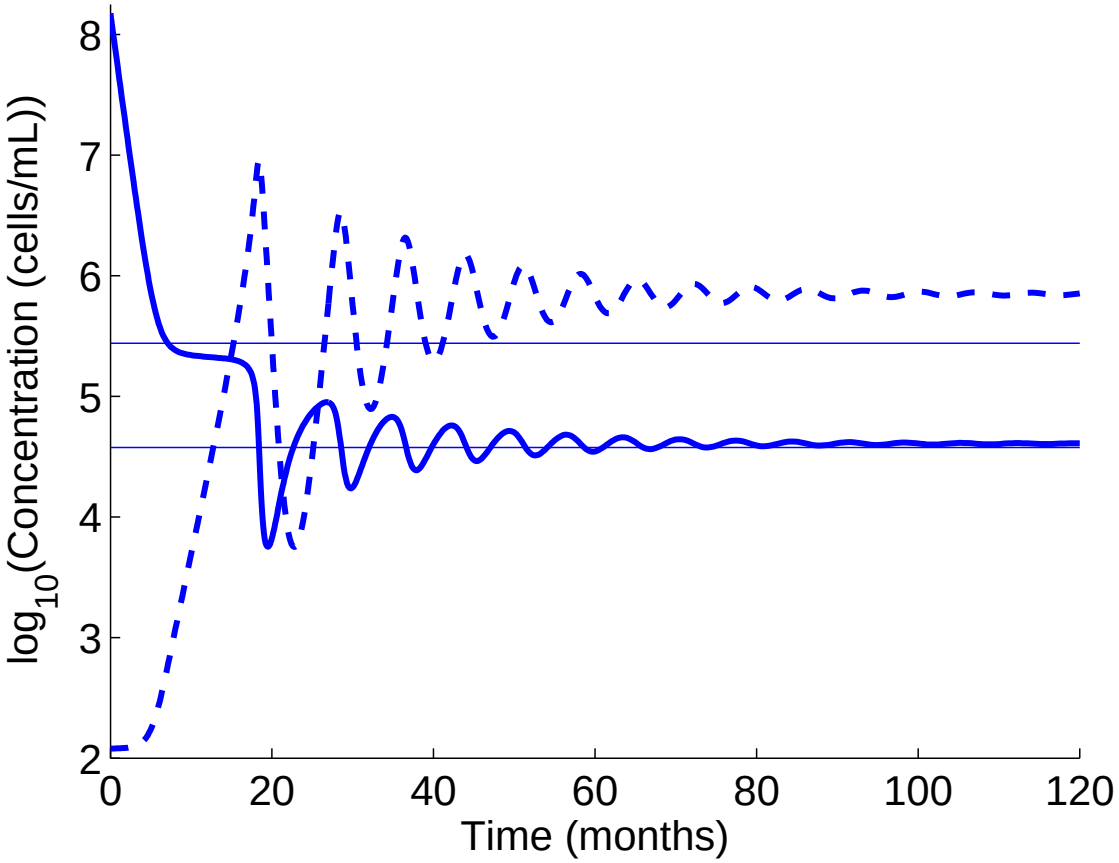

Figure 4.5: Model simulation for a single representative patient. The base-10 log of the leukemia and immune cell populations, in cells/mL, are plotted as a function of time, in months. The thick solid line represents the total leukemic population ($y_{total} = y_0 + y_1 + y_2 + y_3$), and the thick dashed line represents the immune cell population (z). The thin solid lines show the immune window $[y_{min}, y_{max}] = [10^{4.58}, 10^{5.44}]$ cells/mL. For the first twenty months, the patient's leukemia load decreases monotonically, while the immune cells begin to expand. The leukemic population enters the immune window at around month 7. The immune cells mount an attack starting around month 18. This first attack results in the minimum leukemia load achieved during therapy, at around 104 cells/mL. The immune cells drive the leukemia load below the immune window, allowing the leukemic population to partially recover. The two populations oscillate with decreasing amplitudes as they approach their equilibrium concentrations of $(y_{total}, z) = (10^{4.61}, 10^{5.85})$ cells/mL. This simulation corresponds to the plot in Figure 4.3(d) (patient 4 in Table 4.2).

Patient	inh_1	inh_2	d_z	μ	y_{min}	y_{max}
1	9.944	131.016	0.187	$4.021 \cdot 10^{-8}$	$6.001 \cdot 10^{4}$	$1.754 \cdot 10^{5}$
2	33.268	148.517	0.131	$1.515 \cdot 10^{-8}$	$1.443 \cdot 10^{4}$	$4.521 \cdot 10^{4}$
3	4.612	92.3215	0.031	$9.964 \cdot 10^{-7}$	$4.994 \cdot 10^{4}$	$5.598 \cdot 10^{5}$
4	1.456	545.150	0.099	$1.504 \cdot 10^{-8}$	$3.765 \cdot 10^{4}$	$2.759 \cdot 10^{5}$
5	1.872	1700.274	0.128	$3.082 \cdot 10^{-7}$	$2.482 \cdot 10^{4}$	$6.513 \cdot 10^{4}$
6	9.652	43.752	0.238	$1.350 \cdot 10^{-7}$	$1.050 \cdot 10^{5}$	$8.637 \cdot 10^{5}$
7	5.771	155.963	0.019	$4.057 \cdot 10^{-8}$	$4.846 \cdot 10^{4}$	$3.695 \cdot 10^{5}$
8	591.591	14.568	0.040	$2.371 \cdot 10^{-7}$	$3.132 \cdot 10^{3}$	$2.228 \cdot 10^{4}$
9	486.315	226.000	0.075	$2.879 \cdot 10^{-8}$	$3.536 \cdot 10^{2}$	$1.684 \cdot 10^{3}$
10	50.988	79.645	0.005	$1.271 \cdot 10^{-6}$	$1.182 \cdot 10^{3}$	$5.482 \cdot 10^{4}$
11	30.208	359.979	0.371	$2.263 \cdot 10^{-7}$	$4.959 \cdot 10^{3}$	$1.353 \cdot 10^{4}$
12	1.5201	265.6435	0.015	$2.748 \cdot 10^{-8}$	$2.031 \cdot 10^{4}$	$9.352 \cdot 10^{5}$

Table 4.2: Parameter values for patients 1-6 were used to produce Figure 3, while parameter values for patients 7-12 were used to produce Figure 4. Here, y_{min} and y_{max} can be used to obtain immune parameters $\epsilon = 1/(y_{min}y_{max})$ and $\alpha = (y_{min} + y_{max})\epsilon d_z$.

Parameter	$\log(inh_1)$	$\log(inh_2)$	d_z	$\log(\mu)$	$\log(y_{min})$	$\log(y_{min})$	$\log(\frac{y_{max}}{y_{min}})$
Mean	1.132	2.487	0.099	-7.047	3.970	5.024	1.053
STD	0.830	0.754	0.097	0.636	0.888	0.804	0.499
Max	2.772	3.880	0.371	-5.896	5.483	6.024	2.006
Min	0.024	1.073	0.005	-7.954	2.548	3.226	0.197

Table 4.3: Summary of parameter values used in our model simulations. Of the 65 IM patients who do not relapse, develop drug resistance, or progress, 22 change their IM dose during therapy. An additional 6 patients have non-international standard (non-IS) measurements, and 11 patients have five or fewer measurements. We focus on the remaining 25 patients and present the mean, standard deviation, maximum, and minimum parameter values.

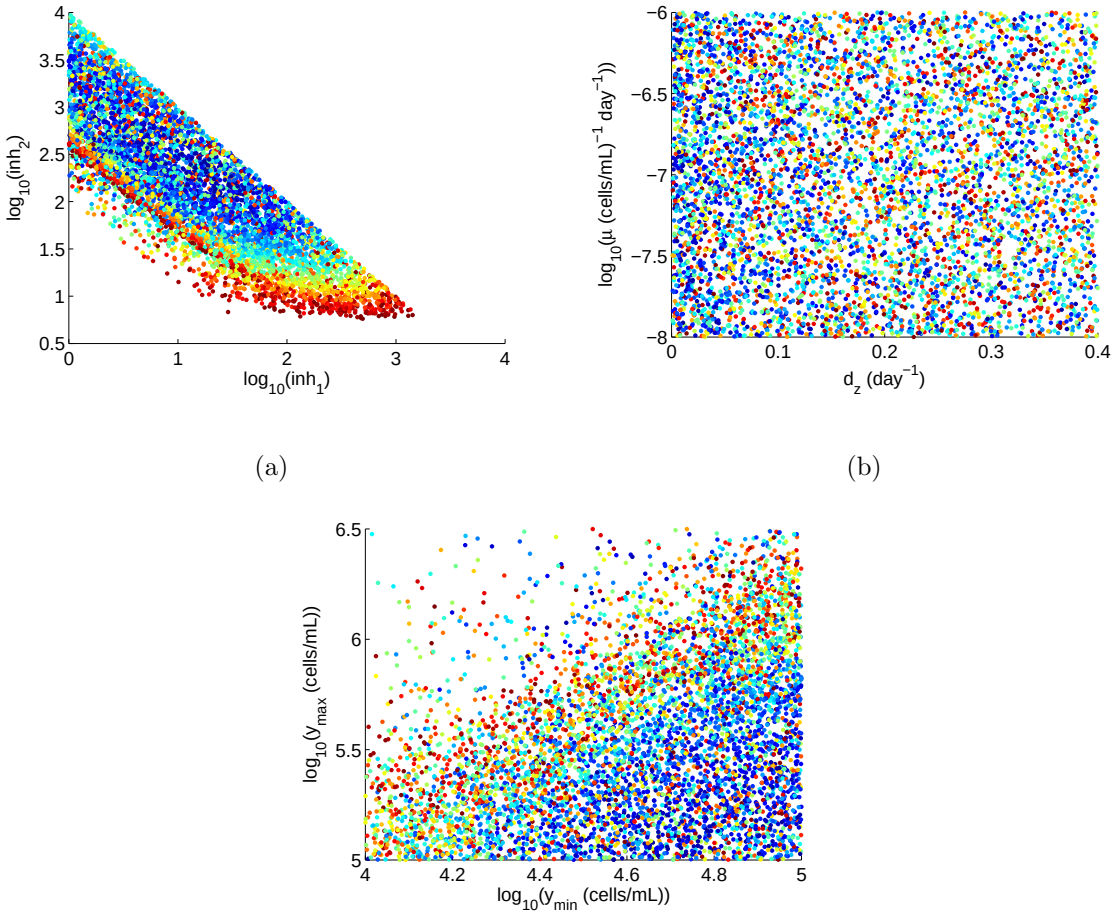

(a) (b)

(c)

Figure 4.6: Quality of the fit as a function of a pair of parameters, for a single representative patient. This is the same patient whose simulation is shown in Figures 4.3(d) and 4.5 (patient 4 in Table 4.2). Red dots indicate worse fits, and dark blue dots indicate better fits. Here, we only show simulations that resulted in a total cost of less than 10, where cost is the squared log-distance between the patient data and model simulation. (a) $\log(inh_2)$ vs. $\log(inh_1)$. For this patient inhibition values satisfying $\log(inh_1 inh_2)$ in [2, 4] were tested. These two parameters are strongly related to the quality of the fit. (b) $\log(\mu)$ vs. d_z. These two parameters seem to be the least important, as it is difficult to see any correlation between the fit and either of these parameters. (c) y_{max} vs. y_{min}. There is a definite relationship between the fit and these two variables. The worse fits tend to be in the upper left corner, while the better fits tend to be in the lower right corner. The parameters y_{max} and y_{min} determine the immune window and therefore affect the timing and magnitude of the autologous immune response.

The parameter values in Table 4.3 suggest that IM alone results in a 3.5-log decrease in the total leukemia load, on average (STD: 0.786, max: 5.158, min: 2.426). This effect is divided into a 2.5-log decrease in the proliferation of mature cells and a 1-log decrease in the proliferation of progenitors. Each patient's immune window covers approximately one order of magnitude of leukemic populations, generally falling between $10^{2.5}$ cells/mL and 10^6 cells/mL. We assume an initial mature leukemic population of $1.5 \cdot 10^8$ cells/mL. Thus, IM must decrease the leukemia load by several orders of magnitude before the leukemia enters the immune window and an immune response is initiated. After the leukemic population enters this window, the leukemia and immune populations oscillate, with the amplitude of oscillations decreasing over time.

4.4 Discussion

Despite the success of IM and other TKI therapies, many questions about the underlying mechanisms of action remain. Mathematical modeling is a complementary tool to clinical and experimental data that can help us understand these mechanisms. Several mathematical modeling groups have already studied various aspects of CML. We briefly review some of these contributions but note that a more thorough review can be found in Chapter 2.

Michor *et al.* [65] constructed an ODE model of CML that divides leukemic cells into stem cells, progenitors, differentiated cells, and terminally differentiated cells. Upon analyzing patients' initial responses to IM therapy, they found that IM often leads to biphasic exponential declines in the leukemic cell populations. Their modeling results suggested that the first, steeper decline represents the action of IM on the differentiated leukemic cell

population, while the second, slower decline represents an effect on the leukemic progenitors. They later hypothesized that long-term therapy leads to a triphasic exponential decline, where the third decline may represent an effect on immature leukemic cells and possibly leukemic stem cells [98].

On the other hand, Roeder *et al.* [85] developed an agent-based model of CML that divides leukemic stem cells into cycling and quiescent compartments. In their model, IM results in the degradation and inhibition of cycling leukemic stem cells while having no direct effect on quiescent leukemic stem cells. They interpreted the biphasic exponential decline as an initial degradation effect, followed by a change in the regulatory response of leukemic stem cells which produces the second decline. A similar interpretation to the biphasic decline is proposed in [48].

Although these modeling frameworks are capable of reproducing the dynamics of some patients during therapy, both are limited to those who show a monotonic decline in their leukemic burdens. Neither model includes a mechanism that would allow patients to show oscillations in leukemia load. However, in our data, we found that many patients who respond well to IM and achieve long-term remissions exhibit increases in leukemic burden. The fact that the Michor and Roeder models are unable to reproduce such oscillations suggests that there may be (an) additional mechanism(s) that contribute(s) to patients' dynamics during therapy.

Motivated by this, we developed a mathematical model that integrates CML and an autologous immune response. As previously discussed in Section 1.3, there is strong evidence that the immune system plays a role in the dynamics of CML. In our modeling framework, we defined an immune window, or a range of leukemic loads that will provoke a strong autologous

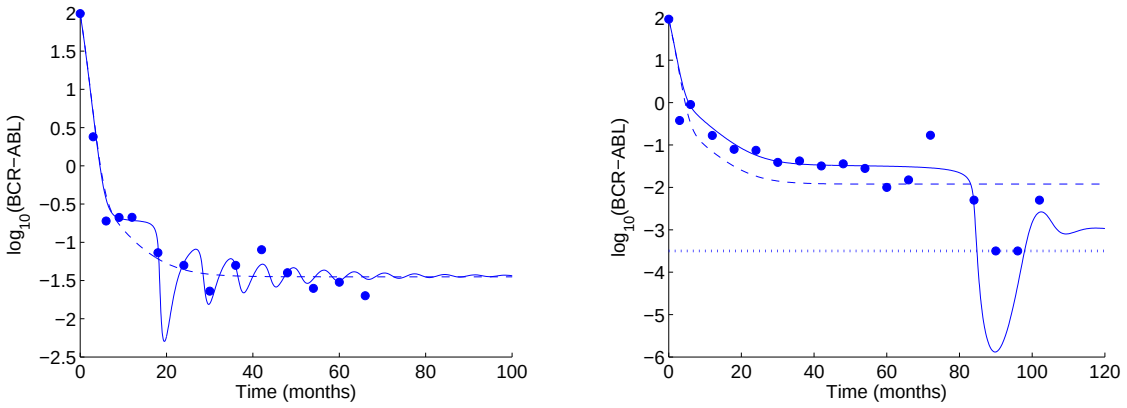

(a) (b)

Figure 4.7: Comparison of the model with and without an autologous immune response. Patients 4 and 10 from Table 4.2 are shown in (a) and (b), respectively. The dots represent patient data, the solid lines represent fits for the model with an immune response, and the dashed lines represent fits for the model without an immune system (set $z(0) = 0$ and $s_z = 0$). The dotted line in (a) approximates the minimum leukemic level that is detectable by RT-PCR. Dots along this line represent zero measurements, meaning CML cells were not detected. For simulations without an immune response, $inh_1 = 17.140$ and $inh_2 = 239.330$ in (a), and $inh_1 = 37.393$ and $inh_2 = 299.235$ in (b). All other parameters, besides s_z and $z(0)$, are set to those given in Table 4.1. Only the model with an autologous immune response is able to produce the non-monotonicity seen in both patients' BCR-ABL ratios.

immune response. At diagnosis, the leukemic load is above this window, and the large leukemic population is able to partially or fully suppress the autologous immune system's response to CML. IM therapy generally reduces a patient's leukemic load by several orders of magnitude, representing a significant reduction in immunosuppression. We hypothesize that IM may drive the leukemic population into the immune window, allowing a patient's autologous immune system to mount a response to CML.

In our model, oscillations in leukemic load occur after the leukemia enters the immune window. Without the autologous immune response, our model produces monotonically de-

creasing cancer loads, as seen in Figure 4.7. Once the autologous immune cells have expanded sufficiently, they attack the residual leukemic population. This first attack by the autologous immune system results in the minimum detectable leukemic load achieved during IM therapy. However, because the leukemia is driven below the immune window, the patient's immune cell population begins to contract. If the leukemia is not eradicated, it is able to rebound, until it reenters the immune window, thus stimulating another weaker immune response. The immune and leukemic cell populations continue to oscillate in this way, with the amplitude of these oscillations decreasing over time. Eventually, the oscillations dampen, and an equilibrium is achieved between the leukemic and autologous immune cells. Our modeling results suggest that oscillations in BCR-ABL ratio during therapy may be partially explained by the patient's autologous immune response to the residual CML population.

Moreover, the oscillations may be a signature of the autologous immune response, that can be used to characterize a patient's individual immune system. This result is reminiscent of previous tumor-immune models, e.g. Kuznetsov *et al.* [50].

Based on a patient's data over the course of TKI therapy, we determine their immune profile in the context of our model. Each patient's immune profile is different, as demonstrated by differences in the immune windows and in the timing and magnitude of the autologous immune response to CML. Our modeling framework provides a potential tool to help quantify these differences, which may play a significant role in designing personalized therapies or combination therapies aimed at further reducing or eradicating the residual CML burden. This framework will serve as a basis for future studies of treatment cessation and personalized combination therapies consisting of TKIs and immunotherapy.

4.5 Conclusion

The potentially significant role of the immune system in the dynamics of IM therapy suggests that immunotherapy may help to eliminate the residual leukemic burden. In our simulations, when IM therapy drives the leukemia into the immune window, an initially strong immune response occurs that weakens over time. Eventually, the immune cell population contracts, allowing the leukemia to partially recover. A combination of IM and immunotherapy may help to maintain a strong immune response, to prevent such a recovery in the leukemic population. As suggested in [43], carefully-timed vaccines may stimulate the patient's immune system when the residual CML burden is no longer sufficient. A sustained immune response may result in a further decrease of the leukemic population and may even drive the leukemia to extinction. An optimal vaccine schedule would depend heavily on each patient's immune profile, and our model offers a tool for characterizing this.

Although we focus on the autologous immune response as a possible explanation of the oscillations that occur during IM therapy, many other factors may contribute to this behavior. The microenvironment of the leukemic cells is known to have a strong influence on both healthy and leukemic cells [51,63], but is not included in our model. Additionally, we do not account for patients who do not properly or regularly take their drugs, which is known to be an important factor [62]. Moreover, for simplicity, we do not distinguish between various subtypes of immune cells, each of which may interact and play different roles in CML. Our model can be expanded in order to achieve a more accurate representation of the autologous immune response to CML. We leave this for a future work.

Still, the oscillations in patients' leukemic loads suggest an additional mechanism dur-

ing therapy that has not previously been included in mathematical models. Our modeling results support the hypothesis that the autologous immune system contributes to the dynamics of IM therapy. If this is the case, our model may serve as a valuable tool for characterizing a patient's immune response to CML. This immune profile may then help in designing personalized combination therapies in order to further control or eliminate the residual leukemic burden.

4.6 Afterthoughts: An Alternate Mechanistic Model

We also consider the following alternative model of CML and the autologous immune system, in which the immune-leukemia interactions are based on [50].

$$\dot{y}_0 = b_1 y_1 - a_0 y_0 - \mu y_0 z, \tag{4.3a}$$

$$\dot{y}_1 = a_0 y_0 - b_1 y_1 + r y_1 (1 - \frac{y_1}{K}) - d_1 y_1 - \mu y_1 z, \tag{4.3b}$$

$$\dot{y}_2 = \frac{a_1}{inh_1} y_1 - d_2 y_2 - \mu y_2 z, \tag{4.3c}$$

$$\dot{y}_3 = \frac{a_2}{inh_2} y_2 - d_3 y_3 - \mu y_3 z, \tag{4.3d}$$

$$\dot{z} = s_z - d_z z + \alpha \frac{y_3 z}{1 + \epsilon y_3} - \alpha_2 y_3 z. \tag{4.3e}$$

This model is similar to Equation (4.1) except in the way in which the immune response is represented. In the previous model, immunosuppression is incorporated by dividing the mass action terms representing immune-leukemia interactions (immunostimulation $\alpha y_3 z$ and the killing of leukemic cells by immune cells $\mu y_i z$) by $1+\epsilon y_3^2$. As was previously mentioned, these terms encode an immune response that is most effective at intermediate levels of leukemic stimulus. This representation is not motivated by a specific mechanism of immunosuppression, although we note that these immunosuppression terms are similar to terms found in [61].

In their model, proliferation rates and renewal fractions are divided by a factor $1+kc_6$, where k is a constant, and c_6 is the mature blood cell population, in order to incorporate the effect of a regulatory cytokine. The presence of two regulatory cytokines would lead to division by a quadratic function of the mature population, producing terms similar to those in Equations (4.1a)-(4.1e).

In the mechanistic model, there are no terms representing immunosuppression of the immune-leukemia interactions. Rather, mature leukemic cells are assumed to have two contrasting effects on immune cells, as seen in the last two terms of Equation (4.3e). The Michaelis-Menten term $(\alpha y_3 z/(1+\epsilon y_3))$ represents the stimulation of immune cells by leukemic cells, with maximum rate $\alpha_2\epsilon^{-1}$ and Michaelis constant ϵ^{-1}. The mass action term $(\alpha_2 y_3 z)$ represents the killing of immune cells by leukemic cells, at a rate α_2.

Although the two models of CML and the autologous immune system represent immune-leukemia interactions differently, they are qualitatively very similar and produce similar fits, as seen in Figures 4.8 and 4.9. The mechanistic model does, however, introduce an additional parameter α_2, and this model seems to be stiff. For convenience, although both models seem plausible and it may be difficult to exclude either until further information about the nature of immunosuppression in CML is known, we choose to focus on our original model given by Equations (4.1a)-(4.1e).

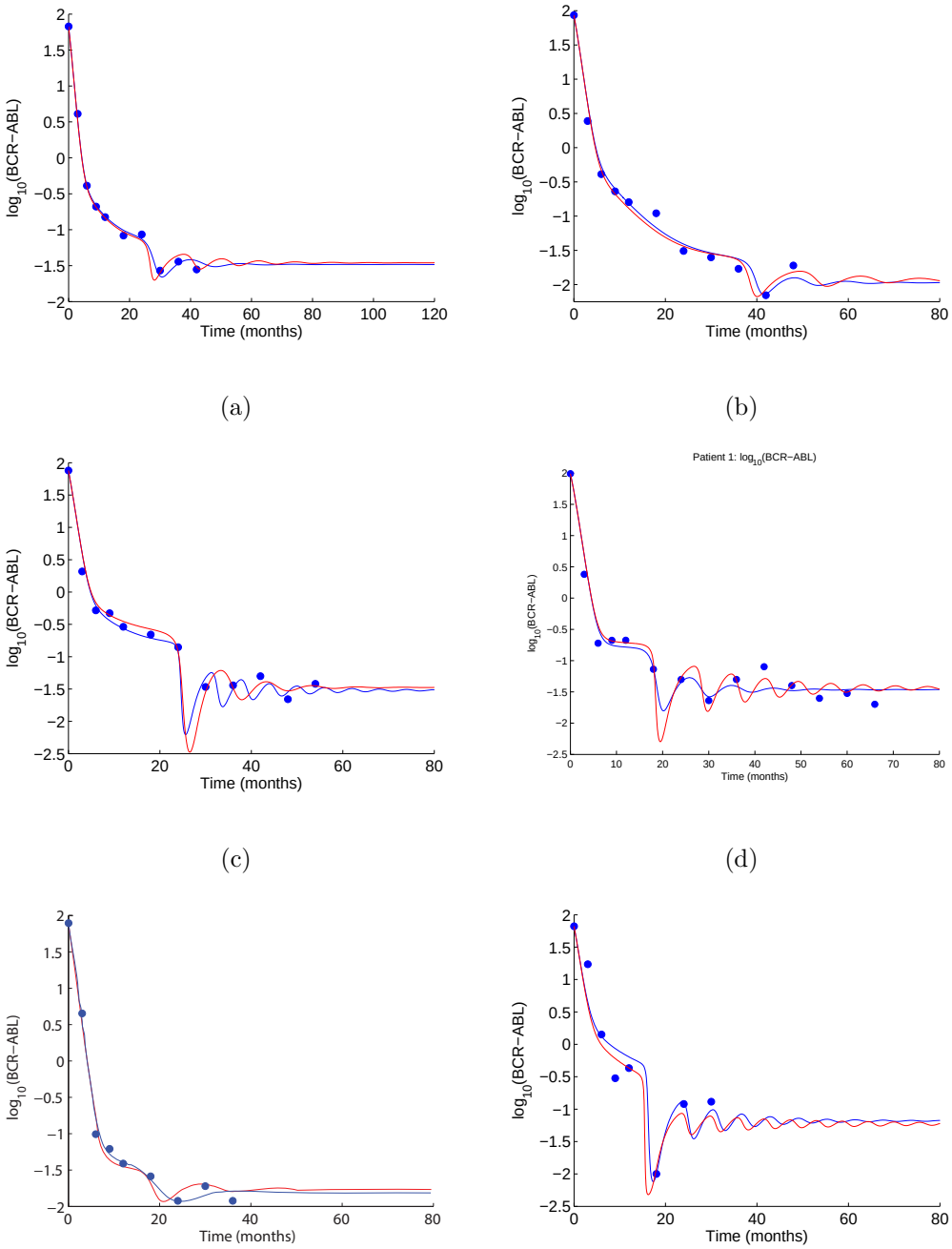

Figure 4.8: Fits of our two models to patient data. Dots indicate patient data. Fits of our original model (Equations (4.1a)-(4.1e)) are shown in red. These fits are obtained as described in Section 4.2. Fits to the alternative mechanistic model (Equations (4.3a)-(4.3e)) are shown in blue. These fits are obtained using a similar strategy, with one additional immune parameter α_2. The two models produce comparable fits.

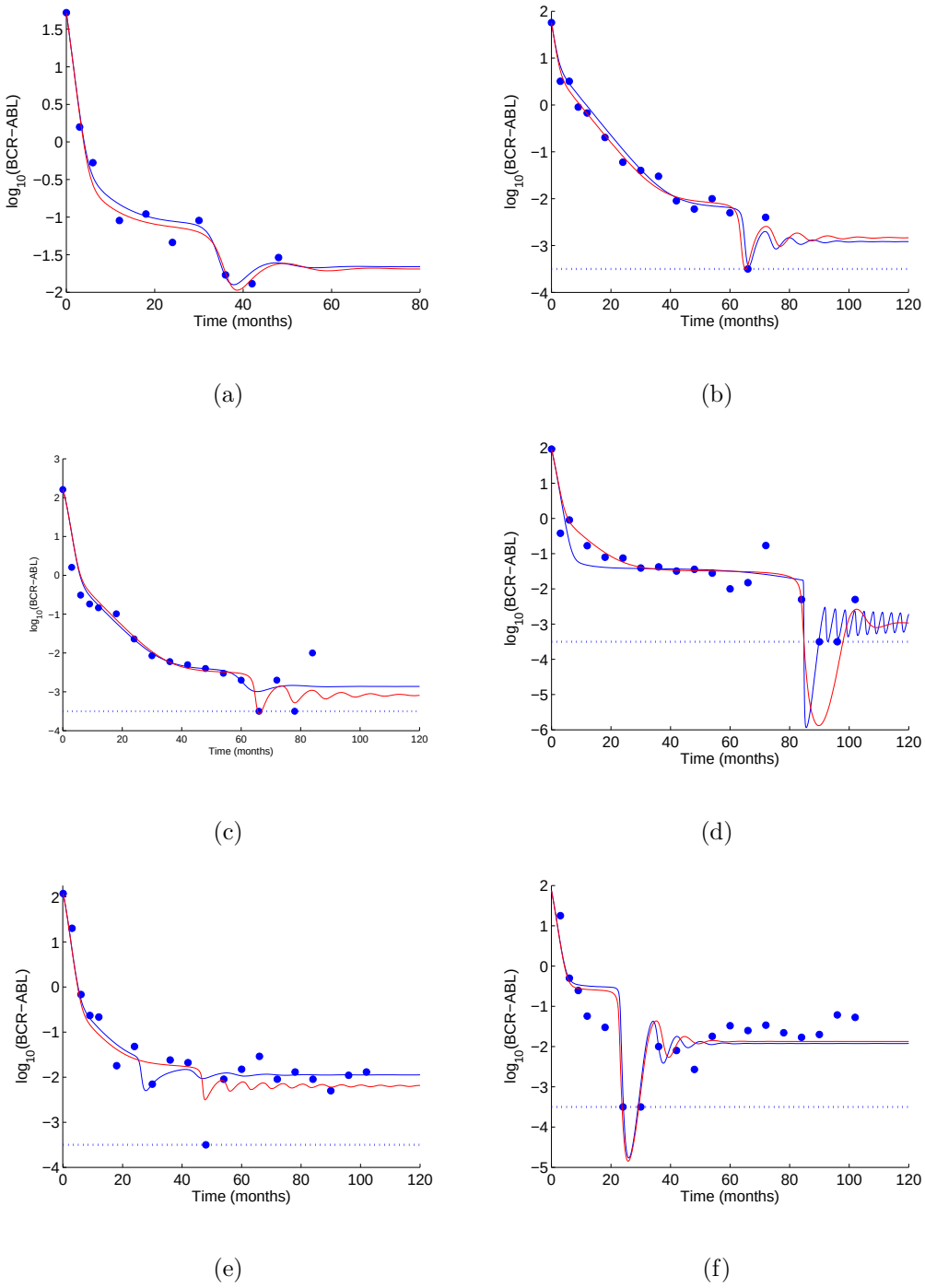

Figure 4.9: Six additional fits of both models to patient data. Fits of our original model (Equations (4.1a)-(4.1e)) are shown in red, while fits to the alternative mechanistic model (Equations (4.3a)-(4.3e)) are shown in blue. Dots indicate patient data. A dotted line approximates the lowest detectable BCR-ABL ratio. Dots along this line indicate zero measurements. Again, the two models produce comparable fits.

Chapter 5: Analysis of a Simplified Model of CML and the Immune System

The analysis that follows is the result of a collaboration with Apollos Besse, a graduate student and member of Inria and the University of Lyon.

5.1 A Simplified Model

We consider the following simplified version of our original model presented in Chapter 4:

$$\dot{y_0} = b_1 y_1 - a_0 y_0, \tag{5.1a}$$

$$\dot{y_1} = a_0 y_0 - b_1 y_1 + r y_1 (1 - \frac{y_1}{K}) - d_1 y_1 - \mu_1 \frac{y_1 z}{1 + \epsilon_1 y_2^2}, \tag{5.1b}$$

$$\dot{y_2} = a_1 y_1 - d_2 y_2 - \mu_2 \frac{y_2 z}{1 + \epsilon_2 y_2^2}, \tag{5.1c}$$

$$\dot{z} = s - dz + \alpha \frac{y_2 z}{1 + \epsilon y_2^2}. \tag{5.1d}$$

In contrast to our original model (Equations (4.1a)-(4.1e)), the simplified model includes only three leukemic subpopulations: quiescent stem cells y_0, cycling stem cells y_1, and mature cells y_2. We exclude the progenitor compartment in order to make the analysis of the system more accessible. Our analysis provides insight into the behavior that should be expected from the full model, although we acknowledge that this simplification may affect the stability properties of the system.

We initially include a term $d_1 y_1$ that represents the natural death of leukemic stem cells. However, we can incorporate this term into the logistic growth term $ry_1(1-\frac{y_1}{K})$ simply by redefining r and K as $r_{new} = r_{old} - d_1$ and $K_{new} = \frac{r_{new}}{r_{old}} K_{old}$.

Additionally, we assume that immune cells have the same effect on both leukemic stem cells and mature leukemic cells, by setting $\mu_1 = \mu_2 := \mu$ and $\epsilon_1 = \epsilon_2$. We arrive at the following system:

$$\dot{y_0} = b_1 y_1 - a_0 y_0, \tag{5.2a}$$

$$\dot{y_1} = a_0 y_0 - b_1 y_1 + r y_1 (1 - \frac{y_1}{K}) - \mu \frac{y_1 z}{1 + \epsilon_1 y_2^2}, \tag{5.2b}$$

$$\dot{y_2} = a_1 y_1 - d_2 y_2 - \mu \frac{y_2 z}{1 + \epsilon_1 y_2^2}, \tag{5.2c}$$

$$\dot{z} = s - dz + \alpha \frac{y_2 z}{1 + \epsilon y_2^2}. \tag{5.2d}$$

Because all coefficients in Equations (5.2a)-(5.2d) are positive, the populations must remain nonnegative and satisfy

$$y_1 \leq K \qquad y_2 \leq \frac{a_1 K}{d_2} := M \qquad z \geq \frac{s}{d}.$$

5.2 Steady States of the Simplified System

We want to determine the steady states of the system given by Equations (5.2a)-(5.2d) and their stability. For now, we assume that $\alpha^2 \geq 4\epsilon d^2$ so that the following quantities will be real:

$$y_{min} = \frac{\alpha - \sqrt{\alpha^2 - 4\epsilon d^2}}{2\epsilon d},$$

$$y_{max} = \frac{\alpha + \sqrt{\alpha^2 - 4\epsilon d^2}}{2\epsilon d}.$$

We will call the interval $[y_{min}, y_{max}]$ an *immune window*. If we define $Y = (y_{min} + y_{max})/2$, then $\epsilon = (y_{min}y_{max})^{-1}$ and $\alpha = 2Y\epsilon d$.

Proposition 5.2.1 *There is one healthy equilibrium given by* $(0, 0, 0, \frac{s}{d})$. *The others satisfy*

$$\begin{aligned} y_0 &= \frac{b_1}{a_0}\frac{(r+d_2)y_2}{(a_1+\frac{ry_2}{K})}, \\ y_1 &= \frac{(r+d_2)y_2}{a_1+\frac{ry_2}{K}}, \\ z &= \frac{s(1+\epsilon y_2^2)}{d\epsilon y_2^2 - \alpha y_2 + d} = \frac{s(1+\epsilon y_2^2)}{d\epsilon(y_2-y_{min})(y_2-y_{max})}, \end{aligned}$$

where y_2 *is a positive root of the polynomial*

$$p(X) = (X-y_{min})(X-y_{max})(X-M)(1+\epsilon_1 X^2) + \frac{\mu s}{\epsilon r d}(M+\frac{r}{d_2}X)(1+\epsilon X^2). \tag{5.3}$$

These roots lie outside $[y_{min}, y_{max}]$.

Proof The equilibria can be found by setting Equations (5.2a)-(5.2d) to zero.

$$\begin{aligned} 0 &= b_1 y_1 - a_0 y_0, \\ 0 &= r y_1(1-\frac{y_1}{K}) - \mu\frac{y_1 z}{1+\epsilon_1 y_2^2}, \\ 0 &= a_1 y_1 - d_2 y_2 - \mu\frac{y_2 z}{1+\epsilon_1 y_2^2}, \\ 0 &= s - dz + \alpha\frac{y_2 z}{1+\epsilon y_2^2}. \end{aligned}$$

The healthy equilibrium $(0, 0, 0, \frac{s}{d})$ clearly satisfies these equations. We now search for equilibria such that $y_i > 0$ for $i = 0, 1, 2$. Then, $\dot{y_0} = 0$ iff $y_0 = \frac{b_1 y_1}{a_0}$. When $y_1 > 0$, the equilibria must also satisfy

$$r(1-\frac{y_1}{K}) = \mu\frac{z}{1+\epsilon_1 y_2^2}, \tag{5.4a}$$

$$a_1 y_1 - d_2 y_2 = \mu\frac{y_2 z}{1+\epsilon_1 y_2^2}, \tag{5.4b}$$

$$dz - s = \alpha\frac{y_2 z}{1+\epsilon y_2^2}. \tag{5.4c}$$

By multiplying Equation (5.4a) by y_2, we can set it equal to Equation (5.4b) and solve for y_1 as a function of y_2. We can also solve Equation (5.4c) for z as a function of y_2. We arrive at the following.

$$y_0 = \frac{b_1}{a_0}\frac{(r+d_2)y_2}{(a_1+\frac{ry_2}{K})}, \tag{5.5a}$$

$$y_1 = \frac{(r+d_2)y_2}{a_1+\frac{ry_2}{K}}, \tag{5.5b}$$

$$z = \frac{s(1+\epsilon y_2^2)}{d\epsilon y_2^2 - \alpha y_2 + d}. \tag{5.5c}$$

When $\alpha^2 \geq 4\epsilon d^2$, we can rewrite the equation for z with respect to y_{min} and y_{max} as follows.

$$z = \frac{s(1+\epsilon y_2^2)}{d\epsilon(y_2 - y_{min})(y_2 - y_{max})}.$$

Thus, $z > 0$ iff either $y_2 < y_{min}$ or $y_2 > y_{max}$. That is, equilibrium values for y_2 must lie outside the immune window.

We have found y_0, y_1, and z with respect to y_2, so all that remains is to find the appropriate y_2 values. We can plug Equation (5.5b) into $1 - \frac{y_1}{K}$, which simplifies to

$$1 - \frac{y_1}{K} = \frac{a_1K - d_2y_2}{a_1K + ry_2} = \frac{M - y_2}{M + \frac{r}{d_2}y_2}.$$

Replacing $1 - \frac{y_1}{K}$ and z in Equation (5.4a), we arrive at

$$r\frac{M - y_2}{M + \frac{r}{d_2}y_2} = \frac{\mu s}{d\epsilon(y_2 - y_{min})(y_2 - y_{max})}\frac{1+\epsilon y_2^2}{1+\epsilon_1 y_2^2}.$$

It follows that y_2 must satisfy

$$(y_2 - y_{min})(y_2 - y_{max})(y_2 - M)(1+\epsilon_1 y_2^2) + \frac{\mu s}{\epsilon r d}(M + \frac{r}{d_2}y_2)(1+\epsilon y_2^2) = 0.$$

∎

We observe that

$$P(0) = M(-y_{min}y_{max} + \frac{\mu s}{\epsilon r d}) = -\frac{M}{\epsilon}(1 - \frac{\mu s}{rd}),$$

where the second equality comes from the fact that $\frac{1}{\epsilon} = y_{min}y_{max}$. Thus, $P(0) < 0$ iff $\mu s < rd$. Later, we will find that we are interested primarily in the case when $\mu s < rd$.

When $P(0) < 0$, since $P(y_{min}) > 0$, it follows that there is a zero of P on $(0, y_{min})$. Additionally, provided $y_{min} < M$, P is positive on the intervals $[y_{min}, min\{y_{max}, M\}]$ and $[max\{y_{max}, M\}, \infty)$. When $y_{min} < y_{max} < M$, if we can find a value $y_2^* \in (y_{max}, M)$ such that $P(y_2^*) < 0$, then it will follow that there are at least two additional roots of P, one in (y_{max}, y_2^*) and another in (y_2^*, M).

Since all steady states (y_1, y_2, z) must satisfy $y_2 < M$, it follows that:

- If $y_{max} \geq M$, then we expect roots only on $(0, y_{min})$.
- If $y_{max} < M$, then we expect roots on $(0, y_{min})$ and possibly (y_{max}, M).

We will soon see that in most cases of interest, there are three equilibria: a large one near $(\frac{b_1 K}{a_0}, K, M, \frac{s}{d})$, an intermediate one $(y_{0,int}, y_{1,int}, y_{2,int} \approx y_{max}, z_{int})$, and a low one $(y_{0,low}, y_{1,low}, y_{2,low} \approx y_{min}, z_{low})$.

5.3 The Healthy Steady State

The healthy equilibrium $(0, 0, 0, \frac{s}{d})$ represents the case when there are no leukemic cells. We can linearize the system about this point to obtain the following.

$$\dot{y_0} = -a_0 y_0 + b_1 y_1, \tag{5.6a}$$

$$\dot{y_1} = a_0 y_0 + (-b_1 + r - \frac{\mu s}{d}) y_1, \tag{5.6b}$$

$$\dot{y_2} = a_1 y_1 - (d_2 + \frac{\mu s}{d}) y_2, \tag{5.6c}$$

$$\dot{z} = \frac{\alpha s}{d} y_2 - dz. \tag{5.6d}$$

Thus, the matrix of this system is

$$A = \begin{pmatrix} -a_0 & b_1 & 0 & 0 \\ a_0 & -b_1 + r - \frac{\mu s}{d} & 0 & 0 \\ 0 & a_1 & -d_2 - \frac{\mu s}{d} & 0 \\ 0 & 0 & \frac{\alpha s}{d} & -d \end{pmatrix}.$$

This matrix has a characteristic polynomial

$$\begin{aligned} \chi_A(X) &= (X + d)(X + d_2 + \frac{\mu s}{d})[(X + b_1 - r + \frac{\mu s}{d})(X + a_0) - a_0 b_1] \\ &= (X + d)(X + d_2 + \frac{\mu s}{d})(X^2 + (a_0 + b_1 - r + \frac{\mu s}{d})X + (-r + \frac{\mu s}{d})). \end{aligned}$$

Define $f(X) = X^2 + (a_0 + b_1 - r + \frac{\mu s}{d})X + (-r + \frac{\mu s}{d})$. It is clear that $\lambda_1 = -d$ and $\lambda_2 = -d_2 - \frac{\mu s}{d}$ are two eigenvalues of A. The other two eigenvalues are the roots of f. Suppose $rd < \mu s$. Then $f(0) > 0$ and $f'(0) > 0$, so the remaining two eigenvalues have negative real part, making the healthy equilibrium stable. If $rd > \mu s$, then $f(0) < 0$, so it follows that one of the remaining eigenvalues is real and positive, making this equilibrium unstable. We are

primarily interested in the latter case, so for the remainder of this discussion, we will assume that $rd > \mu s$. Recall that this assumption implies that $P(0) < 0$, so P will have a zero on $(0, y_{min})$.

5.4 Steady States Without Suppression of Activated Immune Cells

The polynomial P given in Equation (5.3) has degree five. We can simplify the problem by adjusting our immunosuppression parameters ϵ_1 and ϵ in one of two ways.

- Set $\epsilon_1 = 0$. That is, assume that immunosuppression only affects the activation and expansion of immune cells but does not affect an activated immune cell's efficacy at killing leukemic cells.

- Set $\epsilon_1 = \epsilon$. That is, assume that immunosuppression affects the activation and efficacy of immune cells equally.

Both assumptions reduce P to a degree three polynomial. For now, we consider the first case, as parameter estimates suggest that this is reasonable.

By setting $\epsilon_1 = 0$, we arrive at the following model

$$\dot{y}_0 = b_1 y_1 - a_0 y_0, \tag{5.7a}$$

$$\dot{y}_1 = a_0 y_0 - b_1 y_1 + r y_1 (1 - \frac{y_1}{K}) - \mu y_1 z, \tag{5.7b}$$

$$\dot{y}_2 = a_1 y_1 - d_2 y_2 - \mu y_2 z, \tag{5.7c}$$

$$\dot{z} = s - dz + \alpha \frac{y_2 z}{1 + \epsilon y_2^2}. \tag{5.7d}$$

and the polynomial

$$P(X) = (X - y_{min})(X - y_{max})(X - M) + \frac{\mu s}{\epsilon r d}(M + \frac{r}{d_2} X)(1 + \epsilon X^2). \tag{5.8}$$

We can expand this polynomial in the following way:

$$\begin{aligned} P(X) &= X^3(1+\frac{\mu s}{dd_2}) - X^2(M + y_{min} + y_{max} - M\frac{\mu s}{rd}) \\ &\quad + X(My_{min} + My_{max} + y_{min}y_{max} + \frac{\mu s}{\epsilon dd_2}) - (My_{min}y_{max} - M\frac{\mu s}{\epsilon rd}) \\ &= X^3(1+\frac{\mu s}{dd_2}) - X^2(y_{min} + y_{max} + M(1 - \frac{\mu s}{rd})) \\ &\quad + X(My_{min} + My_{max} + y_{min}y_{max}(1+\frac{\mu s}{dd_2})) - My_{min}y_{max}(1 - \frac{\mu s}{rd}) \\ &= X^3\omega_+ - X^2(y_{min} + y_{max} + M\omega_-) \\ &\quad + X(My_{min} + My_{max} + y_{min}y_{max}\omega_+) - My_{min}y_{max}\omega_-. \end{aligned}$$

Here, $\omega_+ = 1 + \frac{\mu s}{dd_2}$ and $\omega_- = 1 - \frac{\mu s}{rd}$. Since we want the healthy equilibrium to be unstable, it follows that $rd > \mu s$ and therefore $\omega_- > 0$. Therefore, P has alternating signs, so by Descartes' rule of signs, P cannot have any negative roots. Because P has odd degree, it must therefore have either 1 or 3 real positive roots.

Proposition 5.4.1 *If M satisfies*

$$M > max\left\{\frac{2Y}{\omega_-}(2\sqrt{\frac{\omega_+}{\omega_-}(\frac{\omega_+}{\omega_-} - 1)} + 2\frac{\omega_+}{\omega_-} - 1), \frac{y_{min}(2\omega_+ - 1) - y_{max}}{\omega_-}\right\}, \tag{5.9}$$

then P has three positive roots, one in $(0, y_{min})$ and two in (y_{max}, M).

Proof Since $P(0) < 0 < P(y_{min})$, P has a root on $(0, y_{min})$. If M satisfies Equation (5.9), then $M > y_{max}$. We will now show that P has two roots on (y_{max}, M) by finding a value of $X \in (y_{max}, M)$ such that $P(X) < 0$. Since $P(y_{max}) > 0$ and $P(M) > 0$ the result will follow immediately.

We begin by searching for $X = cM$ for a positive constant c. Consider $P(cM)$:

$$\begin{aligned} P(cM) &= (cM)^3\omega_+ - (cM)^2(y_{min} + y_{max} + M\omega_-) \\ &\quad +cM(My_{min} + My_{max} + y_{min}y_{max}\omega_+) - My_{min}y_{max}\omega_- \\ &= c^2M^3(c\omega_+ - \omega_-) + cM^2(y_{min}(1-c) + y_{max}(1-c)) \\ &\quad +My_{min}y_{max}(c\omega_+ - \omega_-) \\ &= M[(c^2M^2 + y_{min}y_{max})(c\omega_+ - \omega_-) + M(y_{min} + y_{max})c(1-c)]. \end{aligned}$$

If we assume that $c < \frac{\omega_-}{\omega_+} < 1$, then we can produce the following upper bound:

$$\begin{aligned} P(cM) &< M[c^2M^2(c\omega_+ - \omega_-) + M(y_{min} + y_{max})c(1-c)] \\ &< cM^2[cM(c\omega_+ - \omega_-) + (y_{min} + y_{max})(1-c)] \\ &< cM^2[c^2M\omega+ - c(M\omega_- + 2Y) + 2Y]. \end{aligned}$$

Define $Q(c) = c^2M\omega+ - c(M\omega_- + 2Y) + 2Y$. Then, Q is a degree two polynomial with determinant

$$\begin{aligned} \Delta &= (M\omega_- + 2Y)^2 - 4(M\omega+)(2Y) \\ &= M^2\omega_-^2 + 4MY\omega_-(1 - 2\frac{\omega_+}{\omega_-}) + 4Y^2 \\ &= (M\omega_- + 2Y(1 - 2\frac{\omega_+}{\omega_-}))^2 - 4Y^2((1 - 2\frac{\omega_+}{\omega_-})^2 - 1) \\ &= (M\omega_- - 2Y(2\frac{\omega_+}{\omega_-} - 1))^2 - 16Y^2(\frac{\omega_+}{\omega_-}(\frac{\omega_+}{\omega_-} - 1)). \end{aligned}$$

By solving for M, we find that $\Delta > 0$ when

$$M > \frac{2Y}{\omega_-}(2\sqrt{\frac{\omega_+}{\omega_-}(\frac{\omega_+}{\omega_-} - 1)} + 2\frac{\omega_+}{\omega_-} - 1).$$

When $\Delta > 0$, Q has two real roots and is negative at $c = \frac{M\omega_- + 2Y}{2M\omega_+}$. Since $\frac{\omega_+}{\omega_-} > 1$, it follows

that

$$\omega_-^2(2\sqrt{\frac{\omega_+}{\omega_-}(\frac{\omega_+}{\omega_-}-1)}+2\frac{\omega_+}{\omega_-}-1)>1.$$

Therefore $M>\frac{2Y}{\omega_-}$ which implies that $c<\frac{\omega_-}{\omega_+}<1$. Thus,

$$P(cM)=P(\frac{M\omega_-+2Y}{2M\omega_+}M)<cM^2Q(\frac{M\omega_-+2Y}{2M\omega_+})<0.$$

Since $c<1$ we know that $cM\in(0,M)$. However, it is not clear whether $cM\in(0,y_{min})$ or $cM\in(y_{max},M)$ (we know that P is positive in $[y_{min},y_{max}]$). By ensuring that

$$M>\frac{y_{min}(2\omega_+-1)-y_{max}}{\omega_-},$$

it follows that $cM>y_{min}$ and hence $cM\in(y_{max},M)$. We conclude that P has two roots on (y_{max},M). ∎

When $y_{min}<M<y_{max}$, the theorem does not apply, and there will be one equilibrium $(y_{0,low},y_{1,low},y_{2,low}\approx y_{min},z_{low})$. When $M<y_{min}$, there will again be only one equilibrium, near $(\frac{b_1}{a_0}K,K,M,\frac{s}{d}\frac{y_{min}y_{max}}{(y_{min}-M)(y_{max}-M)})$.

The bound given by Equation (5.9) is not necessarily the minimum lower bound. However, this proposition does provide a sufficient condition that guarantees three equilibria.

5.5 Stability Analysis

We will now shift our attention to the stability of the fixed points of the system given by Equations (5.7a)-(5.7d). To approach this problem, we further simplify our model by no longer distinguishing between cycling and quiescent stem cells. We arrive at the following

model:

$$\dot{y}_1 = ry_1(1-\frac{y_1}{K}) - \mu y_1 z, \tag{5.10a}$$

$$\dot{y}_2 = a_1 y_1 - d_2 y_2 - \mu y_2 z, \tag{5.10b}$$

$$\dot{z} = s - dz + \alpha \frac{y_2 z}{1+\epsilon y_2^2}. \tag{5.10c}$$

We note that all of the analysis up to this point holds for this new system. That is, removing the quiescent stem cell compartment does not affect the number of steady states or the stability of the healthy equilibrium. Although it is possible that this simplification may (in some cases) affect the stability of the other fixed points, this analysis provides valuable insight into the original system.

We start with the low equilibrium $(\bar{y_1}, \bar{y_2}, \bar{z})$ satisfying $\bar{y_2} \in (0, y_{min})$. In general, the matrix of the system (5.10a)-(5.10c) linearized about $(\bar{y_1}, \bar{y_2}, \bar{z})$ is given by

$$B = \begin{pmatrix} r - 2\frac{r}{K}\bar{y_1} - \mu\bar{z} & 0 & -\mu\bar{y_1} \\ a_1 & -d_2 - \mu\bar{z} & -\mu\bar{y_2} \\ 0 & \alpha\bar{z}\frac{1-\epsilon\bar{y_2}^2}{(1+\epsilon\bar{y_2}^2)^2} & -d + \alpha\frac{\bar{y_2}}{1+\epsilon\bar{y_2}^2} \end{pmatrix}.$$

Since $(\bar{y_1}, \bar{y_2}, \bar{z})$ is a positive fixed point, we can rewrite this as

$$B = \begin{pmatrix} -\frac{r}{K}\bar{y_1} & 0 & -\mu\bar{y_1} \\ a_1 & -a_1\frac{\bar{y_1}}{\bar{y_2}} & -\mu\bar{y_2} \\ 0 & \alpha\bar{z}\frac{1-\epsilon\bar{y_2}^2}{(1+\epsilon\bar{y_2}^2)^2} & -\frac{s}{\bar{z}} \end{pmatrix}. \tag{5.11}$$

We wish to prove that the low equilibrium is stable. To do this, we will make use of the following Lemma.

Lemma 5.5.1 *Consider a polynomial $P(X) = X^3 + aX^2 + bX + c$ with positive coefficients a, b, and c. If $ab > c$, then the dominant root of P has negative real part.*

Proof Because P has positive coefficients, it cannot have positive real roots by Descartes' rule of signs. Also, since $P(0) = c > 0$, P must have at least one real negative root λ. The remaining two roots are either negative real or complex. If they are negative, then we are done. If the roots are complex, then we wish to show that the real part is negative. We can factor P as

$$P(X) = (X - \lambda)(X^2 + (a + \lambda)X + (b + a\lambda + \lambda^2)).$$

Denote the complex roots as z and $\bar{z}$. Then since

$$X^2 + (a + \lambda)X + (b + a\lambda + \lambda^2) = (X - z)(X - \bar{z}),$$

then it follows that

$$\begin{aligned} a + \lambda &= -(z + \bar{z}) = -2\,\mathrm{Re}\, z, \\ b + a\lambda + \lambda^2 &= z\bar{z} = (\mathrm{Re}\, z)^2 + (\mathrm{Im}\, z)^2. \end{aligned}$$

Now, we observe that $P(-a) = -ab + c < 0$ since $ab > c$. Since λ is the only negative root of P, it must be that $-a < \lambda$. Hence, $\mathrm{Re}\, z = -\frac{a+\lambda}{2} < 0$. ∎

Proposition 5.5.2 *The low equilibrium* $(\bar{y_1}, \bar{y_2}, \bar{z})$ *satisfying* $\bar{y_2} \in (0, y_{min})$ *is asymptotically stable.*

Proof We first observe that the all terms in Equation (5.11) have sign independent of the fixed point coordinates, except $\alpha\bar{z}\frac{1-\epsilon\bar{y_2}^2}{(1+\epsilon\bar{y_2}^2)^2}$. Define $E = \frac{1-\epsilon\bar{y_2}^2}{(1+\epsilon\bar{y_2}^2)^2}$. Since $\epsilon = \frac{1}{y_{min}y_{max}}$, it follows that $\epsilon\bar{y_2}^2 < 1$, so $E > 0$. (If $\bar{y_2} > y_{max}$, then $E < 0$.)

Consider the characteristic polynomial χ_B of B.

$$\begin{aligned}
\chi_B(X) &= (X - \frac{r}{K}\bar{y_1})((X + a_1\frac{\bar{y_1}}{\bar{y_2}})(X + \frac{s}{\bar{z}}) + \mu\alpha\bar{y_2}\bar{z}E) + a_1\mu\alpha\bar{y_1}\bar{z}E \\
&= X^3 + X^2(\frac{r}{K}\bar{y_1} + a_1\frac{\bar{y_1}}{\bar{y_2}} + \frac{s}{\bar{z}}) \\
&\quad + X(\frac{r}{K}\bar{y_1}(a_1\frac{\bar{y_1}}{\bar{y_2}} + \frac{s}{\bar{z}}) + a_1\frac{\bar{y_1}}{\bar{y_2}}\frac{s}{\bar{z}} + \mu\alpha\bar{y_2}\bar{z}E) \\
&\quad + (\frac{r}{K}\bar{y_1}(a_1\frac{\bar{y_1}}{\bar{y_2}}\frac{s}{\bar{z}} + \mu\alpha\bar{y_2}\bar{z}E) + a_1\mu\alpha\bar{y_2}\bar{z}E)) \\
&= X^3 + X^2(r + d_2 + \frac{s}{\bar{z}}) + X(\frac{r}{K}\bar{y_1}(a_1\frac{\bar{y_1}}{\bar{y_2}} + \frac{s}{\bar{z}}) + a_1\frac{\bar{y_1}}{\bar{y_2}}\frac{s}{\bar{z}} + \mu\alpha\bar{y_2}\bar{z}E) \\
&\quad + (\mu\alpha(r + d_2)\bar{y_2}\bar{z}E + \frac{r}{K}\bar{y_1}a_1\frac{\bar{y_1}}{\bar{y_2}}\frac{s}{\bar{z}}).
\end{aligned}$$

We simplified the above expression using the fact that $\frac{r}{K}\bar{y_1} + a_1\frac{\bar{y_1}}{\bar{y_2}} = r + d_2$.

Since $\bar{y_2} \in (0, y_{min})$, $E > 0$. Thus, χ_B has positive coefficients. We would like to apply the previous lemma to complete our proof. Thus, we consider

$$\begin{aligned}
a_\chi b_\chi - c_\chi &= (r + d_2 + \frac{s}{\bar{z}})(\frac{r}{K}\bar{y_1}(a_1\frac{\bar{y_1}}{\bar{y_2}} + \frac{s}{\bar{z}}) + a_1\frac{\bar{y_1}}{\bar{y_2}}\frac{s}{\bar{z}} + \mu\alpha\bar{y_2}\bar{z}E) \\
&\quad - (\mu\alpha(r + d_2)\bar{y_2}\bar{z}E + \frac{r}{K}\bar{y_1}a_1\frac{\bar{y_1}}{\bar{y_2}}\frac{s}{\bar{z}}) \\
&= (r + d_2)(\frac{r}{K}\bar{y_1}(a_1\frac{\bar{y_1}}{\bar{y_2}} + \frac{s}{\bar{z}}) + a_1\frac{\bar{y_1}}{\bar{y_2}}\frac{s}{\bar{z}}) \\
&\quad + \frac{s}{\bar{z}}(\frac{r}{K}\bar{y_1}(a_1\frac{\bar{y_1}}{\bar{y_2}} + \frac{s}{\bar{z}}) + a_1\frac{\bar{y_1}}{\bar{y_2}}\frac{s}{\bar{z}} + \mu\alpha\bar{y_2}\bar{z}E - \frac{r}{K}\bar{y_1}a_1\frac{\bar{y_1}}{\bar{y_2}}) \\
&= (r + d_2)((r + d_2)\frac{s}{\bar{z}} + \frac{r}{K}\bar{y_1}a_1\frac{\bar{y_1}}{\bar{y_2}}) + \frac{s}{\bar{z}}((r + d_2)\frac{s}{\bar{z}} + \mu\alpha\bar{y_2}\bar{z}E) \\
&> 0.
\end{aligned}$$

By the previous lemma, χ_B has a dominant root with negative real part, so the dominant eigenvalue of B has negative real part. We conclude that the low equilibrium is asymptotically stable. ∎

The low equilibrium should be attracting for sufficiently close initial conditions. However, the basin of attraction is so small that almost all solutions converge to the large

equilibrium. Thus, a successful treatment should either expand the basin of attraction of the low equilibrium or eliminate the larger equilibria.

5.5.1 Special Case: $s_z = 0$

We consider the case when $s_z = 0$ because it allows us to fully classify the equilibria. These classifications provide insights about the stability of the equilibria when s_z is small. We consider the following system:

$$\dot{y}_1 = r y_1(1 - \frac{y_1}{K}) - \mu y_1 z, \tag{5.12a}$$

$$\dot{y}_2 = a_1 y_1 - d_2 y_2 - \mu y_2 z, \tag{5.12b}$$

$$\dot{z} = (\alpha \frac{y_2}{1 + \epsilon y_2^2} - d) z. \tag{5.12c}$$

We will first assume that $\alpha^2 > 4\epsilon d^2$ and $y_{max} < M$. Then we can rewrite $\dot{z}$ as

$$\dot{z} = \frac{-d\epsilon(y - y_{min})(y - y_{max})}{1 + \epsilon y_2^2} z.$$

It follows that $\dot{z} = 0$ iff $z = 0$, $y_2 = y_{min}$, or $y_2 = y_{max}$. The first case produces the equilibria $(0, 0, 0)$ and $(K, M, 0)$. The other two cases produce the equilibria $(y_1(y_{min}), y_{min}, z(y_{min}))$ and $(y_1(y_{max}), y_{max}, z(y_{max}))$ where

$$\begin{aligned} y_1(y_2) &= \frac{(r + d_2) y_2}{a_1 + \frac{r}{K} y_2}, \\ z(y_2) &= \frac{r}{\mu}(1 - \frac{y_1}{K}). \end{aligned}$$

Thus, we have four equilibria. Since $s = 0$, the condition for the healthy equilibrium $(0, 0, 0)$ to be unstable reduces to $rd > 0$. Hence, the healthy equilibrium is always unstable. Further, by Proposition 5.5.2, $(y_1(y_{min}), y_{min}, z(y_{min}))$ is asymptotically stable. We wish to classify the remaining two equilibria.

First, consider $(y_1(y_{max}), y_{max}, z(y_{max}))$. The matrix of the system linearized about this equilibrium C is

$$C = \begin{pmatrix} -\frac{r}{K}\bar{y_1} & 0 & -\mu\bar{y_1} \\ a_1 & -a_1\frac{\bar{y_1}}{\bar{y_2}} & -\mu\bar{y_2} \\ 0 & \alpha\bar{z}\frac{1-\epsilon\bar{y_2}^2}{(1+\epsilon\bar{y_2}^2)^2} & 0 \end{pmatrix}. \tag{5.13}$$

with characteristic polynomial

$$\begin{aligned} \chi_C(X) &= (X + \frac{r}{K}\bar{y_1})[X(X + a_1\frac{\bar{y_1}}{\bar{y_2}}) + \alpha\mu\bar{y_2}\frac{1-\epsilon\bar{y_2}^2}{(1+\epsilon\bar{y_2}^2)^2}] \\ &\quad +a_1\alpha\mu\bar{y_1}z\frac{1-\epsilon\bar{y_2}^2}{(1+\epsilon\bar{y_2}^2)^2} \\ &= X^3 + X^2(\frac{r}{K}\bar{y_1} + a_1\frac{\bar{y_1}}{\bar{y_2}}) + X(\frac{r}{K}a_1\frac{\bar{y_1}^2}{\bar{y_2}} + \alpha\mu\bar{y_2}z\frac{1-\epsilon\bar{y_2}^2}{(1+\epsilon\bar{y_2}^2)^2}) \\ &\quad +\alpha\mu y_1 z\frac{1-\epsilon\bar{y_2}^2}{(1+\epsilon\bar{y_2}^2)^2}(\frac{r}{K}\bar{y_2} + a_1). \end{aligned}$$

Since $\bar{y_2} = y_{max}$, it follows that $1 - \epsilon\bar{y_2}^2 < 0$, so $\chi_C(0) < 0$. Therefore, χ_C must have at least one real positive root, so $(y_1(y_{max}), y_{max}, z(y_{max}))$ is unstable.

The last equilibrium $(K, M, 0)$ represents the case when the leukemic population fully overcomes and suppresses the immune system. The matrix of the linearized system about this fixed point is

$$D = \begin{pmatrix} -r & 0 & -\mu K \\ a_1 & -d_2 & -\mu M \\ 0 & 0 & -d + \frac{\alpha M}{1+\epsilon M^2} \end{pmatrix}. \tag{5.14}$$

The characteristic polynomial is

$$\chi_D(X) = [X + r][X + d_2][X - (\frac{\alpha M}{1 + \epsilon M^2} - d)],$$

so the eigenvalues of (5.14) are $\lambda_1 = -r$, $\lambda_2 = -d_2$, and $\lambda_3 = \frac{\alpha M}{1+\epsilon M^2} - d$. Since $M > y_{max}$, it follows that all three eigenvalues are negative, so $(K, M, 0)$ is a stable node.

K	Stem cell carrying capacity	$4.2872r/(r+d_1)$
d_1	Stem cell death rate	0.00225
a_1	Differentiation and expansion rate	$2.16 \cdot 10^6$
d_2	Mature cell death rate	0.06
s	Immune cell source term	120 * d
$y_1(0)$	Initial stem cell concentration	K
$y_2(0)$	Initial mature cell concentration	a_1K/d_2
$z(0)$	Initial immune concentration	s/d

Table 5.1: Universal parameters and initial conditions for our simplified model.

When $\alpha^2 < 4\epsilon d^2$, no immune window exists, and $\dot{z} < 0$ whenever $z > 0$. Hence, the only positive equilibrium is $(K, M, 0)$, and it is stable, by a similar argument to the one given above. A saddle-node bifurcation occurs when $\alpha^2 = 4\epsilon d^2$, provided $y_{min} = y_{max} < M$.

When $M < y_{min}$, the only positive equilibrium is $(K, M, 0)$, and it is stable. Lastly, when $y_{min} < M < y_{max}$, there is only one positive equilibrium: $(y_1(y_{min}), y_{min}, z(y_{min}))$. By Proposition 5.5.2, it is stable.

Recall that treatment has the effect of decreasing M. As M approaches y_{max} from above, the two equilibria $(K, M, 0)$ and $(y_1(y_{max}), y_{max}, z(y_{max}))$ approach one another. There is a saddle-node bifurcation at $M = y_{max}$, after which $(M < y_{max})$, both equilibria are eliminated.

5.6 Numerical Simulations

Fits of our simplified model (Equations (5.10a)-(5.10c)) to data of two patients are shown in Figure 5.1. The universal parameters and initial conditions used in Figure 5.1 are provided in Table 5.1.

As in Chapter 4, IM is assumed to decrease the leukemic cells' differentiation rate a_1 by a factor inh to $a_1' = \frac{a_1}{inh}$. The treatment parameter, inh, and immune parameters, μ,

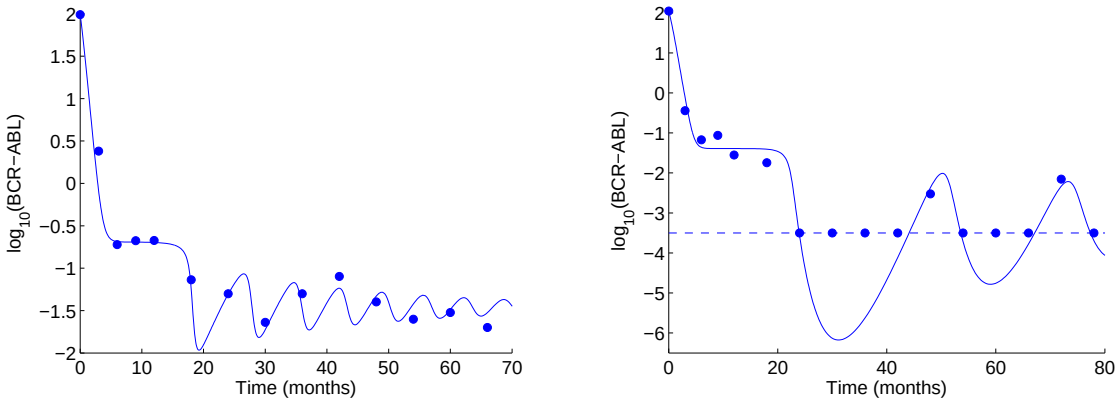

(a) (b)

Figure 5.1: We fit two representative patients to our simplified model given in Equations (5.10a)-(5.10c). Patient data is represented by dots, and our fits are shown as solid lines. The dashed line approximates the detection threshold, or the lowest detectable leukemia level. Dots along this line represent zero measurements, which indicate BCR-ABL ratios below the detection threshold. (a) This data corresponds to patient 4 in Table 4.2. The following patient-specific parameter values were used: $d = 0.127$, $\mu = 10^{-8.18}$, $y_{min} = 10^{4.50}$, $y_{max} = 10^{5.34}$, $inh = 10^{2.85}$, $r = 0.0134$. (b) This patient proved difficult to fit when varying only the drug and immune parameters. By varying both r and d, the model is able to reproduce the slower fluctuations present in the data. The following parameters were used: $d = 0.006$, $\mu = 10^{-9.25}$, $y_{min} = 10^{2.97}$, $y_{max} = 10^{5.26}$, $inh = 10^{3.64}$, and $r = 0.0276$.

α, d, and ϵ, are allowed to vary between patients. We additionally allow r to vary, as it characterizes the aggressiveness of the leukemic clone. Varying both r and d allows us to reproduce slower fluctuations, as seen in Figure 5.1(b).

We now consider the effect of the treatment parameter inh on the number and stability of the steady states. Our results for the patient in Figure 5.1(a) are shown in Figure 5.2. For small values of inh, four equilibria exist: the healthy equilibrium $(0, 0, \frac{s}{d})$ (dark blue), the low equilibrium $(y_{1,low}, y_{2,low} \approx y_{max}, z_{low})$ (green), the intermediate equilibrium $(y_{1,int}, y_{2,int} \approx y_{max}, z_{int})$ (red), and the high equilibrium near $(K, M, \frac{s}{d})$ (light blue). The

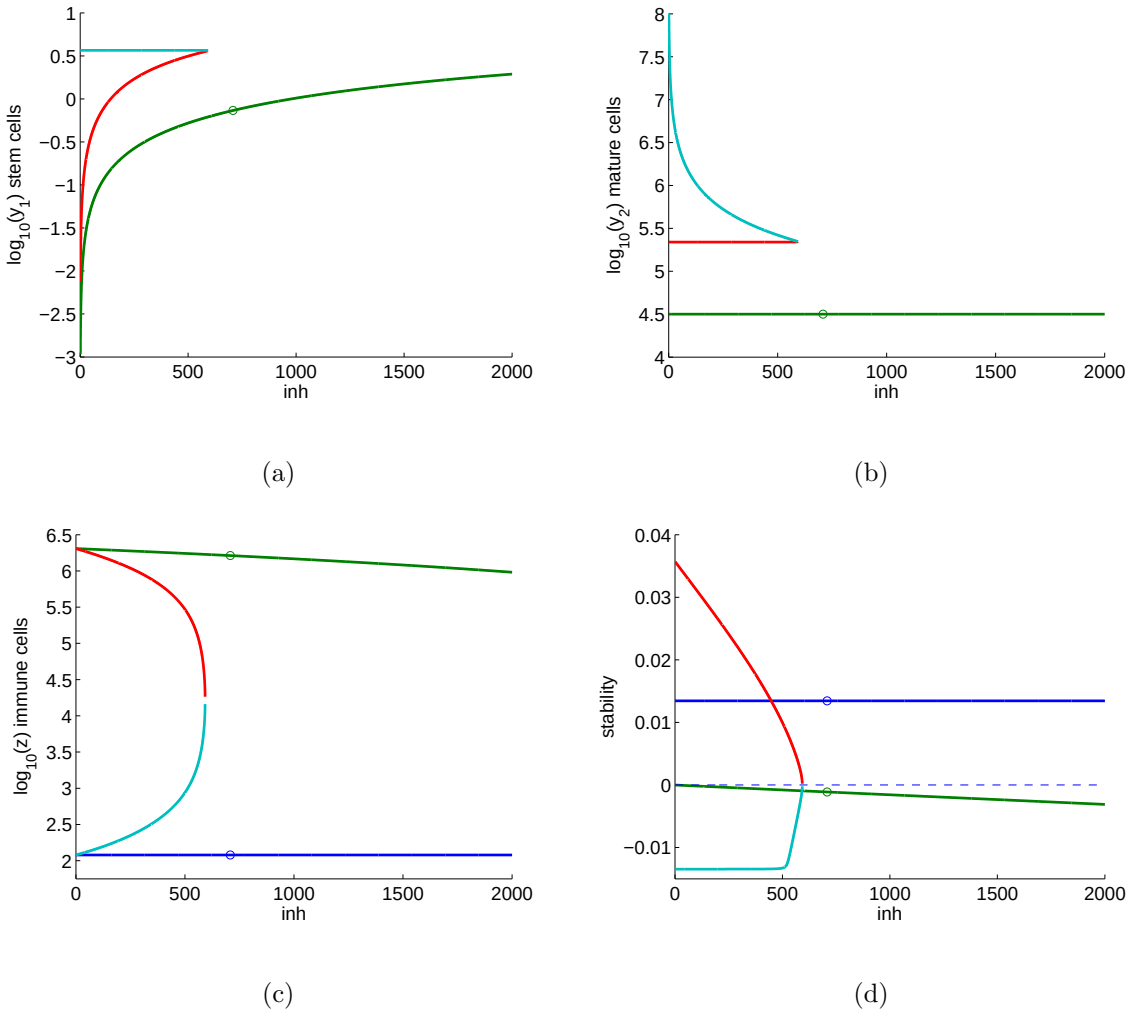

Figure 5.2: The steady states and their stability are plotted as functions of inh. For each value of inh, there are at most four equilibria: the healthy equilibrium $(0, 0, \frac{s}{d})$ represented by dark blue, the low equilibrium $(y_{1,low}, y_{2,low} \approx y_{max}, z_{low})$ represented in green, the intermediate equilibrium $(y_{1,int}, y_{2,int} \approx y_{max}, z_{int})$ represented in red, and the high equilibrium near $(K, M, \frac{s}{d})$ represented in light blue. However, for large values of inh, the middle and high steady states are eliminated. Circles mark the inh value (707.95) used in our model simulation shown in Figure 5.1(a). (a) Stem cell concentration y_1 is plotted against inh. Interestingly, $y_{1,low}$ and $y_{1,int}$ are increasing functions of inh. (b) Mature leukemic concentration y_2 is plotted against inh. A saddle-node bifurcation occurs when $inh \approx 593$, and the low and high equilibria are eliminated. (c) Immune cell concentration z is plotted against inh. (d) The real part of the dominant eigenvalue is plotted against inh. When these values are above (below) the dashed line $\lambda = 0$, the corresponding fixed points are unstable (stable). Hence, we see that the healthy and intermediate steady states are always unstable, while the low and high equilibria are always stable.

healthy and intermediate equilibria are always unstable, as indicated by negative real parts of the dominant eigenvalues in Figure 5.2(d). The low and high equilibria are stable. These stability results are in agreement with our analysis in the previous sections.

Although both the low and high equilibria are stable, the high equilibrium has a larger basin of attraction, so most simulations converge to this equilibrium rather than the low equilibrium. Since we would like treatment to decrease the leukemic population significantly, one possible strategy is to drive the leukemic population toward the low equilibrium, either by expanding the basin of attraction of the low equilibrium or by eliminating the high equilibrium. As we will see, the latter occurs in our simulation.

As inh increases, the mature leukemic concentration of the high equilibrium $y_{2,high}$ decreases. When $inh \approx 593$, there is a saddle-node bifurcation. The high stable equilibrium collides with the unstable intermediate equilibrium, and both are eliminated for larger values of inh. This result also supports our analysis. In our model simulation shown in Figure 5.1(a), $inh = 707.95$. This value is indicated in Figure 5.2 with circles. Thus, during IM therapy, only the stable low equilibrium and unstable healthy equilibrium exist, so the patient converges to the low equilibrium.

Interestingly, in Figure 5.2(a), we see that the steady state leukemic stem cell concentration is an increasing function of inh. Large values of inh, while effective against the mature leukemic population, allow a large residual leukemic stem cell population to persist. As inh increases, the leukemic stem cell concentrations approach the carrying capacity K, which is approximately marked by the light blue line. A large leukemic stem cell population increases the risk of resistant subpopulations that could eventually cause relapse. This result suggests that treatment should achieve an inh value large enough to drive the leukemia to the

low equilibrium but small enough to prevent a large residual leukemic stem cell population.

Chapter 6: Applications and Extensions

In this section, we apply our modeling framework developed in Chapter 4 to studying various aspects of CML. We first present fits of our model to patients treated with second-generation TKIs nilotinib and dasatinib. We then expand our model in order to study drug resistance, treatment cessation, and combination therapy.

6.1 Dynamics During Therapy with Second-Generation TKIs

A group of 46 patients with CML was monitored at the Centre Hospitaller Lyon Sudd during therapy with second-generation TKIs. One group of 21 patients was treated with dasatinib (100 gm daily), while the other 25 patients were treated with nilotinib (600 gm daily). The BCR-ABL ratios were measured at diagnosis, months 3, 6, 9, and 12, and every six months thereafter. The average follow-up time for these patients is 25.14 months (range: 2.06 - 62.33), with an average of 6.98 measurements during this time (range: 2 - 14). Six dasatinib patients change TKIs, one of whose disease progresses. Two nilotinib patients also change TKIs, both of whose disease progresses.

In comparison to the IM data, the average follow-up time is much shorter. Only seven patients (4 dasatinib, 3 nilotinib) have at least ten measurements. We chose not to include any patients taking dasatinib or nilotinib in [17] because of the shorter follow-up times and

the smaller number of patients per drug. A shorter follow-up time makes it more difficult to evaluate our model's ability to fit patients treated with second-generation TKIs. It is also difficult to classify a patient's immune response to CML, as such a response during IM therapy seems to occur only after several months to a few years of therapy. Still, 23 of the 38 patients who do not relapse and whose disease does not progress show at least one increase in BCR-ABL ratio during therapy. Thirteen even show increases that are larger than 0.5-log. Our previous modeling results suggest that these fluctuations may represent a patient's immune response to CML.

In order to further investigate this phenomenon, we applied the model in Equations (4.1a)-(4.1e) to these patients. Fits to patients treated with dasatinib are shown in Figures 6.1(a)-6.1(c), while fits to patients treated with nilotinib are shown in Figures 6.1(d)-6.1(f). The universal parameter values used in these simulations are the same ones in Table 4.1 of Chapter 4. Patient-specific parameters are given in Table 6.1. These particular patients were chosen because they have the largest number of measurements. However, we note that the patients in Figures 6.1(b), 6.1(c), and 6.1(e) change TKIs (at months 20, 28, and 9), and the patient in Figure 6.1(e) shows disease progression (at month 10). The remaining three patients have no adverse events.

Patient	inh_1	inh_2	d_z	μ	y_{min}	y_{max}
1	21.056	349.677	0.119	$3.972 \cdot 10^{-8}$	$1.246 \cdot 10^{4}$	$3.401 \cdot 10^{5}$
2	40.701	14.192	0.122	$1.039 \cdot 10^{-7}$	$1.481 \cdot 10^{5}$	$3.483 \cdot 10^{5}$
3	1.122	810.343	0.046	$6.314 \cdot 10^{-7}$	$4.488 \cdot 10^{4}$	$2.291 \cdot 10^{5}$
4	1.026	11253.417	0.021	$1.558 \cdot 10^{-8}$	$2.309 \cdot 10^{2}$	$2.103 \cdot 10^{4}$
5	83.619	15.117	0.084	$2.488 \cdot 10^{-7}$	$6.478 \cdot 10^{4}$	$2.016 \cdot 10^{5}$
6	18.676	161.473	0.047	$1.492 \cdot 10^{-8}$	$1.456 \cdot 10^{4}$	$8.915 \cdot 10^{4}$

Table 6.1: Patient-specific parameter values for patients shown in Figure 6.1.

Similar to patients treated with IM, patients treated with second-generation TKIs

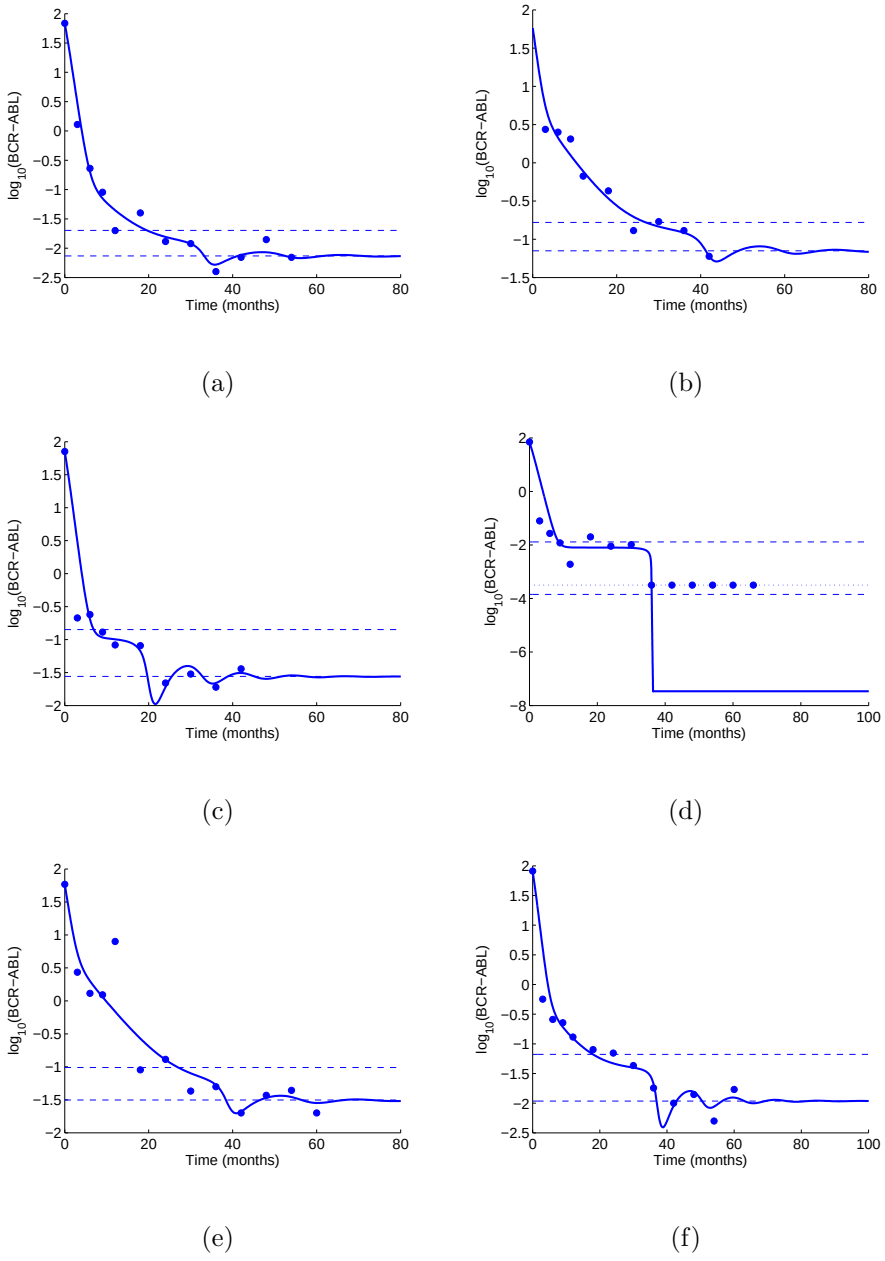

Figure 6.1: Fits of the model given in Equations (4.1a)-(4.1e) to patients treated with second-generation TKIs. Patients were treated with either dasatinib (Figures 6.1(a)-6.1(c)) or nilotinib (Figures 6.1(d)-6.1(f)). The base-10 log of the BCR-ABL ratio is plotted against time, in months. Dots represent patient data, and the solid lines represent the simulations. Dashed lines show the BCR-ABL ratios that correspond to the ends of immune window, y_{min} and y_{max}. Dotted lines approximate the minimum leukemic level that is detectable by RT-PCR. Dots along this line represent zero measurements, meaning CML cells were not detected.

appear to exhibit three phases of leukemia reduction: a first sharp exponential decline, a second slower exponential decline, and a period of fluctuations that may be caused by leukemia-immune interactions. Patients' immune windows tend to span approximately one order of magnitude. The patient shown in Figure 6.1(d) has a larger immune window. Interestingly, our model suggests that this patient's immune response to CML results in eradication of the disease. The patient's BCR-ABL ratio levels off at around 10^{-7} which corresponds to a leukemic stem cell concentration of less than one cell. Overall, these fits to patients' initial responses to second-generation TKIs suggest that this model is capable of capturing the dynamics of patients treated with both IM and second-generation TKIs dasatinib and nilotinib.

6.2 Incorporating Drug Resistance

We study the effects of pre-existing resistant leukemia by incorporating sensitive and resistant subpopulations into our model, resulting in the following system of ODEs.

$$\dot{x}_1 = r_x x_1(1 - \frac{x_1 + y_1}{K_x}) - \frac{\mu x_1 z}{1 + \epsilon(x_2 + y_2)^2}, \tag{6.1a}$$

$$\dot{x}_2 = a_x x_1 - d_2 x_2 - \frac{\mu x_2 z}{1 + \epsilon(x_2 + y_2)^2}, \tag{6.1b}$$

$$\dot{y}_1 = r_y y_1(1 - \frac{x_1 + y_1}{K_y}) - \frac{\mu y_1 z}{1 + \epsilon(x_2 + y_2)^2}, \tag{6.1c}$$

$$\dot{y}_2 = a_y y_1 - d_2 y_2 - \frac{\mu y_2 z}{1 + \epsilon(x_2 + y_2)^2}, \tag{6.1d}$$

$$\dot{z} = s_z - d_z z + \frac{\alpha(x_2 + y_2) z}{1 + \epsilon(x_2 + y_2)^2}. \tag{6.1e}$$

In this model, sensitive leukemic cells x and resistant leukemic cells y are divided into stem cells (x_1 and y_1) and mature cells (x_2 and y_2). For simplicity, we do not further distinguish between cycling and quiescent leukemic cells nor do we include progenitor compartments.

Sensitive and resistant cells are described by the same pair of equations, except that their stem cell carrying capacities K and differentiation rates a may differ. Competition between sensitive and resistant cells is incorporated at the stem cell level with the terms $1 + \frac{x_1+y_1}{K_x}$ and $1 + \frac{x_1+y_1}{K_y}$.

Prior to treatment, sensitive and resistant leukemic populations are assigned the same parameter values. Specifically $r_x = r_y := r$, $K_x = K_y := K$, and $a_x = a_y := a$. TKI therapy is assumed to inhibit the sensitive leukemic population by decreasing its stem cell carrying capacity to $K'_x = \frac{K}{inh_0}$ and its differentiation rate to $a'_x = \frac{a}{inh_1}$. On the other hand, resistant leukemic cells are assumed to be completely resistant to TKIs, that is, $K'_y = K_y = K$ and $a'_y = a_y = a$. Initially, it is assumed that the sensitive population is at its equilibrium for the system without an immune response or a resistant subpopulation (that is $(x_1(0), x_2(0)) = (K_x, \frac{a_x K_x}{d_2})$). A small resistant population is introduced $(y_1(0), y_2(0)) = (1.6667 \cdot 10^{-3}, \frac{1.6667 \cdot 10^{-3} a_y}{d_2})$, and immune cells are set to $z(0) = \frac{s_z}{d_z}$.

We consider the effect of $inh := inh_0 inh_1$ on the time to relapse, which we define as a BCR-ABL ratio exceeding 1. Figure 6.2 shows the time to relapse as a function of inh. Figure 6.3 shows simulations of a patient's BCR-ABL ratio during treatment, for specific values of inh. It is clear from these figures that time to relapse is a nonmonotone function of drug inhibition. Specifically, in some cases, increasing the drug's effect results in an earlier time to relapse.

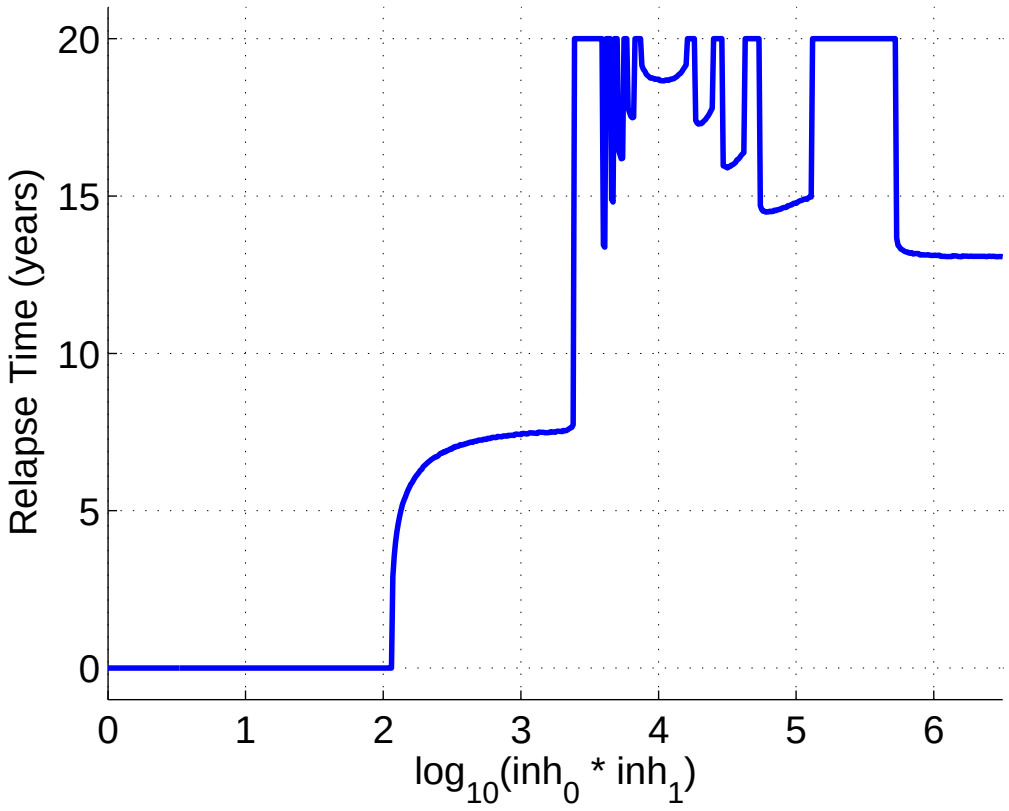

Figure 6.2: Relapse time is plotted as a function of $inh = inh_0 inh_1$. A relapse time of zero indicates that the patient's BCR-ABL ratio never falls below 1 during therapy. Simulations were run for 20 years. A relapse time of 20 years, therefore, indicates that the patient does not relapse during simulation. Initially relapse time is an increasing function of drug time. For larger values of inh, the immune system plays a significant role, and relapse time becomes a nonmonotone function of inh. In fact, an inh value that is too large can result in a faster relapse. The following parameter values are used in these simulations: $r = 0.008$, $K = 41.6667$, $a = 2.16 \cdot 10^5$, $d_2 = 0.06$, $\mu = 10^{-8}$, $s_z = 2.4$, $d_z = 0.02$, $y_{min} = 10^4$, $y_{max} = 10^5$, $inh_0 = 1.32$, $inh_1 = \frac{inh}{inh_0}$.

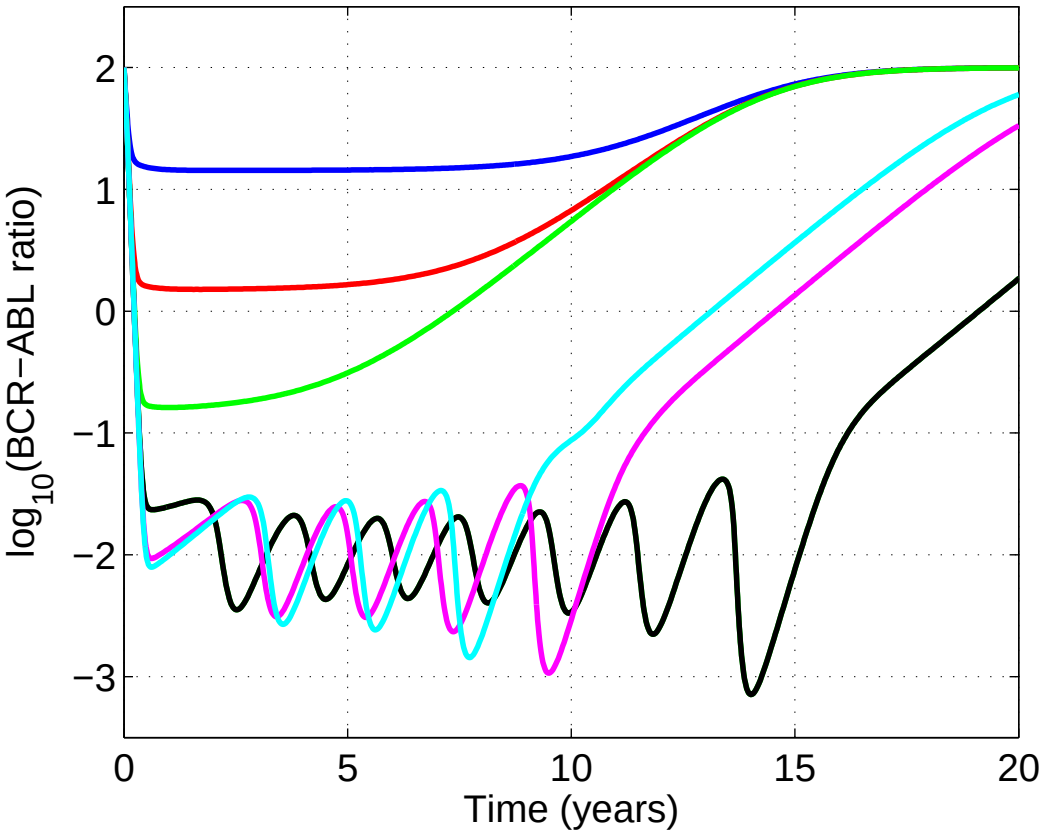

Figure 6.3: Simulations of a patient's BCR-ABL ratio for $inh = inh_0 inh_1 = 10^n$, $n = 1$ (blue), 2 (red), 3 (green), 4 (black), 5 (purple), 6 (light blue). All other parameters are those given in the caption of Figure 6.2. We see that $inh = 10^4$ results in the latest relapse, at about 19 years, which is over four years after the relapse times when $inh = 10^5$ or $inh = 10^6$.

6.3 IM Cessation

We now apply our mathematical model to study the dynamics of IM cessation and the potential benefits of carefully-timed vaccines. We incorporate vaccine cells v into our model as follows:

$$\dot{y}_0 = b_1 y_1 - a_0 y_0 - \frac{\mu y_0 z}{1+\epsilon y_3^2}, \tag{6.2a}$$

$$\dot{y}_1 = a_0 y_0 - b_1 y_1 + r y_1 (1 - \frac{y_1}{K}) - d_1 y_1 - \frac{\mu y_1 z}{1+\epsilon y_3^2}, \tag{6.2b}$$

$$\dot{y}_2 = \frac{a_1}{inh_1} y_1 - d_2 y_2 - \frac{\mu y_2 z}{1+\epsilon y_3^2}, \tag{6.2c}$$

$$\dot{y}_3 = \frac{a_2}{inh_2} y_2 - d_3 y_3 - \frac{\mu y_3 z}{1+\epsilon y_3^2}, \tag{6.2d}$$

$$\dot{z} = s_z - d_z z + \alpha_z \frac{(y_3+v) z}{1+\epsilon y_3^2}, \tag{6.2e}$$

$$\dot{v} = \phi_v(t) - d_v v - \frac{\mu v z}{1+\epsilon y_3^2}. \tag{6.2f}$$

Here, Equations (6.2a)-(6.2d) are the same as in Equations (4.1a)-(4.1e) in Chapter 4. Equation (6.2e) is similar to Equation (4.1e), except that the vaccine cells provide an additional stimulus to the immune cells. We assume that vaccine cells do not contribute to immunosuppression, hence they are not included in the denominators. Vaccine cells, which are represented by Equation (6.2f), are introduced at a rate $\phi_v(t)$ and die naturally at a rate d_v and as a result of an immune response at a maximal rate μ and with suppression constant ϵ. The source term is zero, except for the periods during which the vaccines are administered. Similar to [43], we assume that each vaccine is delivered over the course of a day.

Treatment cessation is simulated by reducing the inhibition parameters inh_1 and inh_2 to the values inh_1' and inh_2', thus resulting in partially restored proliferative capacities of leukemic progenitors and mature cells. If we were to assume that the pre-treatment and

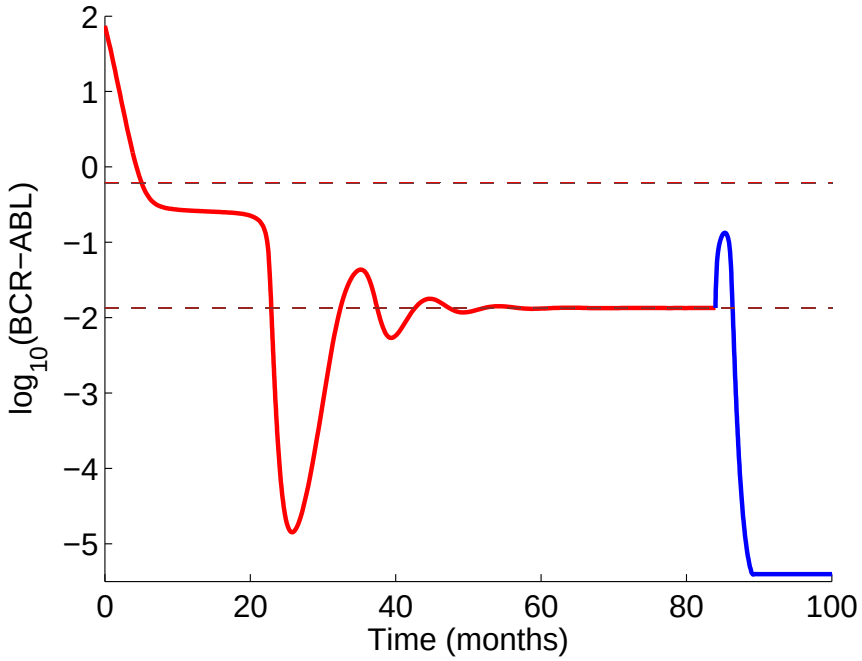

Figure 6.4: Simulation of successful treatment cessation. A patient's BCR-ABL ratio (solid line) is shown as a function of time in months. For the first 84 months, the patient is treated with IM therapy (red). At month 84, the patient stops therapy (blue). Despite having a small residual leukemic population which initially grows, the patient does not relapse. Rather, treatment cessation results in an immune response that eliminates the leukemic population. Thus, this patient will remain in TFR indefinitely. Dotted lines mark the patient's immune window. For this simulation, we set $d_v = 0.35$, $inh_1' = inh_1$, and $inh_2' = inh_2/10$. All other parameters are those of Patient 12 in Chapter 4.

post-treatment leukemic populations have similar growth rates, then we could set $inh_1' = inh_2' \approx 1$ during treatment cessation. However, as suggested in [97], it is possible that IM exerts a selective pressure on the leukemic population that may result in post-treatment cells with less proliferative capacity. We therefore choose $inh_1' = inh_1$ and either $inh_2' = inh_2/10$ or $inh_2/100$. We recall that treatment cessation trials have produced two disparate results. While 60% of patients relapse within the first six months, 40% achieve durable TFR. Moreover, in many patients who achieved TFR, residual levels of leukemia persisted.

In our simulations, the success of treatment cessation depends both on the patient's immune profile and the growth kinetics of the post-treatment leukemic population. For a single representative patient treated with IM (patient 12 in Chapter 4), we simulate treatment cessation starting at month 84. During treatment, IM is assumed to decrease the proliferation of progenitors by a factor $inh_1 = 1.5201$ and to decrease the proliferation of mature cells by a factor $inh_2 = 265.6435$. All other model parameters for this patient are shown in Tables 4.1 and 4.2.

We first consider the case when $inh_2' = inh_2/10$. That is, the proliferative capacity of leukemic cells is partially restored by treatment cessation. Although the leukemia initially grows, the patient's immune system is able to mount an efficient response that eliminates the residual leukemia. Therefore, this patient remains leukemia-free indefinitely without resuming IM therapy. This behavior, shown in Figure 6.4, represents the best possible outcome of treatment cessation. On the other hand, if we assume that the post-treatment leukemia's proliferative capacity is almost fully restored, by setting $inh_1' = inh_1 = 1.5201$ and $inh_2' = inh_2/100 = 2.6564$, then the patient relapses shortly after treatment cessation. In our simulations, we resume IM therapy at month 85, one month after cessation, as this is a likely first follow-up time during cessation. The results of this unsuccessful treatment cessation are shown in Figure 6.5(a).

For patients who relapse, we consider a combination of IM therapy and vaccines. The vaccines are intended to maintain a patient's immune response to CML when the leukemic stimulus alone becomes insufficient. This prolonged immune response may result in further control or even elimination of the residual leukemia. We therefore construct a vaccine schedule based on a patient's individual immune profile and response to IM therapy. For

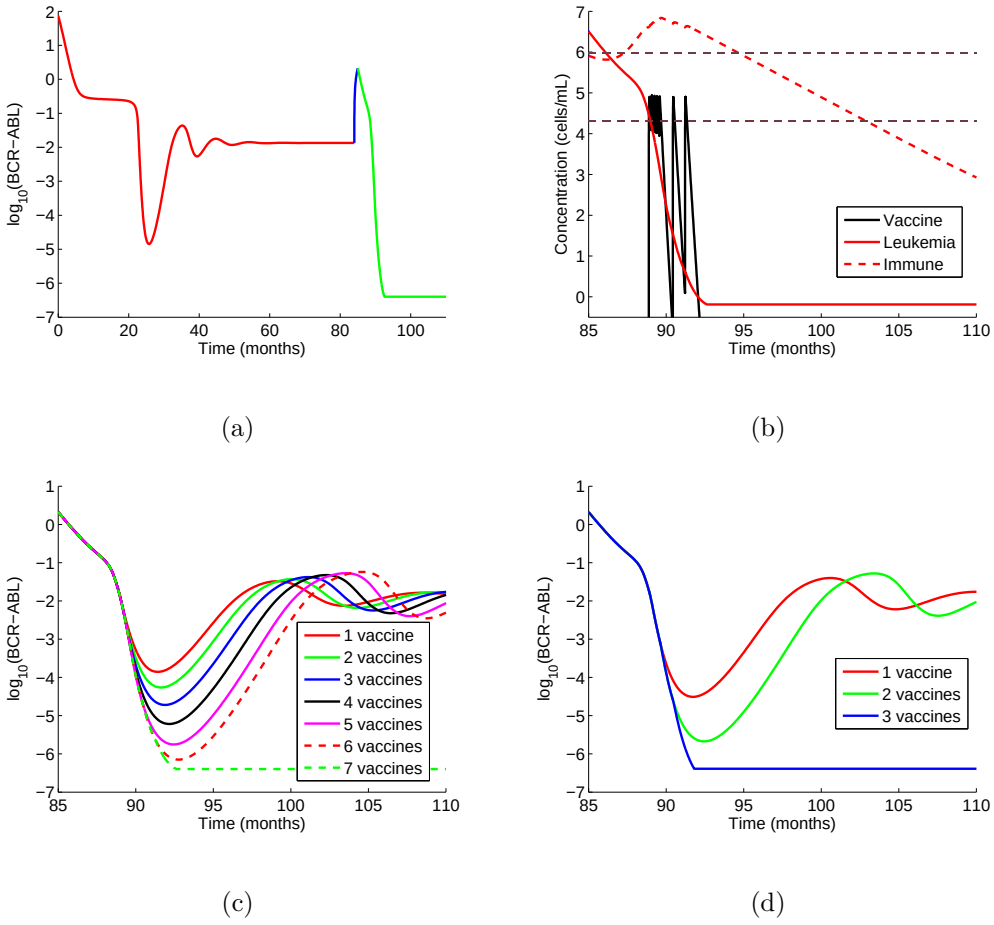

Figure 6.5: Residual leukemia can be eliminated by a sequence of vaccines. (a) This patient is treated with first-line IM and achieved a BCR-ABL ratio around 10^{-2} (red) during treatment. Treatment cessation (blue) starts at month 84. The patient relapses within the first month and resumes therapy starting at month 85 (green). A sequence of seven vaccines during IM therapy results in the elimination of the leukemic burden. (b) This figure focuses on the time during which the vaccines are administered. Each vaccine delivers 10^5 cells/mL over a one-day period. These cells die at a rate $d_v = 0.35$. The solid red line represents leukemia, while the thick dotted red line represents immune cells. The black curve represents vaccine cells, and the immune window is marked by thin dotted red lines. Each of the seven vaccines boosts the total leukemic concentration into the immune window, thus sustaining immune cells that would otherwise contract. (c) The effects of a variable number of vaccines on the mature leukemic population are shown. Administering as many as six vaccines is insufficient to eliminate the leukemia. However, applying seven vaccines sustains the immune response long enough to drive the leukemia to extinction. (d) If we increase the individual vaccines to $2.5 \cdot 10^5$ cells/mL, then only three vaccines are needed to cure the patient.

simplicity, just like in [43], we assume that each vaccine delivers a total of 10^5 cells/mL over a period of one day. Using the MATLAB function fminbnd, we optimize the timing of each vaccine, one at a time. That is, the time of the first vaccine is chosen to minimize the leukemic concentration following the vaccine. Then, the time of the second vaccine is chosen, and so on. Although this is a simplification of the full optimization problem in which all vaccine times are chosen in parallel and doses are allowed to vary, this strategy still produces successful treatment outcomes in many cases.

As previously mentioned, the patient shown in Figure 6.5(a) relapses within one month of IM cessation and resumes treatment at month 85. Figure 6.5(c) shows the effects of administering a variable number of vaccines during IM therapy. Administering up to six vaccines reduces a patient's leukemic temporarily below the immune window. However, once the vaccines are stopped, the leukemia is able to return to its original low-level equilibrium concentration. A sequence of seven vaccines administered during IM therapy results in the elimination of the residual leukemia, as shown in Figure 6.5(b). Increasing each vaccine's dose to $2.5 \cdot 10^5$ cells/mL decreases the number of vaccines necessary to cure the patient to three, as seen in Figure 6.5(d).

In summary, our model is able to reproduce a TFR in a patient with a small residual leukemic population at the time of IM cessation. Surprisingly, our modeling results suggest that treatment cessation alone may result in the elimination of the residual leukemia that remains even after several years of IM therapy. As suggested in [97], TFR may be partially explained by a selection effect caused by long-term IM therapy, resulting in a less aggressive leukemic clone than the one present at diagnosis. However, we acknowledge that many other factors may play a role in successful treatment cessation, including a patient's immune profile

(which may be affected by IM), the partial restoration of the microenvironment, or dynamics at the stem cell level. Our modeling framework offers a quantitative tool for exploring these factors.

For patients who relapse during IM cessation, we propose a combination therapy that involves IM and patient-specific, carefully-timed vaccines. Unlike IFNα, which is limited in may cases due to significant toxicity, vaccines offer a low-risk strategy aimed at boosting a patient's immune response to CML. This combination may improve a patient's likelihood of achieving a TFR if they stop IM therapy a second time. In some cases, these vaccines may even result in cancer elimination, thus guaranteeing a durable disease-free state.

Chapter 7: Conclusion

Thanks to TKI therapy, CML has been transformed into a chronic condition in which patients' life expectancies are similar those of their healthy counterparts. TKIs specifically target the constitutively active tyrosine kinase encoded by the *BCR-ABL* fusion oncogene, a mutation that is present in the majority of CML patients and which drives the disease. While TKIs have significant effects on *BCR-ABL*+ leukemic cells, they leave healthy cells mostly intact, in contrast to IFNα which is toxic to all cells. Because of their superior outcomes and their limited toxicity, TKIs remain the primary first-line therapy in the treatment of CML.

Despite these improvements, several open questions remain regarding the treatment of CML. It is unclear whether TKIs alone are capable of eliminating the leukemic burden. Most CML patients continue TKI therapy indefinitely, which is both expensive and may compromise a patient's quality of life. Although many patients respond extremely well to TKI therapy and achieve deep remissions, most continue to harbor detectable leukemic clones even after several years of therapy [86]. This may be partially explained by the claim that quiescent leukemic stem cells are insensitive to TKIs [29, 80]. The extent of the effects of TKIs on leukemic subpopulations, particularly leukemic stem cells, remains undetermined. A more complete understanding of their global mechanisms of action would allow us to identify any limitations of TKI monotherapy and to propose novel combination therapies

that may be able to target any leukemic subpopulations that are insensitive to TKIs.

Even if TKIs prove incapable of eliminating all leukemic cells, the IM cessation trials [60, 86] have shown that this is not necessary to achieve TFR. These trials found that patients who respond especially well to TKI therapy may be safely taken off these drugs, with about 40% achieving durable TFRs that last for many years. Many of these patients have detectable leukemic populations yet do not relapse. One study [14] detected leukemic stem cells in patients who had remained in TFR for up to eight years. Given the persistence of CML during treatment cessation, there must be some alternate mechanism(s) controlling the residual disease. A better understanding of these mechanisms would help clinicians to identify the best candidates for treatment cessation.

The IM cessation trials suggest that about 10-15% of patients diagnosed with CML will achieve TFR. This low percentage motivates the question of how treatment can be improved to achieve more TFRs. One possible strategy is to modify the inclusion and relapse definitions used in the trials. In STIM [60] and TWISTER [86], patients were included only if they had achieved UMRD for the last two years. Relapse was defined as two consecutive positive measurements (loss of UMRD), where STIM additionally required a 1-log increase between these two measurements. It is possible that these criteria unnecessarily exclude patients and may cause others included in the trials to resume treatment before it is needed. Several recent studies [59, 88, 92] are exploring relaxed criteria, with positive preliminary results. These new criteria may allow up to 20-25% of CML patients to achieve TFR.

Even with these new inclusion and relapse criteria, many patients will not respond well enough to TKI monotherapy to become eligible. Combinations of TKIs with IFNα are being investigated by several groups [32, 72, 78] in order to further control and reduce the

residual leukemic population. Because IFNα and TKIs have very different mechanisms of action [96], it is believed that their combination may have a synergistic effect. While TKIs will likely be responsible for removing the majority of the tumor burden, IFNα may target leukemic stem cells that would otherwise survive TKI therapy. Still, the long-term benefits of these combinations are not yet known. Moreover, the optimal scheduling of these two agents is an open research question that is especially difficult to address strictly through experimentation.

Mathematical modeling is a complementary tool to experimental and clinical data that can provide valuable insights into the treatment of CML. In general, mathematical models can be applied to study the underlying mechanisms driving an observed behavior that are difficult to access directly through experiments. They provide an inexpensive environment for testing hypotheses that are too expensive or unethical to study in a clinical setting. When physical experiments and clinical trials are possible, modeling results can be used to guide the experimental design, by identifying the most important parameters and the times at which they should be measured. They can also provide insight into long-term effects that will not be observable for several years. When combined with experimental and clinical data, mathematical models can lead to improvements in patient care and well-being, which I believe is the ultimate goal of mathematics applied to medicine.

Several mathematical modeling groups have studied various aspects of CML, including hematopoiesis, cancer genesis, treatment, and drug resistance. Michor *et al.* [65] construct an ODE model of CML that divides healthy and leukemic cells into four compartments based on their maturity. Roeder *et al.* [85] develop an ABM that also divides healthy and leukemic cells based on maturity but further divides stem cell into cycling and quiescent

compartments. Both models are able to reproduce the biphasic exponential declines that characterize many patients' initial response to IM. In the Michor model, the first steeper decline is explained by a decrease in the proliferative capacity of differentiated leukemic cells, while the second slower decline is explained by a similar effect on leukemic progenitors. The Roeder model attributes this biphasic decline to two effects on cycling leukemic stem cells: an immediate degradation effect followed by a change in the regulatory response of the remaining cells. Interestingly, both models initially assume that a subset of leukemic stem cells is unaffected by IM. In a later paper analyzing patients' long-term responses to IM with the Michor model, Tang et al. [98] find that some patients show triphasic exponential declines. They hypothesize that the third decline may indicate an effect of IM on immature leukemic cells, possibly leukemic stem cells.

Although both models are able to reproduce the monotonic biphasic and triphasic declines observed in some CML patients during IM therapy, our patient data indicates that many patients show nonmonotonic fluctuations in their BCR-ABL ratios. These fluctuations do not indicate relapse in the majority of cases and seem to be a natural part of the dynamics during therapy. The fact that neither the Michor model nor the Roeder model can reproduce these fluctuations suggests that an additional mechanism not included in either plays a critical role during IM therapy.

We therefore constructed a mathematical model that integrates CML and a patient's autologous immune response (see Chapter 4). Our choice to model the autologous immune response to CML is motivated by clinical evidence that a patient's immune system plays a significant role in the dynamics of the disease. Allogeneic bone marrow transplants and IFNα, two common treatments for CML prior to TKIs, work in part by stimulating an im-

mune response against CML. IFNα has reemerged as a potential treatment in combination with TKIs because of the former's ability to target leukemic stem cells and its immunostimulatory effects. The treatment cessation trials further support a critical role of a patient's immune response during TKI therapy. The fact that some patients achieve TFR despite detectable leukemia suggests that another mechanism, such as the immune system, is controlling the residual disease. This hypothesis is further supported by the observation that TFR is associated with prior IFNα therapy and higher concentrations and functionality of NK cells [39, 66, 74, 81], memory CD8+ T cells [102], and CD86+ dendritic cells [11]. Our model allows us to investigate the effects of an immune response on the dynamics during TKI therapy.

Our modeling framework divides leukemic cells into quiescent and cycling stem cells, progenitors, and mature cells. We additionally include a compartment representing immune cells that are able to detect and eliminate leukemic cells. We encode in our model an immune response in which small leukemic loads are an insufficient stimulus, while large leukemic loads suppress the immune system, thereby limiting its response to CML. However, at intermediate leukemic concentrations, which we call an *immune window*, a balance between immunostimulation and immunosuppression is achieved, and the autologous immune system is able to mount an efficient response against CML. This mechanism allowed us to fit our model to patients showing nonmonotonic variations in leukemic load.

Based on our patient data, modeling results, and analysis, we hypothesize that patients receiving TKI therapy go through three phases of leukemia reduction. The initial two phases are similar to the biphasic decline previously described in [65, 85]. During this time, because leukemic loads are still large, the immune system plays a minimal role, and the decline

in the leukemic population is driven primarily by the drug. However, as a result of the biphasic decline, the leukemic load may be driven into the immune window, which allows the immune population to develop an efficient first response, often resulting in a sudden sharp decline in BCR-ABL ratio. This first response marks the beginning of the third stage of therapy. The leukemic population is driven below the immune window, causing the immune population to contract, allowing the leukemia to partially recover. Eventually the leukemia reenters the immune window, which initiates another weaker immune response. This process repeats, producing oscillations in the leukemic and immune populations as the two populations approach equilibrium. It is during this third phase that fluctuations in BCR-ABL ratio are typically observed.

Our patient data and modeling results suggest that a patient's autologous immune system plays a significant role in the dynamics of TKI therapy. Moreover, the fluctuations that occur following the biphasic exponential decline may be explained by the immune system and therefore serve as a signature of a patient's individual immune profile. Our mathematical model is a potential tool for quantifying such inter-patient differences, in order to design patient-specific therapies aimed at achieving TFR.

The ability of our modeling framework to reproduce the dynamics of many patients during IM therapy suggests that it may serve as a valuable tool in studying other aspects of CML. Our model is able to fit CML patients treated with second-generation TKIs dasatinib and nilotinib, as shown in Section 6.1. We also include in Sections 6.2 and 6.3 preliminary results of applying extensions of this model to drug resistance, treatment cessation, and combination therapy. A more thorough investigation of these topics may require us to add more biological detail to this model which can be done, for instance, by incorporating variable

healthy cell populations, distinguishing between immune subtypes, or introducing the effects of the microenvironment. These directions are left for a future work.

This dissertation is the product of an active collaboration between clinicians, experimentalists, and mathematicians aimed at using adaptive and quantitative tools to improve patient care. Working directly with clinicians has not only given us access to data but has allowed us to construct a more realistic mathematical representation of CML through their feedback. We were then able to apply the model to study clinically-relevant questions. We believe that an interdisciplinary environment is the ideal setting for studying complex diseases like CML, as each group offers unique resources, insights, and perspectives. This project has convinced me that the most efficient path toward advancing our medical knowledge is through an interdisciplinary and collaborative approach in which both data and ideas are shared.

Bibliography

[1] Adimy M, Crauste F, and A. El Abdllaoui. Discrete-maturity structured model of cell differentiation with applications to acute myelogenous leukemia. J Biol Syst 2008;16:395-424.

[2] Adimy M and F Crauste. Delay differential equations and autonomous oscillations in hematopoietic stem cell dynamics modeling. Math Model Nat Phenom 2012;7(6):1-22.

[3] Alarcón T, Marches R, and KM Page. Mathematical models of the cell fate of lymphoma B cells after antigen receptor ligation with specific antibodies. J Theor Biol 2006;240:54-71.

[4] An X, Tiwari AK, Sun Y, Ding P-R, Ashby Jr CR, and Z-S Chen. BCR-ABL tyrosine kinase inhibitors in the treatment of Philadelphia chromosome positive chronic myeloid leukemia: A review. Leukemia Res 2010;34:1255-68.

[5] Arai F, Hirao A, Ohmura M, Sato H, Matsuoka S, Takubo, K, et al. Tie2/Angiopoietin-1 signaling regulates hematopoietic stem cell quiescence in the bone marrow niche. Cell 2004;118:149-161.

[6] Beillard E, Pallisgaard N, van der Velden VH, Bi W, Dee R, van der Schoot E, et al. Evaluation of candidate control genes for diagnosis and residual disease detection in leukemic patients using 'real-time' quantitative reverse-transcriptase polymerase chain reaction (RQ-PCR) - a Europe against cancer program. Leukemia 2003;17(12):2474-86.

[7] Biron CA. Interferons alpha and beta as immune regulators a new look. Immunity 2001;14(6):661664.

[8] Branford S, Rudzki Z, Walsh S, Parkinson I, Grigg A, Szer J, et al. Detection of BCR-ABL mutations in patients with CML treated with imatinib is virtually always accompanied by clinical resistance, and mutations in the ATP phosphate-binding loop (P-loop) are associated with a poor prognosis. Blood 2003;102(1):276-83.

[9] Branford S, Yeung DT, Ross DM, Prime JA, Field CR, Altamura HK, et al. Early molecular response and female sex strongly predict stable undetectable BCR-ABL1, the criteria for imatinib discontinuation in patients with CML. Blood 2013;121:38183824.

[10] Burchert, A. Chronic myeloid leukemia stem cell biology and interferon alpha. Hematology Education 2014;8:87-96.

[11] Burchert A, Inselmann S, Saussele S, Dietz CT, Müller MC, Eigendorff E et al. Frequency of CTLA-4 Receptor Ligand (CD86, B7.2)-Positive Plasmacytoid Dendritic Cells Predicts Risk of Disease Recurrence after Tyrosine-Kinase Inhibitor Discontinuation in Chronic Myeloid Leukemia: Results from a Prospective Substudy of the Euroski Trial. *Blood* (ASH 2015 Annual Meeting Abstracts), Available from: https://ash.confex.com/ash/2015/webprogram/Paper83467.html.

[12] Burchert A, Muller MC, Kostrewa P, Erben P, Bostel T, Liebler S, et al. Sustained molecular response with interferon alfa maintenance after induction therapy with imatinib plus interferon alfa in patients with chronic myeloid leukemia. J Clin Oncol : Off J Am Soc Clin Oncol 2010;28(8):1429 1435. doi:10.1200/JCO.2009.25.5075.

[13] Chen C I-U, Maecker HT, and PP Lee. Development and dynamics of robust T cell responses to CML under imatinib treatment. Blood 2008;111(11):5342-5349.

[14] Chomel JC, Bonnet M-L, Sorel N, Bertrand A, Meunier M-C, Fichelson S, et al. Leukemic stem cell persistence in chronic myeloid leukemia patients with sustained undetectable molecular residual disease. Blood 2011;118(13):3657-60.

[15] Chomel JC, Brizard F, Veinstein A, Rivet J, Sadoun A, Kitzis A, et al. Persistence of BCR-ABL genomic rearrangement in chronic myeloid leukemia patients in complete and sustained cytogenetic remission after interferon-alpha therapy or allogeneic bone marrow transplantation. Blood 2000;95(2):404408.

[16] Chrobak JM, Bodnar M, and H Herrero. About a generalized model of lymphoma. J Math Anal Appl 2012;386: 813-829.

[17] Clapp G, Lepoutre T, El Cheikh R, Bernard S, Ruby J, Labussiere-Wallet H, Nicolini FE, and D Levy. Implication of the autologous immune system in BCR-ABL transcript variations in chronic myelogenous leukemia patients treated with imatinib. Cancer Res 2015;75(19):4053-4062.

[18] Clapp G, Lepoutre T, Nicolini FE, and D Levy. BCR-ABL Transcript Variations in Chronic Phase Chronic Myelogenous Leukemia Patients on Imatinib First-Line: Possible Role of the Autologous Immune System. OncoImmunology 2015. accepted

[19] Clapp G and D Levy. (2014) Incorporating Asymmetric Stem Cell Division in to the Roeder Model for Chronic Myeloid Leukemia. Mathematical Models of Tumor-Immune System Dynamics. Springer Proceedings in Mathematics and Statistics. 107:1-20.

[20] Clapp G and D Levy. (2014) A Review of Mathematical Models for Treating Leukemia and Lymphoma. Drug Discov Today: Dis Model, http://dx.doi.org/10.1016/j.ddmod.2014.10.002

[21] Colijn C and M Mackey. A mathematical model of hematopoiesis – I. Periodic chronic myelogenous leukemia. J Theoret Biol 2005;237:117-132.

[22] Cross NC, White HE, Mller MC, Saglio G, and A Hochhaus. Standardized definitions of molecular response in chronic myeloid leukemia. Leukemia 2012;26(10):2172-5.

[23] DeConde R, Kim PS, Levy D, and PP Lee. Post-transplantation dynamics of the immune response to chronic myelogenous leukemia. J Theor Biol 2005;236:39-59.

[24] Deininger M, Buchdunger E, and BJ Druker. The development of imatinib as a therapeutic agent for chronic myeloid leukemia. Blood 2005;105(7):2640-53.

[25] Diamond MS, Kinder M, Matsushita H, Mashayekhi M, Dunn GP, Archambault JM, et al. Type I interferon is selectively required by dendritic cells for immune rejection of tumors. J Exp Med 2011; 208(10):19892003. doi:10.1084/jem.20101158

[26] Dingli D and F Michor. Successful therapy must eradicate cancer stem cells. Stem Cells 2006;24:2603-2610.

[27] Doumic-Jauffret M, Kim P, and B Perthame. Stability analysis of simplified yet complete model for chronic myelogenous leukemia. Bull Math Bio 2010;72:1732-1759.

[28] Essers MAG, Offner S, Blanco-Bose WE, Waibler Z, Kalinke U, Duchosal MA, et al. IFNα activates dormant haematopoietic stem cells in vivo. Nature 2009;458:904-909.

[29] Gallipoli P, Abraham SA, and TL Holyoake. Hurdles toward a cure for CML: the CML stem cell. Hematol Oncol Clin N Am 2011;25:951966.

[30] Glauche I, Horn K, Horn M, Thielecke L, Essers MAG, Trump A, et al. Therapy of chronic myeloid leukemia can benefit from the activation of stem cells: simulation studies of different treatment combinations. Brit J Cancer 2012;106(11):1742-1752.

[31] Goldman J and M Gordon. Why do chronic myelogenous leukemia stem cells survive allogeneic stem cell transplantation or imatinib: does it really matter? Leuk Lymphoma 2006;47:17.

[32] Hehlmann R, Lauseker M, Jung-Munkwitz S, Leitner A, Mller MC, Pletsch N, et al. Tolerability-adapted imatinib 800 mg/d versus 400 mg/d versus 400 mg/d plus interferon-a in newly diagnosed chronic myeloid leukemia. J Clin Oncol 2011;29:163442.

[33] Hervas-Stubbs S, Riezu-Boj JI, Gonzalez I, Mancheno U, Dubrot J, Azpilicueta A, et al. Effects of IFN-alpha as a signal-3 cytokine on human naive and antigen-experienced CD8(+) Tcells. Eur J Immunol 2010;40(12):33893402. doi:10.1002/eji.201040664.

[34] Hochhaus A, O'Brien SG, Guilhot F, Druker BJ, Branford S, Foroni L, et al. Six-year follow-up of patients receiving imatinib for the first-line treatment of chronic myeloid leukemia. Leukemia 2009;23:10541061.

[35] Hochhaus A, Reiter A, Saussele S, Reichert A, Emig M, Kaeda J, et al. Molecular heterogeneity in complete cytogenetic responders after interferon- therapyfor chronic myelogenous leukemia: low levels of minimal residual disease are associated with continuing remission. Blood 2000;5(1):6266.

[36] Horn M, Glauche I, Müller MC, Hehlmann R, Hochhaus H, Loeffler M, et al. Model-based decision rules reduce the risk of molecular relapse after cessation of tyrosine kinase inhibitor therapy in chronic myeloid leukemia. Blood 2013;121:378-384.

[37] Hughes T, Deininger M, Hochhaus A, Branford S, Radich J, Kaeda J, et al. Monitoring CML patients responding to treatment with tyrosine kinase inhibitors: review and recommendations for harmonizing current methodology for detecting BCR-ABL transcripts and kinase domain mutations and for expressing results. Blood 2006;108(1):28-37.

[38] Hughes T, Kaeda J, Branford S, Rudzki Z, Hochhaus A, Hensley M, et al. International Randomised Study of Interferon versus STI571 (IRIS) Study Group. Frequency of major molecular responses to imatinib or interferon alfa plus cytarabine in newly diagnosed chronic myeloid leukemia. N Engl J Med 2003; 349(15):1423-1432.

[39] Ilander MM, Olsson-Strömberg U, Lähteenmäki H, Kanasen T, Koskenvesa P, Söderlund S, et al. Disease Relapse After TKI Discontinuation in CML is related both to low number and impaired function of NK-cells: data from Euro-SKI. Blood (ASH Annual Meeting Abstracts) 2013; 122: 379.

[40] Kanodia S, Wieder E, Lu S, Talpaz M, Alatrash G, Clise-Dwyer K, et al. PR1-specific T cells are associated with unmaintained cytogenetic remission of chronic myelogenous leukemia after interferon withdrawal. PLoS One 2010;5(7):e11770. doi:10.1371/journal.pone.0011770.

[41] Kantarjian HM, Giles F, Quintas-Cardama A, and J Cortes. Important therapeutic targets in chronic myelogenous leukemia. Clin Cancer Res 2007;13:108997.

[42] Kim P, Lee P, and D Levy. A PDE model for imatinib-treated chronic myelogenous leukemia. Bull Math Biol 2008;70:1994-2016.

[43] Kim P, Lee P, and D Levy. Dynamics and potential impact of the immune response to chronic myelogenous leukemia. PLoS Comput Biol 2008;4(6):e1000095.

[44] Kim P, Lee P, and D Levy. Modeling imatinib-treated chronic myelogenous leukemia: Reducing the complexity of agent-based models. Bull Math Biol 2008;70:728-744.

[45] Klaus J, Herrmann D, Breitkreutz I, Hegenbart U, Mazitschek U, Egerer G, et al. Effect of CD34 cell dose on hematopoietic reconstitution and outcome in 508 patients with multiple myeloma undergoing autologous peripheral blood stem cell transplantation. Eur J Haematol 2007;78:21-28.

[46] Kolb HJ, Schattenberg A, Goldman JM, Hertenstein B, Jacobsen N, Arcese W, et al. Graft-versus-leukemia effect of donor lymphocyte transfusions in marrow grafted patients European Group for Blood and Marrow Transplantation Working Party Chronic Leukemia. Blood 1995;86(5):2041-50.

[47] Komarova N and D Wodarz. Drug resistance in cancer: Principles of emergence and prevention. PNAS 2005;102(27):9714-9719.

[48] Komarova N, and D Wodarz. Effect of Cellular Quiescence on the Success of Targeted CML Therapy. PLoS ONE 2007;10:e990.

[49] Komarova N, Katouli A, and D Wodarz. Combination of two but no three current targeted drugs can improve therapy of chronic myeloid leukemia. PLoS ONE 2009;4(2):e4423.

[50] Kuznetsov VA, Makalkin IA, Taylor MA, and AS Perelson. Nonlinear dynamics of immunogenic tumors: parameter estimatuion adn global bifurcation analysis. Bull Math Bio 1994;56(2):295-321.

[51] Laperrousaz B, Jeanpierre S, Sagorny K, Voeltzel T, Ramas S, Kaniewski B, et al. Primitive CML cell expansion relies on abnormal levels of BMPs provided by the niche and BMPRIb overexpression. Blood 2013;122(23):3767-77.

[52] Lenaerts T, Pacheco JM, Traulsen A, and D Dingli. Tyrosine kinase inhibitor therapy can cure chronic myeloid leukemia without hitting leukemic stem cells. Haematologica 2010;95(6):900-907.

[53] Leder K, Foo J, Skaggs B, Gorre M, Sawyers CL, and F Michor. Fitness conferred by BCR-ABL kinase domain mutations determines the risk of pre-existing resistance in chronic myeloid leukemia. PLoS ONE 2011;6(11):e27682.

[54] Lee CK, Rao DT, Gertner R, Gimeno R, Frey AB, and DE Levy. Distinct requirements for IFNs and STAT1 in NK cell function. J Immunol 2000;165(7):35713577.

[55] Lei J and M Mackey. Multistability in an age-structured model of hematopoiesis: Cyclical neutropenia. J Theoret Biol 2011;270:143-153.

[56] Mahmud N, Devine S, Weller K, Parmar S, Sturgeon C, Nelson M, et al. The relative quiescence of hematopoietic stem cells in nonhuman primates. Blood 2001;97:3061-3068.

[57] Mahon FX, Delbrel X, Cony-Makhoul P, Fabères C, Boiron JM, Barthe C, et al. Follow-up of complete cytogenetic remission in patients with chronic myeloid leukemia after cessation of interferon alfa. J Clin Oncol 2002;20:214220.

[58] Mahon F-X. Discontinuation of tyrosine kinase therapy in CML. Ann Hematol 2015;94(Suppl 2):S187-S193.

[59] Mahon FX, Nicolini F, Noel MP, Escoffre M, Charbonnier A, Rea D, et al. Preliminary Report Of The STIM2 Study: a multicenter Stop Imatinib trial for chronic phase chronic myeloid leukemia de novo patients on imatinib. Blood (ASH Annual Meeting Abstracts) 2013 [abstract 654]

[60] Mahon FX, Réa D, Guilhot J, Guilhot F, Huguet F, Nicolini F, et al. Discontinuation of imatinib in patients with chronic myeloid leukaemia who have maintained complete molecular remission for at least 2 years: the prospective, multicentre Stop Imatinib (STIM) trial. Lancet Oncol 2010;11(11):1029-1035.

[61] Marciniak-Czochra A, Stiehl T, Ho AD, Jäger W, and W Wagner. Modeling of asymmetric cell division in hematopoietic stem cells – Regulation of self renewal is essential for efficient repopulation. Stem Cells and Dev 2009;18:377-385.

[62] Marin D, Bazeos A, Mahon F-X, Eliasson L, Milojkovic D, Bua M, et al. Adherence is the critical factor for achieving molecular responses in patients with chronic myeloid leukemia who achieve complete cytogenetic responses on imatinib. J Clin Onc 2010;28(14):2381-8.

[63] Mendelson A and PS Frenette. Hematopoietic stem cell niche maintenance during homeostasis and regeneration. Nature Medicine 2014;20(8):833-46.

[64] Metcalf D. Hematopoietic cytokines. Blood 2008;111(2): 485-491.

[65] Michor F, Hughes TP, Iwasa Y, Branford S, Shah NP, Sawyers CL, et al. Dynamics of chronic myeloid leukemia. Nature 2005;435(7046):1267-1270.

[66] Mizoguchi I, Yoshimoto T, Katagiri S, Mizuguchi J, Tauchi T, Kimura Y et al. Sustained upregulation of effector natural killer cells in chronic myeloid leukemia after discontinuation of imatinib. Cancer Sci 2013;104(9):1146-1153.

[67] Molldrem J, Dermime S, Parker K, Jiang YZ, Mavroudis D, Hensel N, et al. Targeted T-cell therapy for human leukemia: cytotoxic T lymphocytes specific for a peptide derived from proteinase 3 preferentially lyse human myeloid leukemia cells. Blood 1996;88(7):24502457.

[68] Molldrem JJ, Lee PP, Kant S, Wieder E, Jiang W, Lu S, et al. Chronic myelogenous leukemia shapes host immunity by selective deletion of high-avidity leukemia-specific T cells. J Clin Invest 2003;111:639-647. doi:10.1172/JCI200316398.

[69] Molldrem JJ, Lee PP, Wang C, Felio K, Kantarjian HM, Champlin RE, et al. Evidence that specific T lymphocytes may participate in the elimination of chronic myelogenous leukemia. Nat Med 2000;6(9):10181023.

[70] Moore H and N Li. A mathematical model for chronic myelogenous leukemia (CML) and T cell interaction. J Theoret Biol 2004;227:513-523.

[71] Murphy K and P Travers. Janeway's Immunobiology 8th ed. New York: Garland Science, 2012. Print.

[72] Nicolini F, Etienne G, Dubruille V, Roy L, Huguet F, Legros L, et al. Nilotinib and pegylated interferon alfa 2a for newly diagnosed chronic phase chronic myeloid leukaemia patients Results of a multicentric phase II study. Lancet Haematol 2015;2:e37-45.

[73] O'Brien SG, Guilhot F, Larson RA, Gathmann I, Baccarani M, Cervantes F, et al. Imatinib compared with interferon and low-dose cytarabine for newly diagnosed chronic-phase chronic myeloid leukemia. N Engl J Med 2003;348(11):994-1004.

[74] Ohyashiki K, Katagiri S, Tauchi T, Ohjashiki JH, Maeda Y, Matsumura I, et al. Increased natural killer cells and decreased CD3+CD8+CD62L+ T cells in CML patients who sustained complete molecular remission after discontinuation of imatinib. Brit J Heaematol 2012;157:249-277.

[75] Panetta JC, Evans WE, and MH Cheok. Mechanistic mathematical modelling of mercaptopurine effects on cell cycle of human acute lymphoblastic leukaemia cells. Brit J Cancer 2006;94:93-100.

[76] Panetta JC, Sparreboom A, Pui C-H, Relling MV, and WE Evans. Modeling mechanisms of in vivo variability in methotrexate accumulation and folate pathway inhibition in acute lymphoblastic leukemia cells. PLoS Comput Biol 2010;6(12):e1001019.

[77] Panetta JC, Wall A, Pui C-H, Relling MV, and WE Evans. A mathematical model of in vivo methotrexate accumulation in acute lymphoblastic leukemia. Cancer Chemoth Pharm 2002;50:419-428.

[78] Preudhomme C, Guilhot J, Nicolini FE, Guerci-Bresler A, Rigal- Huguet F, Maloisel F, et al. Imatinib plus peginterferon alfa-2a in chronic myeloid leukemia. N Engl J Med 2010;363(26):25112521. doi:10.1056/NEJMoa1004095.

[79] Price TH, Chatta GS, and DC Dale. Effect of recombinant granulocyte colony stimulating factor on neutrophil kinetics in normal young and elderly humans. Blood 1996;88:335-340.

[80] Rea D, Rousselot P, Guilhot J, Guilhot F, and FX Mahon. Curing chronic myeloid leukemia. Curr Hematol Malignancy Rep 2012;7:103108.

[81] Rea D, Dulphy N, Henry G, Guilhot J, Guilhot F, Nicolini FE, et al. Low Natural Killer (NK) Cell Counts and Functionality Are Associated With Molecular Relapse After Imatinib Discontinuation In Patients (pts) With Chronic Phase (CP)-Chronic Myeloid Leukemia (CML) With Undetectable BCR-ABL Transcripts For At Least 2 Years: Preliminary Results From Immunostim, On Behalf Of STIM Investigators. Blood (ASH Annual Meeting Abstracts). 2013; 122: 865.

[82] Rizza P, Moretti F, and F Belardelli. Recent advances on the immunomodulatory effects of IFN-alpha: implications for cancer immunotherapy and autoimmunity. Autoimmunity 2010;43(3):204209. doi:10.3109/08916930903510880.

[83] Rodriguez-Brenes IA, Komarova NL, and D Wodarz. Evolutionary dynamics of feedback escape and the development of stem-cell-driven cancers. PNAS 2011;108(47):18983-18988.

[84] Roeder I, Herberg M, and M Horn. An age-structured model of hematopoietic stem cell organization with application to chronic myeloid leukemia. Bull Math Biol 2009;71:602-626.

[85] Roeder I, Horn M, Glauche I, Hochhaus A, Mueller MC, and M Loeffler. Dynamic modeling of imatinib-treated chronic myeloid leukemia: functional insights and clinical implications. Nature Med 2006;12(10):1181-1184.

[86] Ross DM, Branford S, Seymour JF, Schwarer AP, Arthur C, Yeung DT, et al. Safety and efficacy of imatinib cessation for CML patients with stable undetectable minimal residual disease: results from the TWISTER study. Blood 2013;122:515-522.

[87] Ross DM and TP Hughes. How I determine if and when to recommend stopping tyrosine kinase inhibitor treatment for chronic myeloid leukemia. Brit J Hematol 2014;166:3-11.

[88] Rousselot P, Charbonnier A, Cony-Makhoul P, Agape P, Nicolini FE, Varet B, et al. Loss of major molecular response as a trigger for restarting tyrosine kinase inhibitor therapy in patients with chronic-phase chronic myelogenous leukemia who have stopped imatinib after durable undetectable disease. J Clin Oncol 2014;32:424430.

[89] Rousselot P, Huguet F, Rea D, Legros L, Cayuela JM, Maarek O, et al. Imatinib mesylate discontinuation in patients with chronic myelogenous leukemia in complete molecular remission for more than 2 years. Blood 2007;109:5860.

[90] Rufer N, Brummendorf T, Kolvraa S, Bischoff C, Christensen K, Wadsworth L, et al. Telomere fluorescence measurements in granulocytes and T lymphocyte subsets point to a high turnover of hematopoietic stem cells and memory T cells in early childhood. J Exp Med 1999;190(2):157-167.

[91] Sato T, Onai N, Yoshihara H, Arai F, Suda T, and T Ohteki. Interferon regulatory factor-2 protects quiescent hematopoietic stem cells from type I interferon-dependent exhaustion. Nature Med 2009;15(6):696-700.

[92] Saussele S, Richter J, Guilhot J, Mller MC, Dietz C, Porkka K, et al. First interim analysis of a Pan-European Stop trial using standardized molecular criteria: results of the EURO-SKI trial. 19th Congress of the European Hematology Association, Milan, Italy, June 1215, 2014. Haematologica 99(supl. 1):LB-621418.

[93] Silva M, Grillot D, Benito A, Richard C, Nuñez G, and JL Fernández-Luna. Erythropoietin can promote erythroid progenitor survival by repressing apoptosis through bcl-1 and bcl-2. Blood 1996;88:1576-1582.

[94] Stiehl T and A Marciniak-Czochra. Mathematical modeling of leukemogenesis and cancer stem cell dynamics. Math Model Nat Phenom 2012;7(1):166-202.

[95] Swann JB, Hayakawa Y, Zerafa N, Sheehan KC, Scott B, Schreiber RD, et al. Type I IFN contributes to NK cell homeostasis, activation, and antitumor function. J Immunol 2007;178(12):7540-7549.

[96] Talpaz M, Mercer J, and R Hehlmann. The interferon-alpha revival in CML. Ann Hematol 2015;94(Suppl 2):S195-S207. DOI 10.1007/s00277-015-2326-y.

[97] Tang M, Foo J, Gönen M, Guilhot J, Mahon F-X, and F Michor. Selection pressure exerted by imatinib therapy leads to disparate outcomes of imatinib discontinuation trials. Haematologica 2012;97(10):1553-1561.

[98] Tang M, Gonen M, Quintas-Cardama A, Cortes J, Kantarjian H, Field C, et al. Dynamics of chronic myeloid leukemia response to long-term targeted therapy reveal treatment effects on leukemic stem cells. Blood 2011;118(6):1622-31.

[99] Tomasetti C. A new hypothesis: imatinib affects leukemic stem cells in the same way it affects all other leukemic cells. Blood Cancer J 2011;1(19): doi:10.1038/bcj.2011.17 (http://www.nature.com/bcj/index.html).

[100] Tomasetti C and D Levy. Role of symmetric and asymmetric division of stem cells in developing drug resistance. PNAS 2010;107(39):16766-16771.

[101] Tough DF, Borrow P, Sprent J. Induction of bystander T cell proliferation by viruses and type I interferon in vivo. Science 1996;272(5270):19471950.

[102] Usuki K, Yokoyama K, Nagamura-Inoue T, Ito A, Kida M, Izutsu K et al. CD8+ memory T cells predominate over naive T cells in therapy-free CML patients with sustained major molecular response. Leukemia Res 2009;33:e164-e165.